

Development of a Canine Knee Implant

by
Oscar Röhrs

*Thesis presented in partial fulfilment of the requirements for the degree
of Master of Engineering (Mechanical) in the Faculty of Engineering at
Stellenbosch University*



Supervisor: Dr J. van der Merwe
Co-supervisor: Dr J.H. Muller

March 2020

Declaration

By submitting this thesis electronically, I declare that the entirety of the work contained therein is my own, original work, that I am the sole author thereof (save to the extent explicitly otherwise stated), that reproduction and publication thereof by Stellenbosch University will not infringe any third party rights and that I have not previously in its entirety or in part submitted it for obtaining any qualification.

Date: March 2020

Copyright © 2020 Stellenbosch University
All rights reserved

Abstract

Patient-specific canine knee implants have the potential to restore lost mobility to knees experiencing joint degradation. Due to high costs associated with current implant solutions, this research focused on creating and implementing an open-source design approach for a non-cruciate-ligament-sparing total knee replacement. Femoral and tibial canine knee implant components were generated for three different canine specimens. Open-chain knee joint kinematics and kinetics were studied using an Oxford-type test rig and a 3D motion tracking system. Pre- and post-implant knee joint results were obtained for flexion-extension, internal-external rotation, adduction-abduction, mediolateral shift, anterior-posterior drawer, joint compression-distraction and quadriceps forces during joint extension. The open-source design approach was implemented for three different cases, with encouraging results being achieved for the total knee replacement implants compared to the kinematic and kinetic performance of healthy canine knees.

Uittreksel

Pasiëntspesifieke honde-knievervangings het die potensiaal om verlore mobiliteit te herstel in knieë wat gewrigsdegradasie ondergaan. Weens die hoë koste wat met huidige knie vervangingsoplossings gepaard gaan, het hierdie navorsing gefokus op die skepping en implementering van 'n ontwerpsbenadering wat van vrylik beskikbare bronne gebruik maak om 'n nie-kruisligament-sparende totale knieveranging te skep. Femorale en tibiale hondeknie vervangingskomponente was gegeneer vir drie verskillende honde-beenmonsters. Oop-ketting lit kinematika en kinetika was bestudeer met die gebruik van 'n Oxford-tipe toetstuiw en 'n 3D-bewegingsopsporing sisteem. Voor- en na-knieveranging resultate was verkry vir fleksie-uitbreiding, interne-eksterne rotasie, adduksie-wegtrekking, mediale-laterale verskuiwing, anterior-agterste verskuiwing, litkompressie-spanning en quadricep-spierkragte tydens lituitbreiding. Die vrylik-beskikbare-bron-ontwerpsbenadering was geïmplementeer vir drie verskillende gevalle, waarvoor belowende resultate bereik is nadat die totale knievervangings met kinematiese en kinetiese verrigting van gesonde hondeknieë vergelyk is.

Acknowledgements

I would like to thank my supervisors, Dr. Johan van der Merwe and Dr. Cobus Muller, for giving me the opportunity and for your continual guidance throughout the research process.

Thank you Dr. Morne de Wet for your valuable input and guidance, and the friendly assistance of the Cottage Vet staff.

Thank you to Dr. Gary Kruger and the Cape of Good Hope SPCA for their help.

Thank you Ebard, Musa and my fellow BERG members for sharing the post-graduate journey and helping me throughout my Master's experience.

To my parents, Adri and Bernd, thank you so much for your constant love and support and for providing me with this opportunity. Without you this would never have been possible.

To my partner, Lee, thank you for being there for me, for your constant patience, understanding and love. You supported me through thick and thin and I will be forever grateful.

Dedications

*To Him Whose mercies are new every morning
For from Him and through Him and to Him are all things*

Table of contents

Declaration	ii
Abstract	iii
Uittreksel	iv
Acknowledgements	v
Dedications	vi
Table of contents	vii
List of figures	ix
List of tables	xii
1 Introduction	1
1.1 Background.....	1
1.2 Motivation.....	1
1.3 Aim and objectives	1
1.4 Outcomes.....	2
2 Literature review	3
2.1 Canine knee anatomy	3
2.2 Knee kinematics.....	5
2.3 Condition leading to total knee replacement (TKR)	8
2.4 Total knee replacement.....	8
2.5 Design considerations of TKR implants.....	9
2.6 Current implant sizing methods	11
2.7 Current tibial cut approach	13
2.8 Current femoral cut approach.....	15
2.9 Trial reduction and downsizing method	17
2.10 Current implantation method	17
2.11 Design modelling.....	18
3 Implant Design	19
3.1 Overview.....	19
3.2 Functional requirements of design.....	20
3.3 Selection of canines	20
3.4 CT scans.....	20
3.5 Segmentation and 3D reconstruction using 3DSlicer.....	21
3.6 Smoothing procedure using Meshlab	23
3.7 Design using Blender	28
3.7.1 Overview.....	28

3.7.2	Cutting plane selection.....	29
3.7.3	Design of femoral implant.....	31
3.7.4	Implant thickness calculations.....	36
3.7.5	Design of tibial implant.....	37
3.7.6	Design of instrumentation.....	42
4	Testing procedure.....	45
4.1	Overview.....	45
4.2	Steps taken to generate test model and implants.....	45
4.3	Specimen preparation for kinematic tests.....	49
4.4	Testing procedure using open-chain configuration.....	50
4.5	Surgical procedure and implantation.....	55
4.6	Angle and translation calculation method.....	60
5	Results.....	65
5.1	Obtained data.....	65
5.2	Casted bone model results.....	65
5.3	Labrador specimen results.....	69
5.4	German Shepherd specimen results.....	73
6	Discussion and conclusion.....	78
6.1	Discussion and recommendations.....	78
6.2	Conclusion.....	81
	References.....	82
	Appendices.....	87
A	3DSlicer segmentation protocol.....	87
B	Meshlab smoothing protocol.....	88
C	Blender infographic map.....	91
D	Kinematic calculations code.....	93

List of figures

Figure 1: Canine Stifle (Knee) [10]	3
Figure 2: Canine anatomical views [11]	4
Figure 3: Joint coordinate system [12]	6
Figure 4: Cartesian coordinate system and joint angle definitions [12]	6
Figure 5: Joint translations [12]	7
Figure 6: Progression of degenerative joint disease (osteoarthritis) [14].....	8
Figure 7: BioMedtrix (a)[4] and GenuSys (b)[18] total knee replacements	10
Figure 8: CaCr view of tibia in A. ML view of femur in B. ML view of tibia in C. CaCr view of femur in D [4]	12
Figure 9: Tibial cut in A. Exposed cancellous bone of proximal tibia in B. Removed proximal tibial piece in C. [4].....	13
Figure 10: Medial and cranial views of the ETAG [4]	14
Figure 11: Aligned cutting block [4].....	14
Figure 12: Tibial trial handle (TTH) used to align tibial trial block [4]	15
Figure 13: Femoral cut sequence [4]	15
Figure 14: Model of FCB and fixed FCB [4]	16
Figure 15: FCB model fixation & femoral cuts [4].....	16
Figure 16: FCB and femoral implant with datum pin shown [4]	17
Figure 17: Femoral trial component for drilling [4].....	18
Figure 18: Design Overview	19
Figure 19: CT scan specimen positioning.....	21
Figure 20: CT scan image exposure adjustments.....	22
Figure 21: 3DSlicer generated 3D model from selected label map volumes	23
Figure 22: Geometric visualisation of umbrella operator	24
Figure 23: Mesh components before (a) and after (b) Laplacian smoothing	25
Figure 24: Mesh before (a) and after (b) surface reconstruction	25
Figure 25: Vertex quality histogram and distance map for Labrador femur	27
Figure 26: Femur before (a) and after (b) smoothing protocol	27
Figure 27: Design Process	28
Figure 28: Femoral cutting profiles for humans and canines.....	30
Figure 29: Femoral alignment in the lateral, ventro-dorsal and caudal planes ...	31
Figure 30: Bezier circle profile generation	32
Figure 31: Curve to mesh transformation	33
Figure 32: Mesh resolution increase.....	33
Figure 33: Triangulated mesh before and after smoothing.....	34

Figure 34: Femoral implant cut-plane interface generation	34
Figure 35: Femoral implant cut surface and fixation pin generation	35
Figure 36: Distal femur pre- and post-implant.....	36
Figure 37: Free body diagram and loaded beam problem setup.....	36
Figure 38: Tibial alignment in the lateral, ventro-dorsal and caudal planes	38
Figure 39: Ventro-dorsal proximal tibial cut	38
Figure 40: Nurbs circle generation and mesh conversion	39
Figure 41: Femoral condyle scaling for tibial implant articulating surface generation	40
Figure 42: Tibial implant articular geometry generation	41
Figure 43: Generated tibial implant.....	41
Figure 44: Tibial tester.....	42
Figure 45: Tibial cutting alignment guide components	43
Figure 46: Femoral cutting guide components.....	44
Figure 47: Mould box.....	47
Figure 48: Moulding process	47
Figure 49: Casted bone models between FDM printed bone models.....	48
Figure 50: Free-standing pre-implant casted models (a) and post-implant casted models in joint test rig (b)	49
Figure 51: Specimen leg pre- and post-preparation for potting	50
Figure 52: Oxford knee test rig as described by Zavatsky et al. [44].....	51
Figure 53: Labelled open-chain test rig setup	52
Figure 54: Polaris Spectra Measurement Volume (Northern Digital Inc.) [51]	53
Figure 55: Virtual marker point locations shown for a posterior femur and anterior tibia in a. Quadricep-angle description from an anterior view in b.	54
Figure 56: Open-chain experimental setup for knee joint in flexion.....	55
Figure 57: Fixation of the tibial alignment guide.....	56
Figure 58: Tibial cut being made and resultant flat tibial surface.....	57
Figure 59: Fixation of FCGB with FCA still attached	58
Figure 60: Proximal fixation pin added proximally and exposed cancellous bone after femoral cuts have been made	59
Figure 61: Knee with implants inserted before and after suturing	59
Figure 62: Joint coordinate and cartesian coordinate systems relationship	61
Figure 63: Tibial tool positioning and orientation relationship.....	63
Figure 64: Flexion-extension angle measurement convention	65
Figure 65: Pre- and post-implant kinematic results for casted bone model tests	66
Figure 66: Difference comparison between pre- and post-implant results for casted bone model tests	67

Figure 67: Pre- and post-implant kinematic results for Labrador specimen.....	70
Figure 68: Difference comparison between pre- and post-implant results for Labrador specimen.....	71
Figure 69: Pre- and post-implant kinematic results for German Shepherd specimen.....	74
Figure 70: Difference comparison between pre- and post-implant results for German Shepherd specimen.....	75
Figure 71: Blender infographic map adapted from Giudansky [54]	91

List of tables

Table 1: Smoothing process parameters	26
Table 2: Proposed femoral cutting profile data	29
Table 3: Actual femoral cutting profile data.....	30
Table 4: Kinematic comparison between tests for pre-implant and post-implant casted bone models	68
Table 5: Pre- and post-implant correlation data for casted bone models	69
Table 6: Kinematic comparison between tests for pre-implant and post-implant Labrador specimen.....	72
Table 7: Pre- and post-implant correlation data for Labrador specimen.....	72
Table 8: Kinematic comparison between tests for pre-implant and post-implant German Shepherd specimen.....	76
Table 9: Pre- and post-implant correlation data for German Shepherd specimen	77

1 Introduction

1.1 Background

Canines often incur injury in the knee joint, which can mostly be treated by conservative means. When the pain or injury in the knee joint does not resolve after making use of rehabilitation or pain relief methods one has to look to total canine knee replacement in order to make such pain subside [1]. The pain experienced due to knee joint degradation can be so severe that the canine loses full mobility in the knee joint [2]. Some examples of knee joint degradation caused are due to knee arthritis, osteoarthritis, degenerative joint disease, cranial cruciate ligament rupture, abnormal development of the knee or trauma to the knee [3]. Total canine knee replacement may be a good option to consider, which involves removing the articulating surfaces of the knee joint and replacing it with full knee joint implants [4], [5]. A rest period after surgery is required, where movement should be monitored and kept to a minimum to ensure that the canine makes a full recovery without damaging or misaligning the implant in the initial stages of recovery. After such a time period the canine can slowly but surely increase activity of the leg as recovery time continues [3], [4], [6]. Total canine knee replacement is done to relieve the pain and restore some of the lost mobility due to injury, as close as possible to that of what the non-diseased natural knee joint would have had, so that the patient can experience as close to normal joint function as possible once again.

1.2 Motivation

There are a limited number of solutions available for canine knee replacements and the ones that are available are expensive [7]. These high costs have a clear buffering impact on the attainability and accessibility to this type of technology, especially in South Africa. Some costs need to be decreased, without impacting the quality of the product produced. This dramatically increases the relevance of looking towards open source software to fulfil the modelling and image processing needs of a user. If an open source design solution can be implemented for the entire design procedure, from start to finish, then a major step towards accessibility of a product such as this will have been taken.

1.3 Aim and objectives

The aim of this research is to generate a knee implant design, following a workflow which can be used to reproduce a patient specific solution of a similar outcome for another patient. The objectives were:

- To design a canine knee implant modelled after healthy knee joint geometry.
- To use open source software throughout in order to lower the overall cost of the design process.

- To implement a patient-specific implant with a kinematic performance level similar or close to that of healthy knee kinematics.

1.4 Outcomes

A canine knee implant modelled after healthy knee geometry was achieved for three different specimens. The femoral component was modelled after healthy canine articular surface geometry, whilst the tibial component was modelled after the complementary articular surface geometry of the generated femoral implant. Throughout the design process, open-source software was used, and a repeatable work-flow process was generated. Healthy knee kinematics were successfully compared with knee kinematics after implementation of a patient-specific implant, with promising results being achieved.

2 Literature review

2.1 Canine knee anatomy

The canine knee, otherwise known as the stifle, has some anatomical similarities to that of a human. The biggest observable difference between the two joints being that the fully extended position in humans and dogs differ significantly, with the extension position of a human being at about 0° and the extension position of a standing dog being at about 35° [8], differing depending on the dog breed. Carpenter et al. described a thorough review of the canine knee joint anatomy [9], with Figure 1 and Figure 2 assisting in the visualisation of anatomical descriptions discussed in this section.

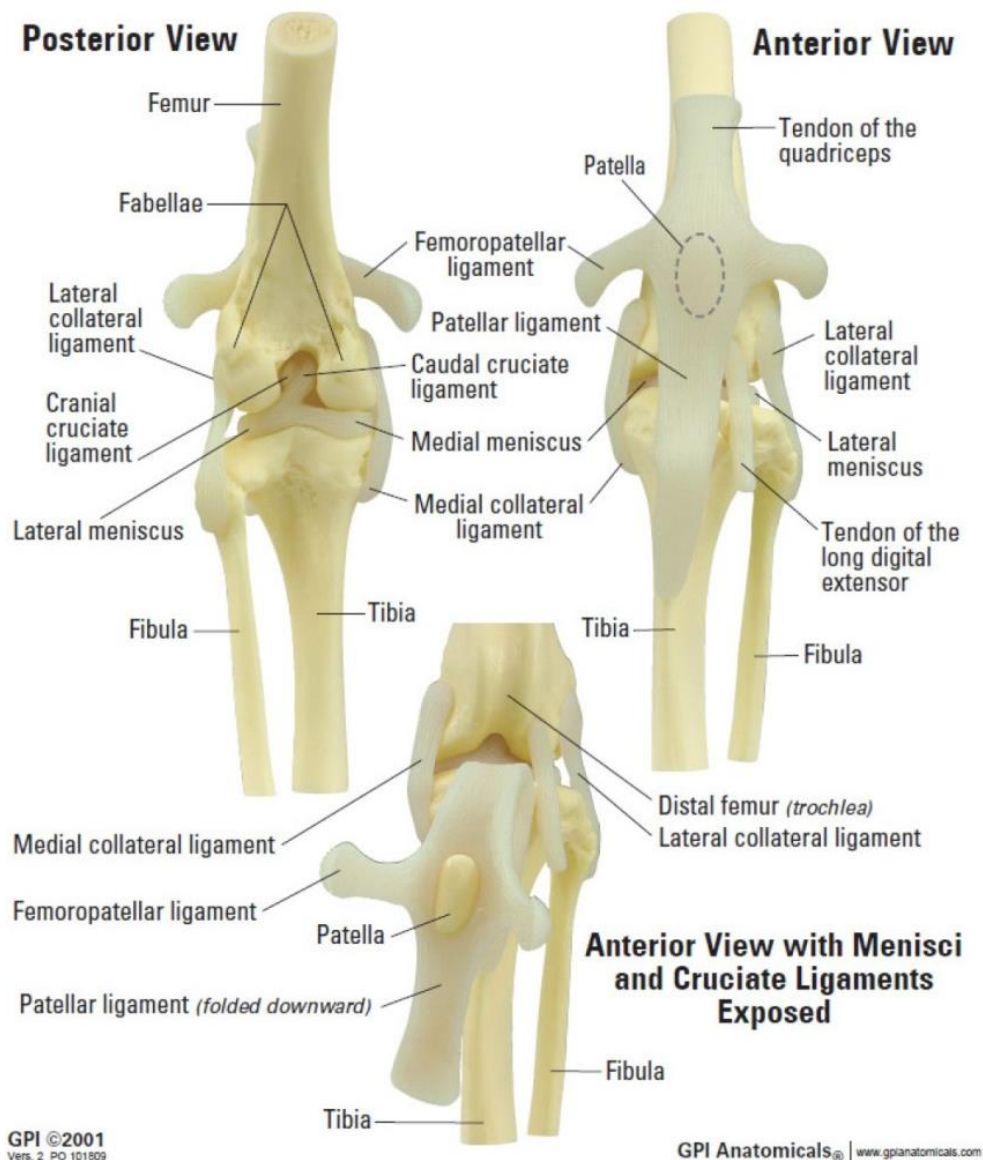


Figure 1: Canine Stifle (Knee) [10]

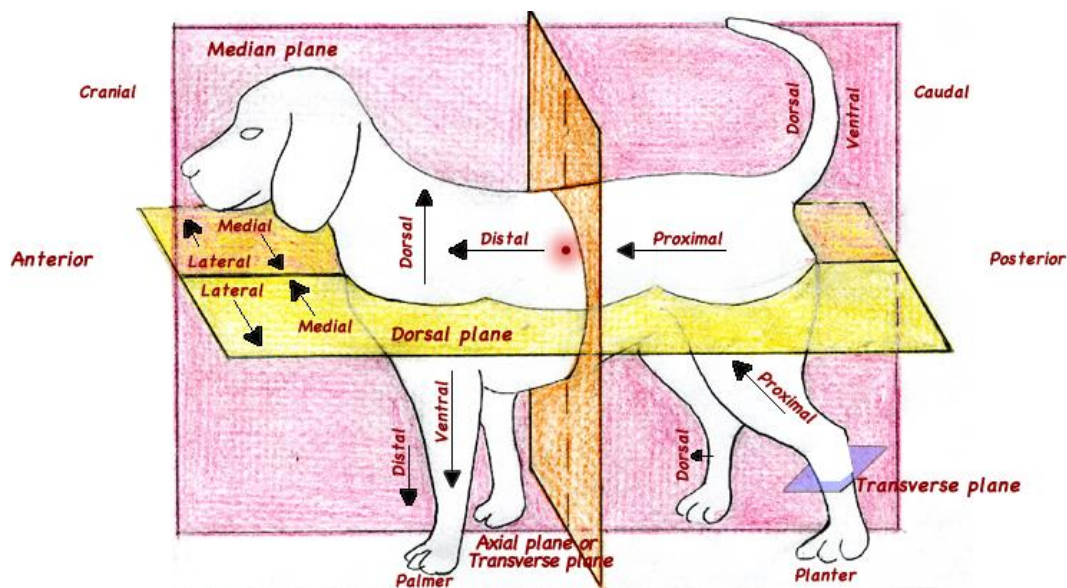


Figure 2: Canine anatomical views [11]

The canine knee joint consists of three major long bones and four sesamoids. The three long bones consist of the tibia, fibula and femur. The patella is the most notable of the sesamoids, with the medial, popliteal and lateral sesamoids making up the rest, which can also be referred to as fabellae. Fabellae may be present, displaced or completely absent, depending on the individual being studied. The femur forms three articulating surfaces, one with the patella, and two with the tibia, forming the patellofemoral and tibiofemoral articulations. A smooth groove at the cranial surface of the distal femur forms the trochlea. The patella has an ovoid shape, with the convex caudal surface of the patella articulating with the trochlear groove of the femur during joint motion. The trochlear groove ridges are continuous with the distally located femoral condyles, with the distally continuing trochlear groove separating the femoral condyles into medial and lateral. These femoral condyles articulate with the proximal tibial condyles, forming the tibiofemoral articulation. The medial and lateral condyles of the tibia are separated by two small ridges forming the intercondylar eminence.

The patella is held in place by the quadriceps tendon, femoropatellar ligaments and patellar ligament. The medial and lateral femoropatellar ligaments hold the patella firmly in place in the trochlear groove, keeping it from dislocating during joint motion. The patellar ligament is attached at the tibial tuberosity. The quadriceps tendon inserts proximally of the patella to form part of the quadriceps femoris muscle group, which forms a vital part of the flexion-extension motion of the knee joint, with extension being initiated with the activation of the quadriceps muscle group.

The proximal fibula is used as an insertion point for most of the distal lateral collateral ligament, with the proximal lateral collateral ligament insertion point being located at the lateral femoral epicondyle. The medial collateral ligament has insertion points located at the medial femoral epicondyle and the proximal medial region of the tibia. Menisci are located between the tibial and femoral condyles and

have a biconcave C-shape. There are two attachment points present for each meniscus, located on the proximal tibial plateau, with the lateral meniscus having one more attachment point located at the lateral surface of the medial femoral condyle. Functionally, cruciate ligaments consist of two bands each. The cranial cruciate ligament inserts at the proximal cranial intercondyloid tibial area and at the caudomedial aspect of lateral femoral condyle. The caudal cruciate ligament inserts at the medial aspect of the proximal tibia and at the proximal aspect on the lateral side of the medial femoral condyle.

The cranial cruciate ligament is the inner knee's main source of stability, assisted by the caudal cruciate ligament, lateral and medial collateral ligaments and the menisci. Most mediolateral (internal-external) rotation occurs in the flexed knee, as the collateral and cruciate ligaments are tensed more as extension occurs, preventing mobility in the joint. Lateral (external) rotation is especially resisted by the lateral collateral ligament, while medial rotation is especially resisted by the cruciate ligaments coiling around one another. The anterior cruciate ligament can have a significant impact on the anterior displacement of a joint. For stability to be maintained in a knee, the ligaments and musculotendinous stabilizing structures work together, making it difficult to assign a single role to each stabilizing component, as a modified hinge joint is created.

2.2 Knee kinematics

The generalized joint coordinate system for the knee, as described by Grood et al. [12], consists of three rotational axes, as seen in Figure 3. The first two axes are embedded into the bodies of which relational motion is to be described and the third axis is perpendicular to both the body fixed axes. This third axis is referred to as the floating axis, as it is not attached to any of the bodies of interest, moving only perpendicularly relative to the bodies. The nonorthogonal unit base vectors for the body fixed axes are described as \mathbf{e}_1 and \mathbf{e}_3 respectively, with \mathbf{e}_2 being described for the floating axis, where the positioning for the floating axis can be calculated by finding the cross product of the fixed body axes nonorthogonal base units. Three relative rotations occur about the three described axes, where the angular coordinates obtained can be seen as a general geometric version of Euler angles (α , β , γ). Relative translational positioning can be determined by calculating the translational vector components from one fixed body to the other, with each component lining up with one of the three described axes.

For application in the knee, a cartesian coordinate system describing the shape of each bone has to be created for the proximal tibia and the distal femur, relative to the joint coordinate system, with reference points used for translational description located at the origins of the cartesian coordinate systems, so that rotation and translation can be described that is clinically relevant with regards to tibial and femoral motion, as seen in Figure 4. The cartesian coordinate system axes for the tibia are denoted by x , y and z , along with \mathbf{i} , \mathbf{j} and \mathbf{k} describing the base vectors for each respective axis. The same denotation is used for the femur, but with capitalised letters, hence X , Y and Z , along with \mathbf{I} , \mathbf{J} and \mathbf{K} .

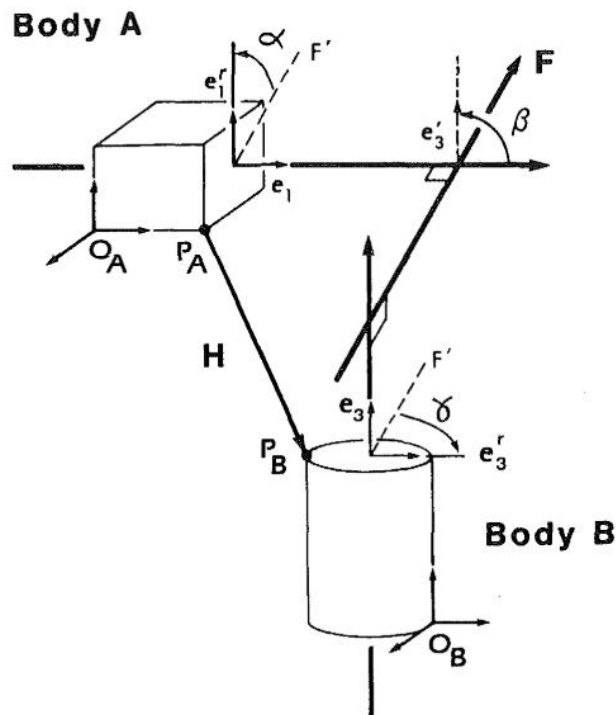


Figure 3: Joint coordinate system [12]

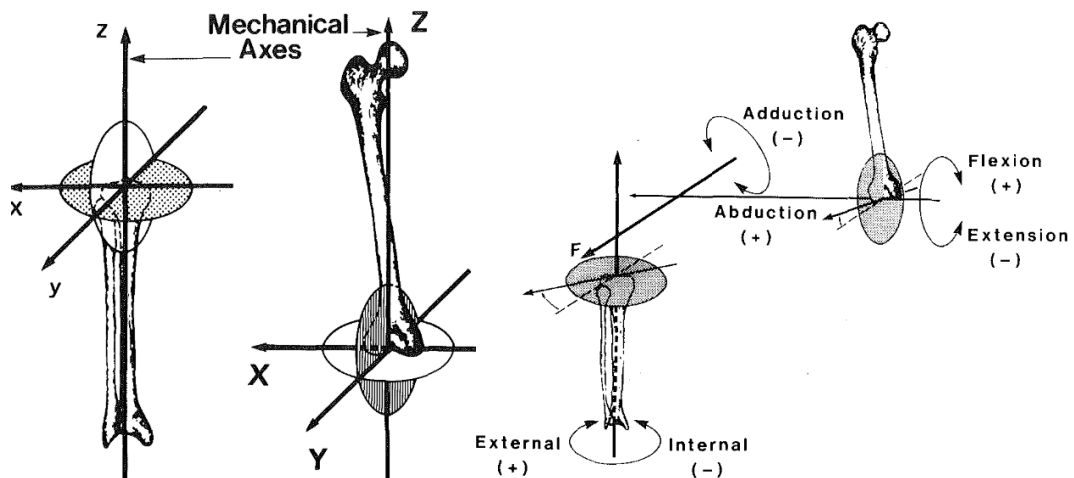


Figure 4: Cartesian coordinate system and joint angle definitions [12]

For the femur, the body fixed axis is chosen such that flexion-extension angular rotation occurs about it, which is done in the sagittal plane. The sagittal plane is similar to the median plane, with the exception that it can divide the body into medial and lateral parts at any point throughout the body and not exclusively in the middle, which is done in the midpoint of the knee for this case. In order to achieve this, the X-axis is chosen as the femoral fixed axis, being perpendicular to the sagittal plane, as displayed in Figure 4. The Z-axis of the femur is created by choosing an axis that flows from the proximal femoral head to the distal femoral

intercondylar groove, otherwise known as the mechanical axis of the femur. The Y-axis is perpendicular to the other specified axes. For the tibia, the body fixed axis is chosen so that internal-external rotation occurs, which is done about the tibial mechanical axis, denoted as the z-axis in Figure 4. This axis flows from the proximal tibial intercondylar eminence to the midpoint of the distal tibia. The y-axis is defined as positive in the anterior direction, with the x-axis being defined as positive to the right, hence being medially positive in a left knee and laterally positive in a right knee.

With this system in place the medically relevant rotational movements can be identified. Flexion-extension angular rotation occurs about the femoral fixed axis, with the internal-external angular rotation occurring about the tibial fixed axis. The final angular rotation of interest, adduction-abduction, occurs about the floating axis. The vector denoted by H describes the translational movement, taking place from the femoral origin to the tibial origin, as seen in Figure 5. The vector can be described by taking the nonorthogonal base vectors and combining them with translations, denoted as s . Taking medically relevant translations into account, one can describe a clinical translational term along each nonorthogonal base vector. Denoted by q_1 , mediolateral tibial shift can be described along the e_1 -axis. Denoted by q_2 , anterior-posterior drawer can be described along the e_2 -axis. Denoted by q_3 , distraction or compression of the joint can be described along the e_3 -axis.

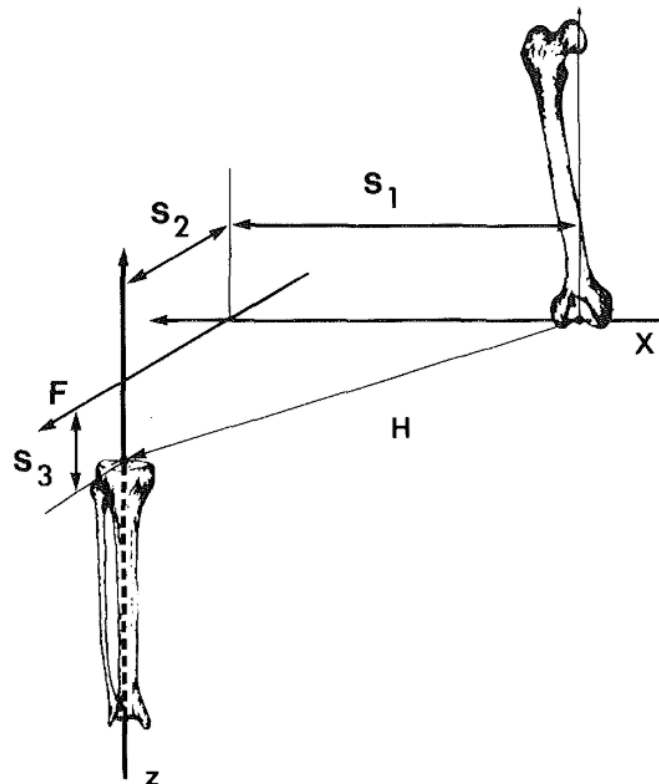


Figure 5: Joint translations [12]

2.3 Condition leading to total knee replacement (TKR)

The most prominent condition which leads to TKR is osteoarthritis [13]. Knee osteoarthritis is caused by joint tissues that break down due to inflammation or mechanical loading in the joints. Hence the joint articular cartilage erodes and osteophytes (bone spurs) form at the articular margins as the degenerative joint disease progresses, as displayed in Figure 6.

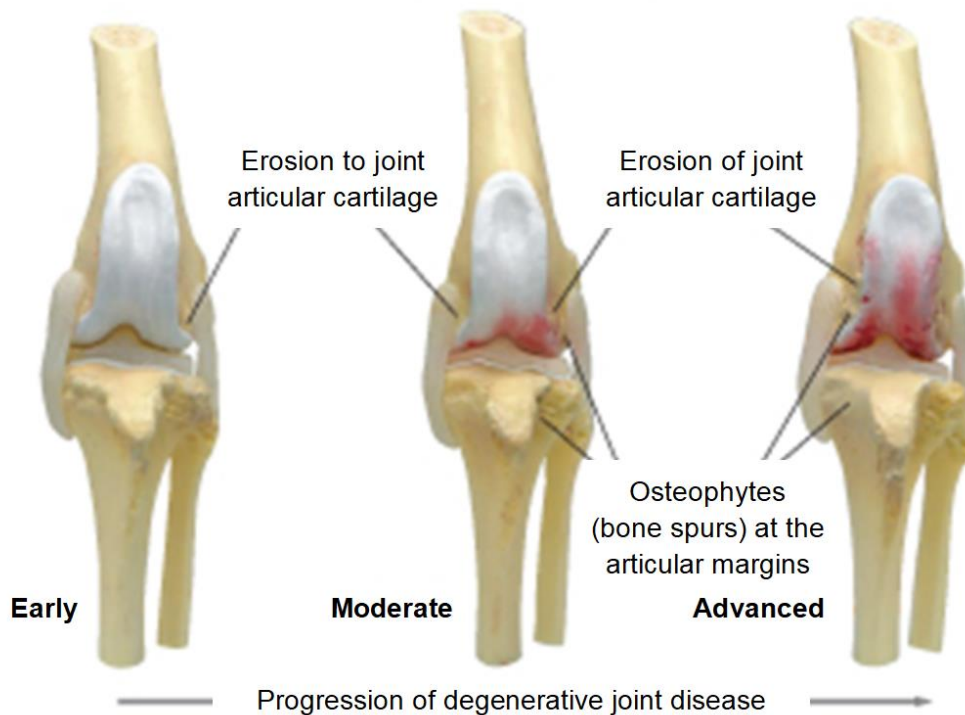


Figure 6: Progression of degenerative joint disease (osteoarthritis) [14]

There are a few risk factors which attribute to having osteoarthritis. Obesity can cause higher loading of the joint. Increasing age causes more wear and tear on the joint resulting in a higher likelihood of erosion occurring. Trauma and infection of the knee joint also increase the risk of having osteoarthritis. Depending on the stage of development of the osteoarthritis, this disease can lead to swelling, pain, deformity, stiffness, loss of function and creation of a grating sensation or sound between cartilage and bone or even the fractured parts of a bone otherwise known as crepitus [3]. If this disease has progressed too far to prevent or treat by conservative means then operative treatment is considered, resulting in either an arthroscopy, osteotomy or knee replacement surgery having to be done.

2.4 Total knee replacement

Total knee replacement or arthroplasty has been in development and received steadily growing interest for the past forty years. The first types of replacements to be tested in the early stages (1970's) of TKR development were hinged or unicompartmental. In 1971 a metal on plastic knee replacement was developed by Frank

Gunsten, and in 1973 John Insall designed a TKR which has become the prototype for modern TKR [15]. This prototype consisted of three components; resurfacing the patella, tibia and the femur. The current canine total knee replacements are based on the designs used on humans, however, current canine TKR's do not resurface the patella. Hence the canine TKR usually only consists of two components, the tibial and femoral components [8].

Total knee replacement surgeries are very common and successful with more than 860000 surgeries having been done on humans in 2017 in the United States of America alone [16]. Patient specific designed components, however, have not been implemented as widely as non-specific type products, despite some clinical benefits. This is due to multiple contributing factors such as the complexity in developing such implants and the skills required, as well as the challenges that come with multi-disciplinary communication and collaboration. The cost of this type of technology is also a big contributing factor, especially in developing countries such as South Africa. Modelling tools and image processing software that is used in the biomodelling industry can range anywhere from 20,000 USD to 50,000 USD. Machines that are used in the rapid prototyping industry range from 50,000 USD to 200,000 USD [7].

2.5 Design considerations of TKR implants

Materials used for the prosthesis of total canine knee implants are the same as those that have been seen to have good performance in humans as well. Materials suitable for implants have good biocompatibility, meaning that a material has a favourable reaction when in the presence of biological materials. This is usually characterised by good cytotoxicity levels and corrosion resistance. Further favourable properties of an implant biomaterial include a modulus of elasticity comparable to bone (18 GPa), high yield and compressive strength to prevent brittle fracture under cyclic loading, good hardness to decrease wear and good toughness to decrease the likelihood of implant fracturing [17]. The tibial component that forms part of the friction surface of the implanted joint in modern implants is made from ultra-high molecular weight polyethylene (UHMWPE). The component forming part of the frictional surface on the distal femur in modern implants is usually manufactured from a titanium alloy or cobalt-chromium [8].

In humans the tibial component for implantation usually has a metal baseplate attached to the underside, as this is reasoned to make the tibial component less susceptible to deformation when exerted to loads. The one-piece polyethylene (UHMWPE) component, however, also has a long and successful history in human TKR application [8]. With lighter loads expected in knee joints of dogs, it stands to reason that the UHMWPE component will also perform well in canine application with regards to performance and longevity of the tibial component.

There are currently two main commercial products available with regards to TKR for canines, manufactured by BioMedtrix and GenuSys (INNOPLANT Medizintechnik), displayed in Figure 7. The difference between these two commercial products lies in the tibial component, where the component manufactured by BioMedtrix is made entirely from UHMWPE, compared to the component manufactured by GenuSys which is also made from UHMWPE, but it

has a tray-like base plate made from a titanium nitride-coated cobalt chromium alloy [8]. No long-term data comparing these two products is available yet.



Figure 7: BioMedtrix (a)[4] and GenuSys (b)[18] total knee replacements

The goal of the designed components is to restore motion as close to normal as possible in the joint. When looking at the sagittal plane, which controls flexion and extension in the joint, the implanted BioMedtrix component curvature is made up of 2 radii for the femoral component. The lower radius is the smaller radius, which is derived by looking at the centre of rotation of the condyle of the femur, and the larger radius is based on the patellofemoral curvature of the joint. These two radii are combined to create the implanted femoral component curvature, creating a joint that is stable throughout movement in the sagittal plane, for flexion and extension. The groove of the implanted femoral component (trochlea) is usually very deep and symmetrical. This is done in order to lower the risk of patellar subluxation when movement in the sagittal plane takes place. The symmetry is ideal for manufacturing purposes, as the implant can then be used on both the left and right knee as required. Rotation of the knee in the dorsal plane is also controlled by the implants, with the BioMedtrix knee allowing for -15° to $+15^{\circ}$ knee rotation, in order to mimic natural movement as close as possible for the swing and stance phases. GenuSys has no data available in this regard [8].

In order to attain an effective canine TKR, the kinematic motion of a healthy stifle joint must be mimicked as close as possible. The main contributors to normal kinematic motion must be identified. This is done not only for successful implant design, but also to make knowledgeable decisions when it comes to cadaveric specimen preparation, so as not to remove or impact important parts contributing to knee joint kinematics. Amiri et al. [19], Pandit et al. [20] and Fitzpatrick et al. [21] identified that articular surface geometry had a big impact on kinematic knee joint motion. Amiri et al. found that the ligaments and articular contacts within the human knee capsule are the key to providing the characteristic kinematic motion of the knee during passive flexion, with the shape of the medial and lateral menisci encouraging and discouraging internal rotation respectively. Pandit et al.

conducted a study involving fifty-five human patients undergoing one of four different designed types of TKR to determine which effects could be seen affecting knee kinematics. It was determined that the main contributing factors to knee kinematic motion were the shape of the trochlear groove and patella, as well as the articular surface shape of the tibia and femur. Fitzpatrick et al. generated a statistical shape model of the patella-femoral knee joint in humans, as the articular surface shape geometry was considered to have a direct impact on knee function. In another study, Cottrell et al. established that surface geometry changes impact the contact patterns experienced in a human knee, hereby changing the kinematic motion experienced in the knee [22]. The biomechanics of the human knee joint were investigated by Mesfar et al. and a finite element model was generated of the femur, tibia and patella along with their respective articular cartilage layers and the patellar tendon. Additionally, models were created for the joint capsule ligaments, menisci and quadriceps muscle. Mesfar et al. found an increase in contact areas/forces for the patellar tendon, anterior cruciate ligament and the joint resistant moment, during quadriceps-induced extension. A decrease of the contact area/forces was observed during flexion, with the exception of the patellofemoral contact area/force, which increased during flexion [23]. Rong et al. showed that a mobile-bearing knee implant designed for a specific patient had better stress distribution than that of a hinged knee implant [24], encouraging a design approach that is patient-specific orientated.

These studies indicate that the joints articular surface shapes, joint ligaments and musculature surrounding the joint capsule are important determinant factors when considering knee joint kinematics. Implants should therefore mimic the articular surface shapes of the joint as close as possible for the specific patient, considering which ligaments might be lost during the surgical procedure and implementing a plausible design solution to counter that loss, in an attempt to restore optimal joint kinematics. During the preparation of knee specimens for testing, one should also consider that the knee joint capsule is the most important determining factor for kinematic analysis and therefore care should be taken in maintaining the structural integrity of the joint capsule, including the quadriceps muscle, which plays a significant role throughout the flexion-extension phase of the knee.

2.6 Current implant sizing methods

In order to do implant sizing, templates of different sized tibial and femoral implants can be superimposed either with a clear plastic acetate image over an X-ray image or similar radiograph image or it can be superimposed digitally. The primary views used for this type of component selection are the mediolateral (ML) view and the caudocranial (CaCr) view, as shown in Figure 8. Liska et al. made use of this method for the sizing procedure in their study [4].

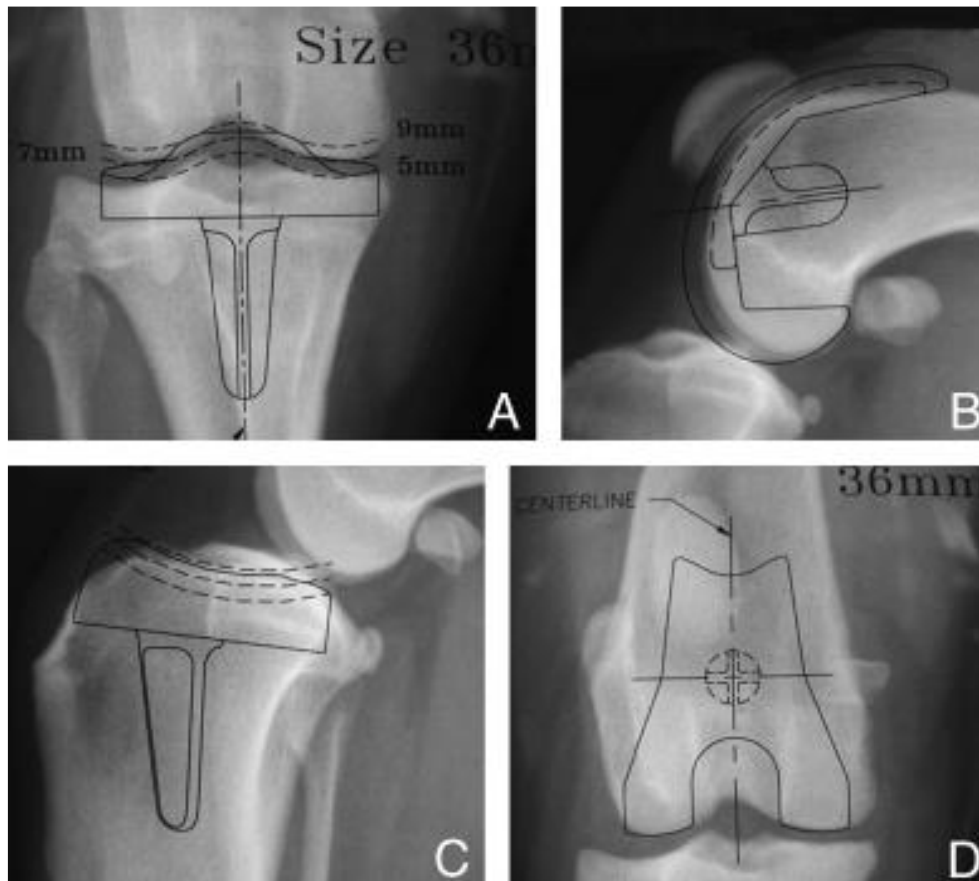


Figure 8: CaCr view of tibia in A. ML view of femur in B. ML view of tibia in C. CaCr view of femur in D [4]

For the tibial component of the implant, the CaCr view was primarily used to determine correct sizing. Lining up of the superimposed tibial template was done in such a way so that the fixation rod of the tibial component reached into the medullary canal. The lower surface of the tibial component was positioned so that cancellous bone would be present at the friction interface in order to promote bone ingrowth between the tibia and the tibial implant. The tibial template did not reach over the medial or lateral cortex, ensuring that the collateral ligaments are not affected. Different tibial thickness sizes can be seen which could be selected to make sure that the joint has the correct stiffness after implantation. This can be used as an additional guideline to check that the correct tibial component size was chosen.

For the femoral component of the implant, the ML view was primarily used to determine the correct sizing. First, the inside surfaces of the template, which are to become the cut surfaces of the distal femur, are positioned so that all four cut surfaces are on cancellous bone, once again to promote bone ingrowth. The external profile of the implant template is very close or a bit larger to the actual size of the distal femur, which is acceptable for sizing when viewing that part of the anatomy. There is no overhanging notch present with the placement of the implant template when looking at the cranial cortical bone, with the implant rounding

smoothly into the bone. This is important to note as a notch at this position could result in forces which add undesired extra stress on the bone or joint. The implant fixation rod is positioned so that it extends directly into cancellous bone and stops before it reaches past the caudal cortex. The CaCr view is used to make sure that the femoral implant template does not extend across the outer dimensions of the condyle.

2.7 Current tibial cut approach

Liska et al. detailed a very detailed surgical procedure for a canine TKR. The tibial cut is made before the femoral cut and there are a few important points to note for a successful tibial cut to be had. The cut to be made on the proximal tibia should be about 6mm deep and expose cancellous bone at a six degree angle when looking at the proximal tibial caudal slope. Figure 9 shows the tibial cut in A, with the cancellous bone exposure achieved in B and the removed proximal tibial piece in C. During this process the goal is not to injure any collateral ligaments, as these will help hold the implant in position. A Hohmann retractor is used to dislocate the knee in order to expose the knee for an easier tibial cut. The cutting blade then has an exit point at the caudal osteochondral junction. In order to achieve these goals an extramedullary tibial alignment guide (ETAG) is used, so that the cut can be made successfully on the aligned cutting block [4].



Figure 9: Tibial cut in A. Exposed cancellous bone of proximal tibia in B. Removed proximal tibial piece in C. [4]

To make this cut an ETAG is attached at the distal end of the tibia, being able to move caudally, cranially, laterally and medially, as the user requires, displayed in Figure 10. Two fixation points are used to attach the device at the distal end of the tibia. Once the cutting block is aligned at the correct location, the third fixation point can be used to attach the ETAG at the tibial tuberosity. An adjustment knob can be turned at the proximal end of the ETAG to make final adjustments of the cutting block, so as to ensure that correct alignment of the cutting surface is achieved.

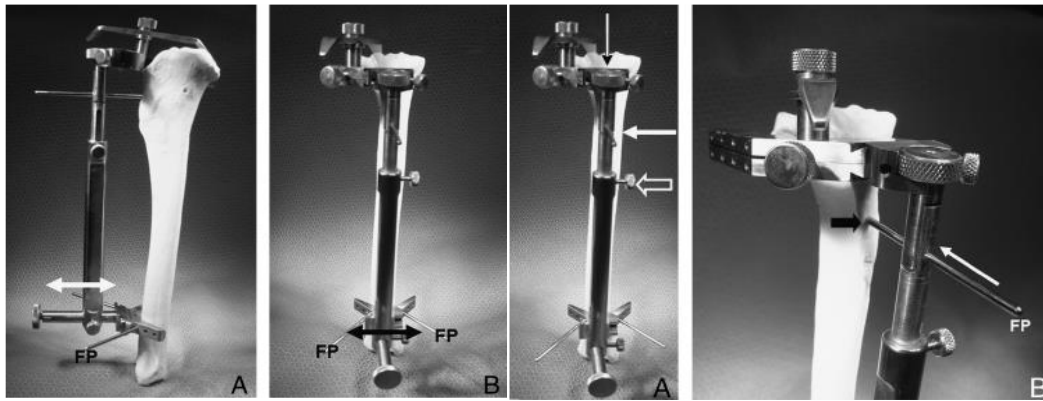


Figure 10: Medial and cranial views of the ETAG [4]

The cutting block has provisions for more fixation points, so that the cutting block can be secured more firmly as required. Cutting block alignment can be seen to be achieved at a six degree angle when looking at the proximal tibial caudal slope, as shown in Figure 11.

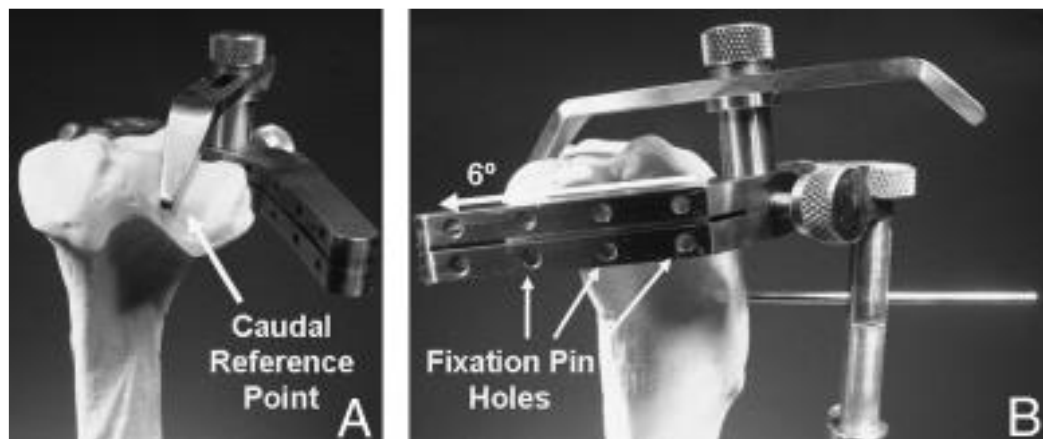


Figure 11: Aligned cutting block [4]

The tibial trial block is placed on the cut surface and alignment is checked, as shown in Figure 12. A hole is drilled 22 mm into the cancellous bone of the proximal tibia, with a diameter of 7 mm. Some further smaller holes (2 mm diameter) are also drilled into the cancellous bone of the proximal tibia. These holes are all made to assist with the attachment of the prostheses via cement, so that the cement has a larger surface area to attach to during fixation of the tibial prosthesis.

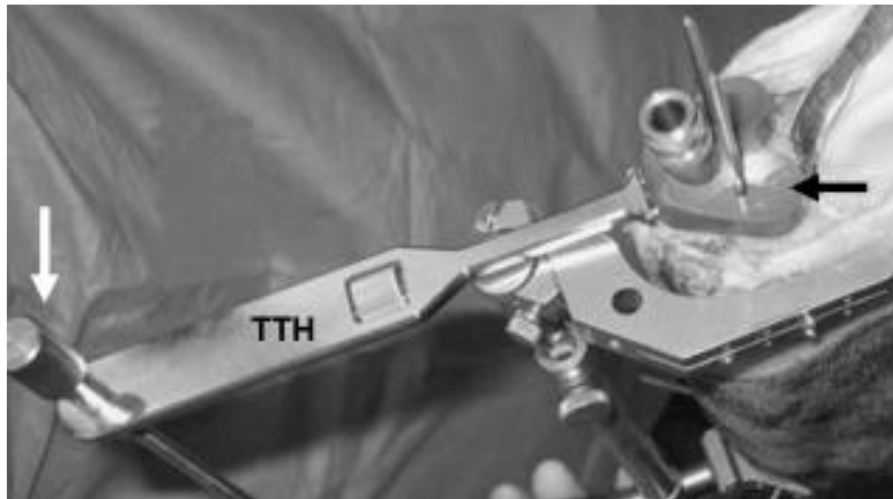


Figure 12: Tibial trial handle (TTH) used to align tibial trial block [4]

2.8 Current femoral cut approach

The femoral cut, as described by Liska et al., is made once the tibial cut has been completed. Traditionally there are four cuts to be made in a femoral cut for canines, always in the same order. First the cranial cut is made, then the caudal cut, followed by the distal cut and finally the cranial-distal cut, as displayed in Figure 13 [4].

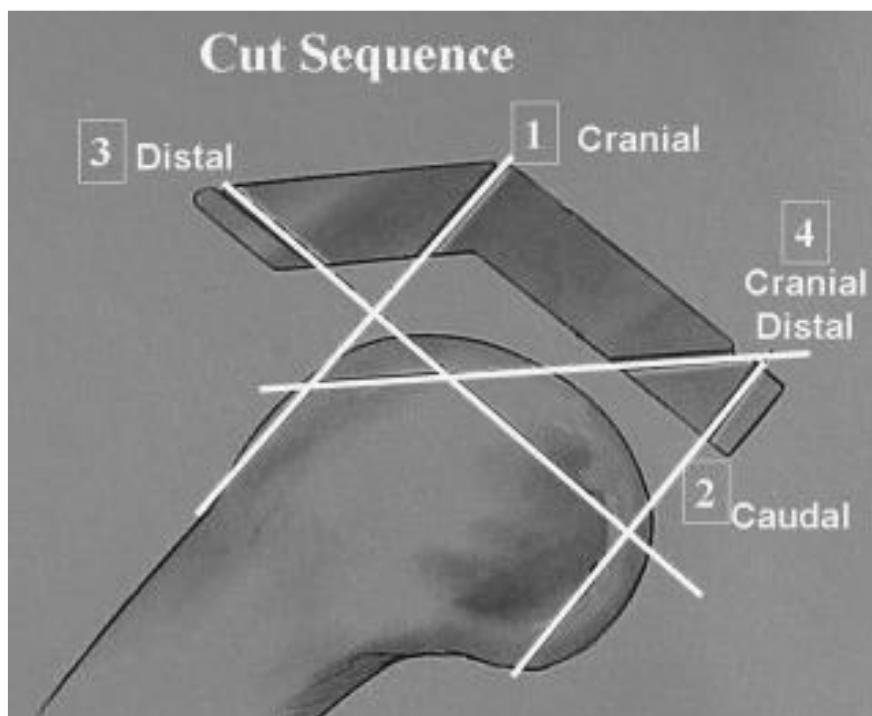


Figure 13: Femoral cut sequence [4]

The correct cutting block for the distal femur (FCB) needs to be chosen according to implant size, so that the correct cut can be made. There are at least three fixation pins holding the FCB in place, with the main fixation points being on the medial, lateral and cranial sides of the distal femur, as shown in Figure 14. Sometimes an incomplete cut can occur and in such a scenario it should be carefully completed once the FCB has been removed and done free hand in the same plain and direction as that of the original intended cut.

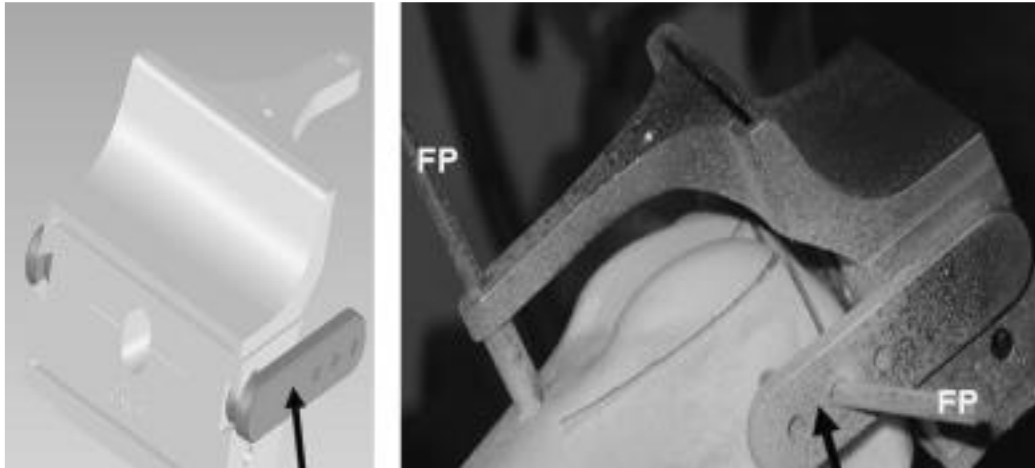


Figure 14: Model of FCB and fixed FCB [4]

A generated completed model was used by Liska et al. to make the sequential femoral cuts. The fixation pins were perfectly placed so that the cuts could be completed fully without any interference. The datum pin should also be noted, shown in Figure 15, as this was used if downsizing of a prosthesis was required, should the size cause the collateral ligaments to be excessively tight, resulting in loss of range of motion and mobility.

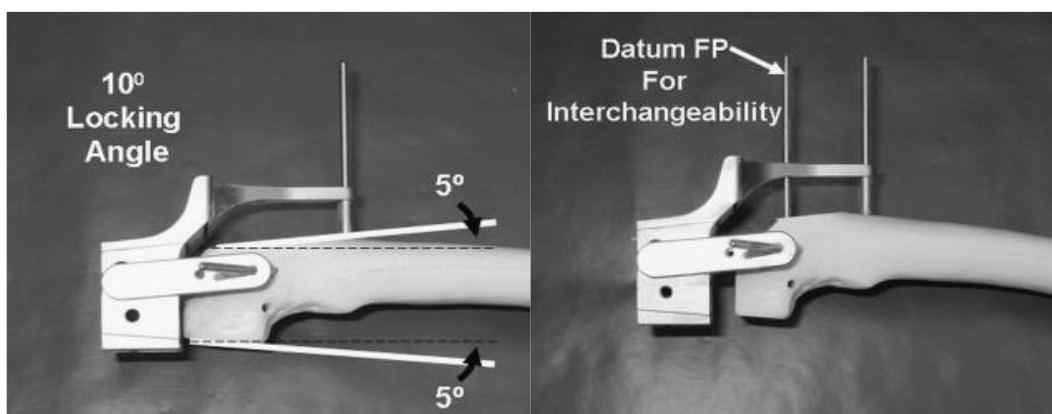


Figure 15: FCB model fixation & femoral cuts [4]

2.9 Trial reduction and downsizing method

Once the tibial and femoral cuts were completed, Liska et al. used trial implants to check that the sizing was correct. If the ligaments of a knee were too tight during flexion of the knee, downsizing needed to take place. This was done by using a femoral cutting block of one size smaller to that of the original cutting block used for the initial femoral cut. Once this was selected, it could be aligned with the datum hole which was made during the initial femoral cut and fixed into place on the bone. Only one cut must be made to downsize the implant in this method of implantation approach, shown in Figure 16. Once this cut was made, another trial implant could be used to check that the correctly sized implants were now being used. If the ligaments of the knee were not tight enough, a thicker tibial implant could be selected to ensure that the ligaments were tighter [4].

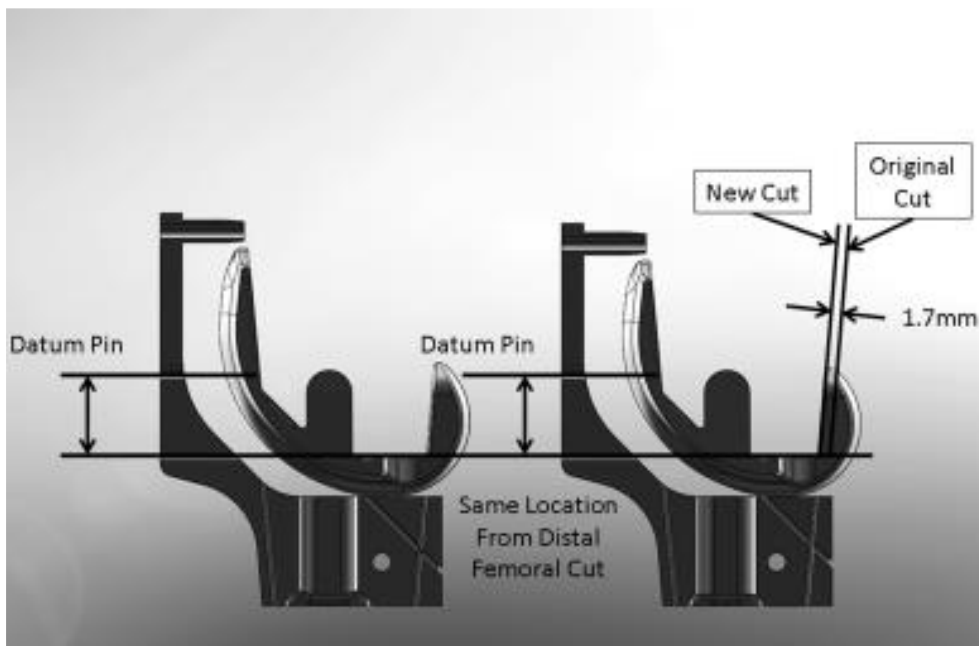


Figure 16: FCB and femoral implant with datum pin shown [4]

2.10 Current implantation method

Having selected the correct size implant, the trial femoral component was used by Liska et al. to drill the hole in the trochlear groove in which the femoral implant's fixation pin was inserted, as displayed in Figure 17. Once this was done the cancellous bone surface had to be cleaned and readied for implantation. The tibial implantation surface area is prepared with cement (for a cemented tibial implant) and the tibial implant is placed accurately and pressed into position using a tibial impactor. Once enough force has been exerted and the implant is pressed in place, the tibial impactor can be removed. The cement that gets pressed out from underneath the implant must be cleaned up before it hardens. The femoral implant is pressed into place next, making use of a femoral impactor. Should cement be used in the femoral implant, the excess cement also must be cleaned up before it hardens.



Figure 17: Femoral trial component for drilling [4]

2.11 Design modelling

There are a multitude of software programs to choose from when implementation of a design orientated solution is needed. In order to make a design procedure accessible to everybody however, one must look towards open-source software. Chosen free-to-use tools should be capable of being used in conjunction with one another to create a design process from start to finish.

3DSlicer (v4.9.0) is an open-source software platform which can convert geometry data into three-dimensional computer models, process images and be used as a medical tool to gain image information. It is a free to use program that allows anyone to use effective cross-platform processing tools. It has been effectively used in research as a reconstruction tool for bones in a hand and to segment endo-sinus bones. [25], [26]

Meshlab (2016.12) is another open-source software system which can be used to re-mesh, edit, render, smooth, clean and convert an existing 3D triangular mesh. It can process unprocessed data produced from a different program, such as 3DSlicer (4.9.0), and get an existing model ready for 3D printing purposes. It is also useful tool in validating the correctness of a smoothed or cleaned model when compared to that of the original unprocessed mesh model. [27]–[29]

Blender (v2.79) is a very powerful open-source software tool which can be used for an array of things found in the three-dimensional computer aided design pipeline, such as modelling, rendering, simulation, compositing, designing and motion tracking. It is traditionally used for motion animation production purposes; however, it has all the fundamentals to be an effective computer aided design (CAD) software as well [30].

3 Implant Design

3.1 Overview

In order to acquire a patient specific canine knee implant solution, several steps had to be followed. Taking the high cost of design software and patient specific implants into account, the decision was made to create a design process that was entirely reliant on open-source software, so that any person would be able to follow these steps in order to create a design that would be plausible for implantation purposes. Figure 18 outlines an overview of the steps required in the proof of concept design process of the implant components.

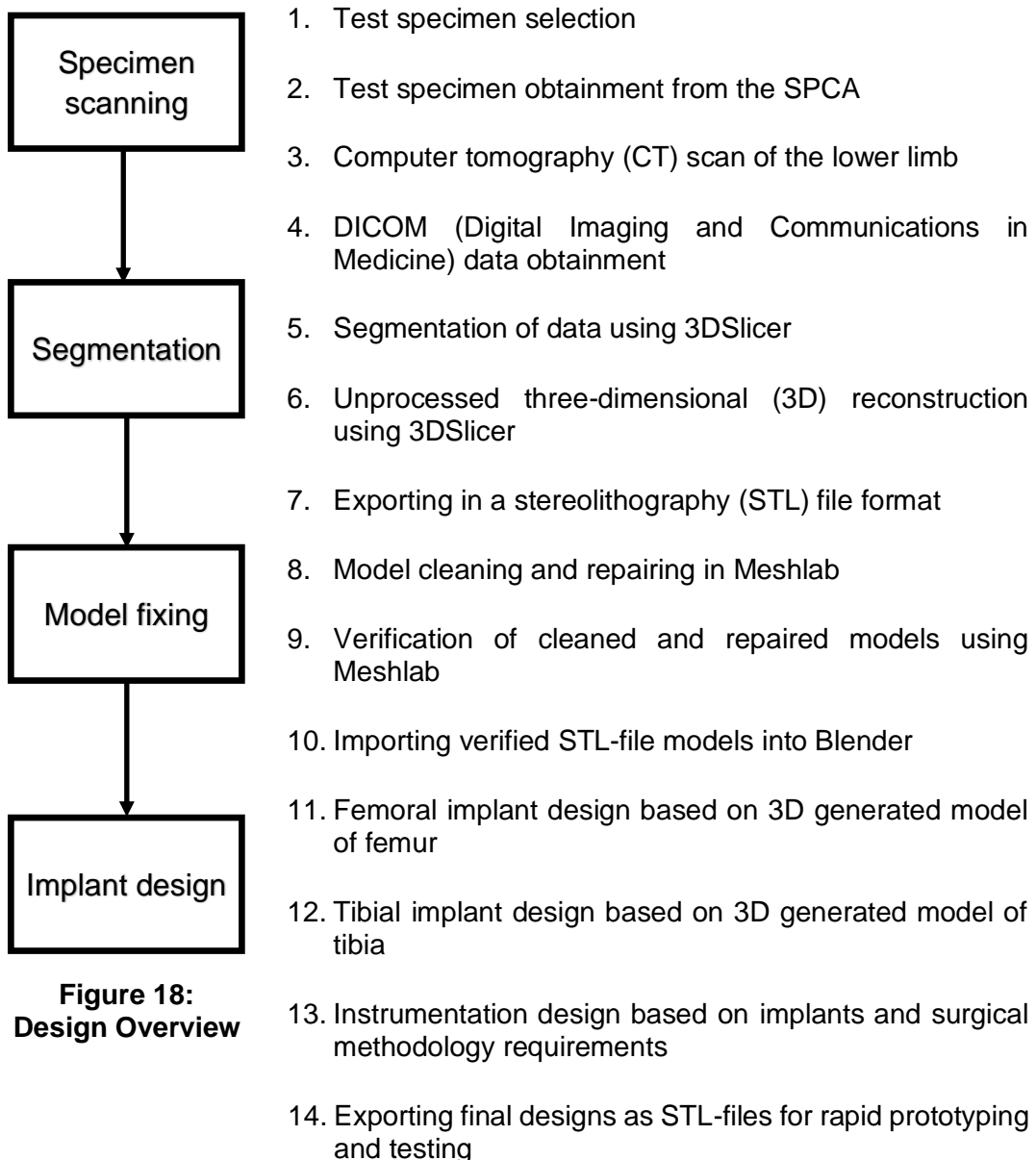


**Figure 18:
Design Overview**

Prototypes could be created for testing, and verification of the designed models and workflow steps to generate the implant components.

3.2 Functional requirements of design

The main objective of this implant is to mimic or restore kinematic mobility as close as possible to that of the original healthy knee, with as little compromise as possible, especially in the flexion-extension phase of the knee. This motion is affected most by health issues in canines needing this type of surgical procedure. The design of the implants should also take the surgical procedure into account, making ease of insertion of the implants a priority. Sizing of the implant should be done as closely as possible to that of the original knee, to avoid any tissue damage and excessive ligament laxity or tightness, which could further impact the range of motion gained. Surface interfaces where the implants are joined to the bone after surgical cuts have been made, should be where cancellous bone is present, to promote bone ingrowth and subsequently improve recovery time.

3.3 Selection of canines

Knee health problems can be present in all sizes and breeds of canines due to a range of health issues such as having had a traumatic injury or osteoarthritis in the knee joint. Larger breeds of dogs must bear larger loads in the load bearing joints, resulting in more wear and tear. Due to this there is a higher risk of developing pain, injury and loss of mobility. Therefore, larger breeds are considered as the primary patients for which full knee replacements could be needed. Specimens with good knee health were required, so that one could compare the range of mobility before and after implant insertion. The specimens had to be selected taking these considerations into account.

Ethical clearance for the use of animal tissue in this research was approved by the local research ethics committee for animal care and use (ACU-2019-9396). Selection was done with the help of the Grassy Park SPCA and Cottage Vet Clinic. A fully-grown bull terrier, a 25 kg Labrador-cross and a fully-grown German Shepherd were selected as suitable specimens for research. The Labrador-cross and German Shepherd specimens were used for cadaveric tests as well as concept generation purposes, with the bull terrier specimen being used for concept generation purposes only. Only the hind limbs were removed for testing, during this research, as the research focus was on the kinematics of the canine knee located in the hind limb.

3.4 CT scans

Designing an implant requires surface geometry data of the bone being replaced, making the acquisition of CT scans the first step in the design process. CT scanning makes use of X-rays, which is especially useful in identifying bone tissue in the body, making it a commonly used tool in the medical field to identify orthopaedic related problems or injuries. A circular system is used in a CT scanner, where ceramic scintillators emit an automated X-ray dose from one direction and receives it from the other direction. Automated radiation levels, depending on the

specimen, are emitted about the ceramic scintillators as the patient is slowly moved through the circular scanning area until the entire region of interest is scanned in a constant helical fashion. The data is then converted into a series of two-dimensional images.

CT scans were obtained at the Winelands Radiology, Mediclinic Stellenbosch. The removed hind limbs were placed flat on the scanning bed when referring to the median plane, being fed into the scanner starting at the proximal end of the femur and finishing at the distal end of the hind limb, as shown in Figure 19. Scanned images were obtained in 1 mm slices at a 0° gantry tilt. Using the workstation of the CT scanner, the data was written onto a CD in a DICOM image file format. This file format is widely used in the medical industry, containing patient and CT scan information, such as bed positioning, for each image.



Figure 19: CT scan specimen positioning

3.5 Segmentation and 3D reconstruction using 3DSlicer

The canine CT scan data was imported into 3DSlicer to start the process of unprocessed 3D model reconstruction, by raising the DICOM module for loading DICOM datasets and selecting and loading the relevant data series into the 2D

viewing windows. The 3DSlicer software picks up the bed positioning for each image and rearranges the images so that a uniform sequential image data set is created. The data was then displayed in three windows showing the axial, coronal and sagittal views. The exposure and frequency values were adjusted for these views until the desired image quality was achieved, as shown in Figure 20. The resulting grey scale image should have bone displayed as white and empty space as black for ease of navigation.

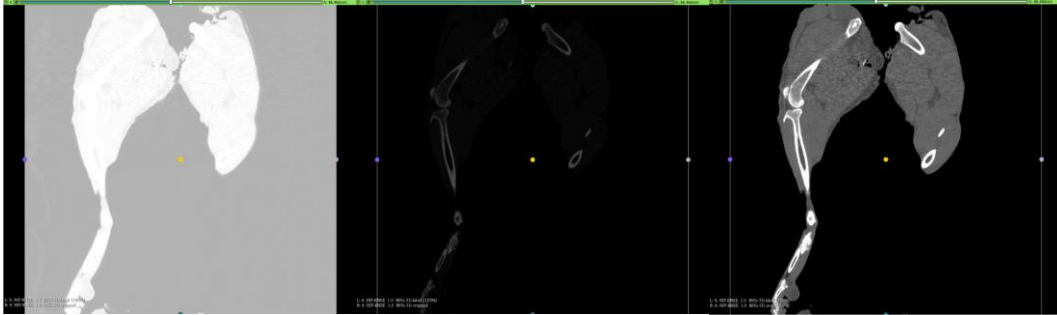


Figure 20: CT scan image exposure adjustments

Region of interest parameters were displayed so that manual cropping of the images could be done. Only the desired region of interest could be displayed in this way. This was done in order to minimise the amount of data analysed and displayed on screen, hereby decreasing the amount of computation time required for the software to respond to given commands.

Segmentation of the selected master volume was performed next. Generic anatomical colours were selected as the colour table node to be used for the segmentation labels. The paint effect was selected in which threshold paint was enabled. The basic principle behind this effect is to use the correct frequency range to separate the bone from the surrounding soft tissue. It is important to make the correct threshold selection, as this will have an impact on the area of interest to be highlighted. Hounsfield units are used to display frequency, where the frequency range can be selected as anywhere from -1024 to 2884. It should be noted that the typical soft tissue range of grey value for canines is from -74 to 226, whereas the typical bone range of grey values for canines is from 226 to 2766 [31]. Threshold painting could be performed for every 1 mm image segment, making sure to select only the relevant information, starting at the distal end of the tibia and ending at the proximal end of the femur. The threshold paint frequency range and radius of the paint brush could be manually adjusted to make sure that no soft tissue was selected or to paint precise regions where bone pieces were very close together, making sure to keep them separate throughout the process, as in the physical leg.

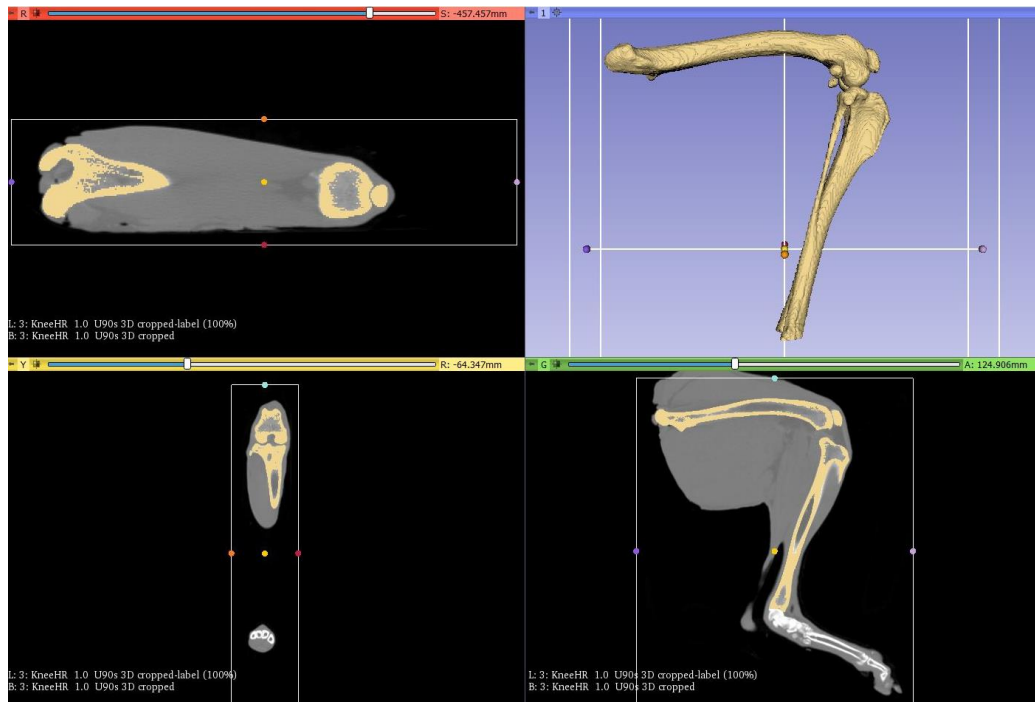


Figure 21: 3DSlicer generated 3D model from selected label map volumes

A 3D model of the resulting label map volume was created, as shown in Figure 21. This model could be used to verify the final smoothed model created, making sure that no excessive shrinkage or shape distortion took place during the cleaning and smoothing process. This 3D model generation process was followed for each bone segment of interest, which in this case were the femoral, tibial, fibular and patellar bone segments. The models of interest were exported as STL files, which is a common file type used in the rapid-prototyping industry and is supported by most 3D printer software. A STL file is a mesh or a faceted surface representation representing a solid computer model, where a watertight mesh is ideally generated. A segmentation protocol of the method described above can be found in Appendix A.

3.6 Smoothing procedure using Meshlab

Meshlab was used as the tool for the next step in the design generation process to process and edit the unstructured 3D meshes that were generated in 3DSlicer. In order to get an anatomically correct geometrical shape model on which implant designs can be based, one must clean, repair, remesh and smooth the unprocessed model. A smoothing protocol developed for the human knee was used as a guide for this step [32], with the full protocol used in this research described in Appendix B. An overview of the process is as follows:

1. Load the unprocessed STL file into Meshlab.
2. Perform volume preserving smoothing and remeshing.

3. Check and repair the mesh constantly throughout as required.
4. Perform paired mesh distance mapping to ensure volumetric retention and geometric shape similarities between the original and smoothed mesh.
5. Export the STL file.
6. Repeat the process for every generated model of interest.

Performing volume preserving smoothing is a vital step in the design process and it follows the same list of steps each time it is done. It can be called the LSTIT smoothing process. This acronym is taken from the five main steps taken during the smoothing process: Laplacian smoothing, Surface Reconstruction, Taubin smoothing, Isometric Parametrization and Taubin smoothing once again. Cleaning and repairing of the mesh should be done repeatedly throughout the process as required. Each step was performed and applied in the same described order to each unprocessed 3D generated model.

Laplacian smoothing is a type of additive smoothing algorithm used to assign a new vertex position for each vertex based on local vertex positioning information, with the newly generated vertex lying almost on the original surface. Considering a triangulated surface, Laplacian smoothing can be described mathematically as follows [33]. For a local vertex point, P , the umbrella-operator vector can be defined as shown in Equation 3.6.1, where w_i are positive weights. A geometric visualisation of the umbrella operator is displayed in Figure 22. The local update rule for each inner vertex of a triangulated surface is described by Equation 3.6.2. Hence the Laplacian smoothing operation has a tendency to flatten and reduce the high frequency of a surface. An example of the Laplacian smoothing step, that was implemented during the design process, can be seen in Figure 23.

$$U(P) = (1/\sum_i w_i) \sum_i w_i Q_i - P \quad (3.6.1)$$

$$P_{new} \leftarrow P_{old} + \lambda U(P_{old}) \quad (3.6.2)$$

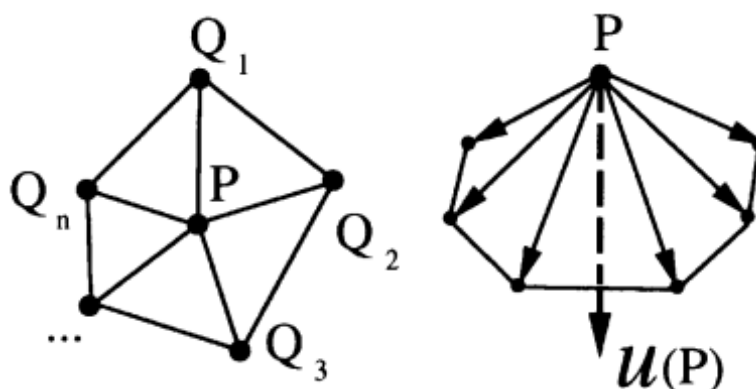


Figure 22: Geometric visualisation of umbrella operator

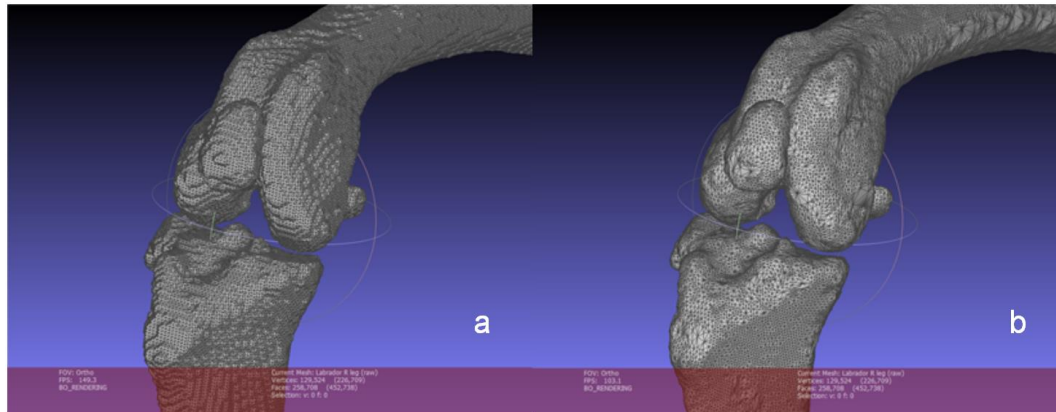


Figure 23: Mesh components before (a) and after (b) Laplacian smoothing

Surface reconstruction is an approach implemented to build a volumetric distance field of a mesh, so that a cleaner mesh is achieved, with local vertex distances that are more constant throughout the mesh. An example of the performed surface reconstruction can be seen in Figure 24. Isometric parametrization builds an abstract domain mesh representing the isoparametrization of a watertight two-dimensional manifold triangular mesh. Remeshing of the input mesh then takes place by making use of the generated abstract mesh. In other words, this filter creates a rough surface triangulation that can be projected onto the new mesh without much distortion from the original mesh. Lastly, repeated subdivision of the triangulated surface is implemented.

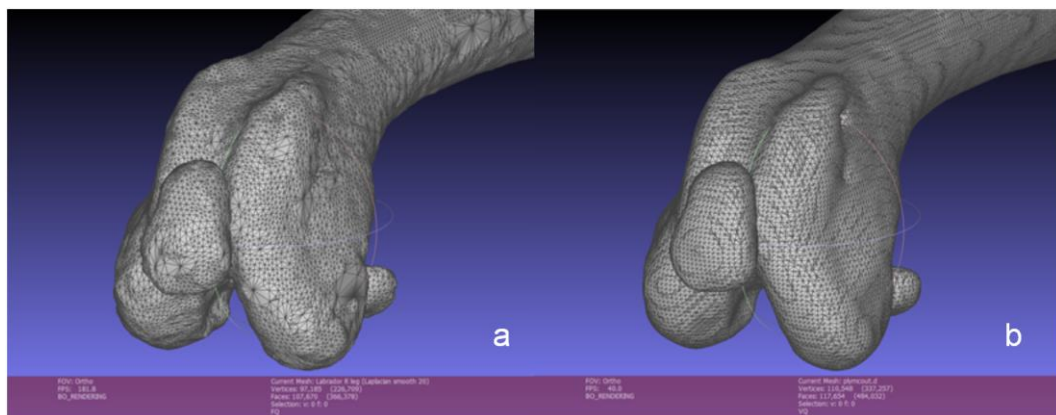


Figure 24: Mesh before (a) and after (b) surface reconstruction

The Taubin smoothing filter is especially useful in smoothing over any sharp edges on a mesh. It is a volume preserving smoothing method for fair surface design, utilizing two steps of smoothing, back and forth, for each iteration. Lower frequencies of the umbrella operator, described in Equation 3.6.1, are enhanced and preserved, while the higher frequencies are suppressed. The Taubin smoothing local update rule for each inner vertex of a triangulated surface is described by Equation 3.6.3, where μ and λ are implemented weighting factors [33].

$$P_{new} \leftarrow (1 - \mu U)(1 + \lambda U)P_{old} \quad , \mu > 0, \lambda > 0 \quad (3.6.3)$$

Taubin smoothing was applied twice, as previously described, to finish the smoothing process. The final Taubin smoothing step corrects any twisted triangles, should any have been created in the previous remeshing step. The parameters used for all smoothing steps can be found in Table 1. The same order of smoothing steps was followed every time.

Table 1: Smoothing process parameters

	Laplacian smoothing steps	VCG surface reconstruction voxel side value	Taubin smoothing λ and μ values	Iso parametrization sampling rate	Taubin smoothing λ and μ values
Femur	20	0.7	0.5, -0.53	10	0.5, -0.53
Tibia	20	0.7	0.5, -0.53	10	0.5, -0.53
Patella	20	0.5	0.5, -0.53	7	0.5, -0.53
Fibula	20	0.5	0.5, -0.53	5	0.5, -0.53

Having created a smoothed mesh, one must verify that the smoothed mesh matches the original mesh as close as possible to be valid. Paired mesh distance mapping was used for this step, more specifically the Hausdorff distance method. This method computes the distance between two meshes, where a vertex point from one mesh is chosen and the closest possible vertex point from the other mesh is used to calculate the distance between the two mesh surfaces [34]. This method was used to determine how similar the unprocessed and smoothed meshes of generated bone models were to one another. A vertex quality histogram was generated along with a projected distance map, where the vertex quality histogram described the maximum distance frequency for each compared point along with the colour code designating of the displayed distance. Figure 25 displays a vertex quality histogram and distance map that was generated for the right femur of a Labrador, showing that more than 95% of the smoothed mesh surface was within 0.3 mm of the original unprocessed surface mesh to which it was compared. This was considered to be a satisfactory result. Once it was ascertained that the volumetric integrity of the smoothed surface mesh was maintained from the original unprocessed surface mesh, the mesh could be exported as an STL file. This procedure was repeated for every model to be used in the design process. An example of a unprocessed surface mesh compared to the generated smooth surface mesh of a labrador femur can be seen in Figure 26.

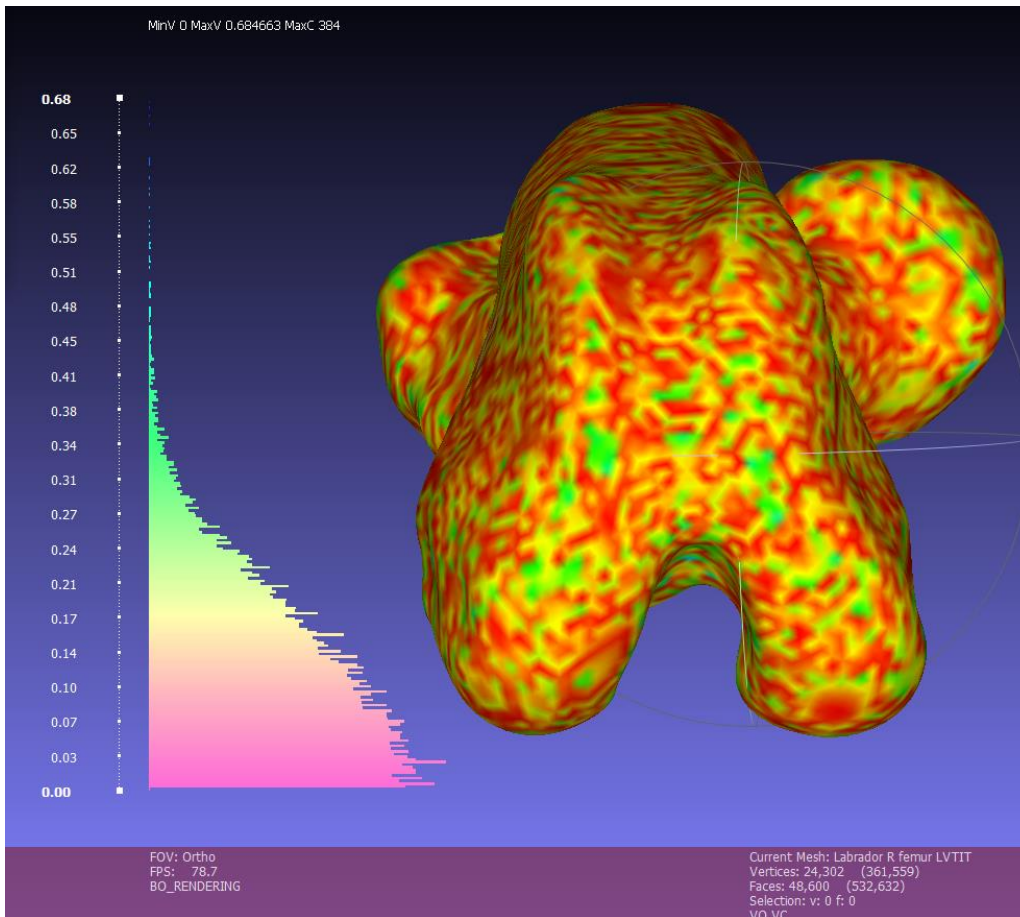


Figure 25: Vertex quality histogram and distance map for Labrador femur

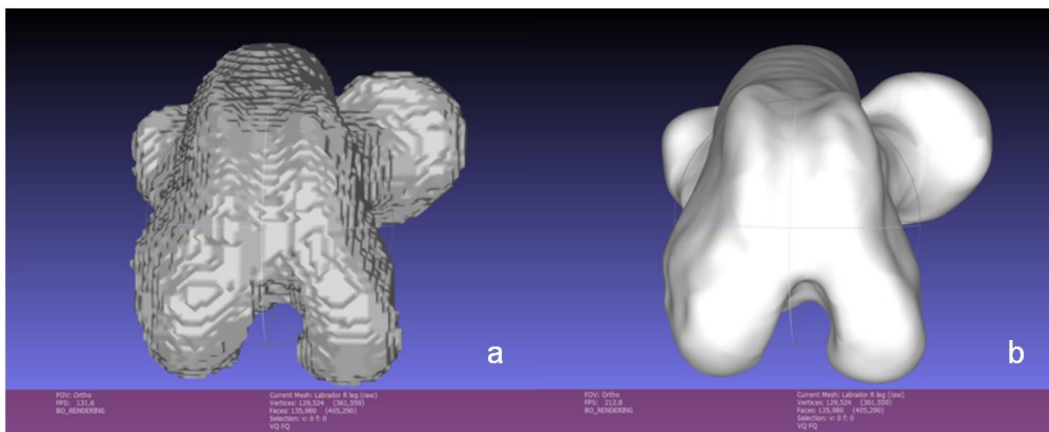


Figure 26: Femur before (a) and after (b) smoothing protocol

3.7 Design using Blender

3.7.1 Overview

Most research in the field of knee implant design has been done with humans in mind. Many of the design attributes implemented in the human knee replacement can be used in the design process of the canine implant. However, there are fundamental differences that make the implementation of current human implant knee design unsuitable for the canine knee. The most notable difference is the fact that only four cutting surfaces are required for a canine femoral implant, compared to the five cutting surfaces seen in a human femoral implant [4], [8]. This is because the canine patellofemoral groove is much longer than the condylar width of the distal femur when compared to the same relationship in humans, hence making the fifth cutting surface unnecessary. The patellofemoral groove of a canine implant would also have to be longer when compared to that of its human counterparts, to keep the probability of patellar subluxation low, as the hyperextension of the knee is a very common problem in canines. The direction of the fixation pin, however, should mimic the results found in humans, meaning that the fixation pin should be in parallel with the mechanical axis of the joint to promote bone ingrowth in the correct direction. Surface shape geometry design will have the greatest impact on restoring movement to a patient as close as possible to that of its natural healthy state. By mimicking the natural articular shape of the joint, optimal joint kinematics can be achieved.

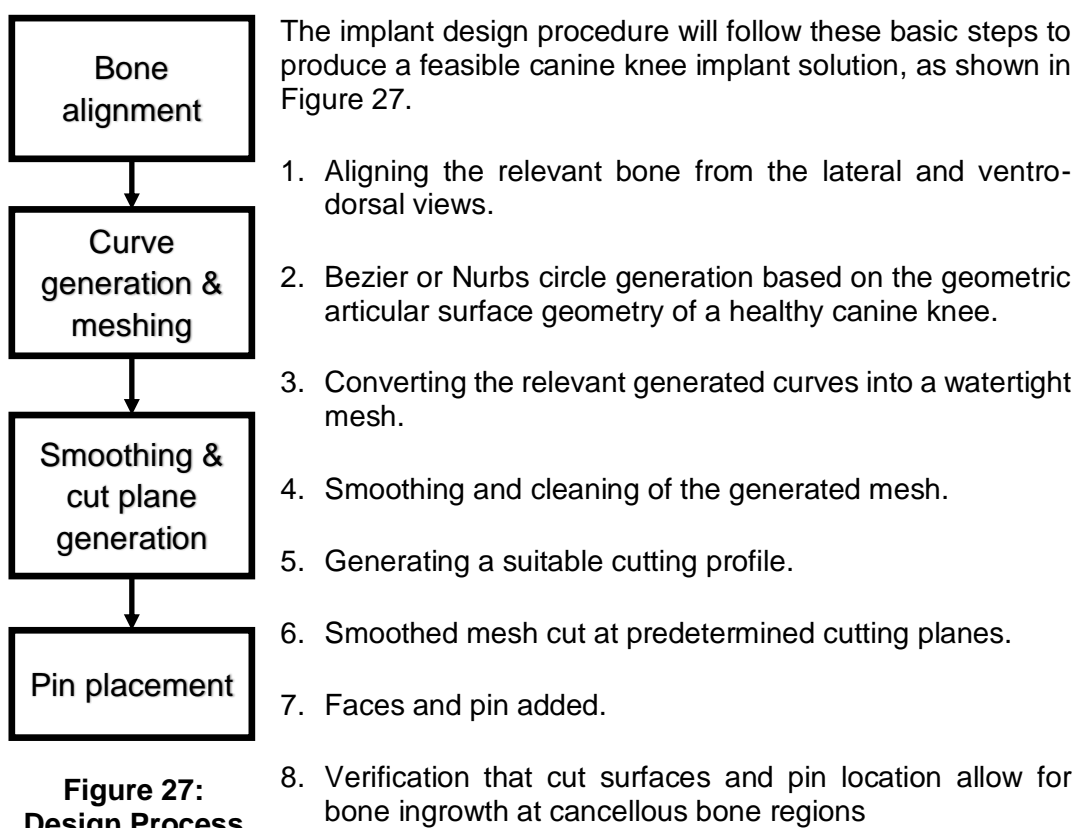


Figure 27:
Design Process

It should be noted that the design steps taken for the tibial and femoral components of the implant are somewhat different, and that the design process overview is only a simplified summary of the process to garner better initial understanding. Blender was chosen as the open-source tool to take on the task of computer aided design. It is unlike traditional CAD software used in the Engineering industry today, in that it is mainly structured towards use for animation purposes, with many of the basic commands different to that of traditional design software. Nevertheless, it has all the fundamentals to be an effective CAD software as well. A Blender infographic map is shown in Appendix C.

3.7.2 Cutting plane selection

There is no cutting profile data available for the femoral implant in canines, hence data from humans was considered in order to get an estimation of what a canine implant could look like. Taking the biological differences of the distal femoral shape geometry between humans and canines into account, and using data acquired from a study looking at the comparisons between different manufactured femoral implants in industry for a human [31], a proposed cutting profile could be created, as shown in Table 2. Referring to Figure 28, cuts 'a' and 'b' took the longer patellofemoral groove of the canine into account. The angular difference between cuts 'a' and 'd' was increased to a difference of ten degrees, to ensure that no undercutting could occur, as well as to improve the ease of insertion of the component for the surgeon, as the smaller size of the canine can make surgery quite difficult. Total cut length was obtained by the summation of 'a' to 'e' or 'a' to 'd' values for the human and canine data respectively, hence each cut length percentage could be obtained by calculating the percentage contribution of each cut to the total length of the cutting profile. For canines, 'a' represents the cranial cut, 'b' the cranial distal cut, 'c' the distal cut and 'd' the caudal cut.

Table 2: Proposed femoral cutting profile data

Cutting face	Average human cut angle from literature [31]	Average human cut length percentage compared to total cut length from literature [31]	Proposed canine cut angle	Proposed canine cut length percentage compared to total cut length
a	95°	27%	97°	31%
b	130°	19%	130°	21%
c	0°	23%	0°	28%
d	136°	13%	93°	20%
e	88°	18%	N/A	N/A

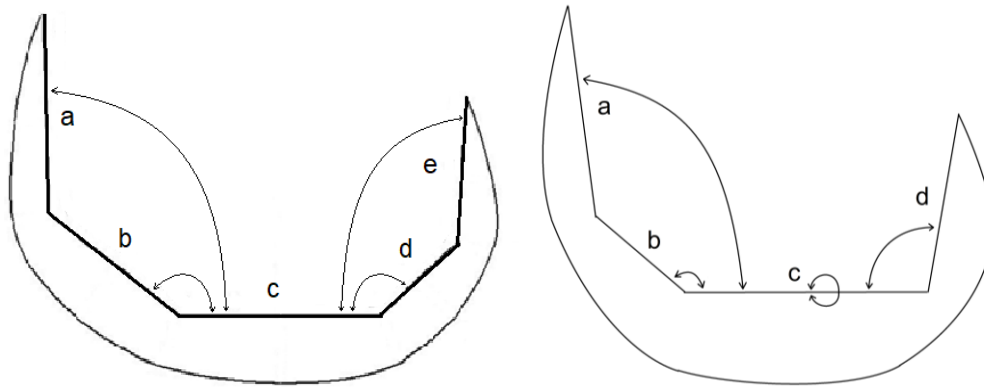


Figure 28: Femoral cutting profiles for humans and canines

As seen from the data in Table 3, the cuts that were implemented mimicked the proposed canine cut lengths when compared to the total length of the cutting profile for the cranial and cranial distal cuts. The data for the distal and caudal cuts differed considerably when compared to the proposed cut lengths, but at a constant amount, hence this new data was considered to be the more natural cutting profile for canine legs and applied as the new standard. All the implemented cutting angles remained the same as the proposed cutting angles.

Table 3: Actual femoral cutting profile data

Cutting face	Proposed canine cut length percentage compared to total cut length	Actual canine cut length percentage compared to total cut length achieved in Pitbull	Actual canine cut length percentage compared to total cut length achieved in Labrador	Actual canine cut length percentage compared to total cut length achieved in German Shephard	Average implemented cut length percentage compared to total cut length achieved
a	31%	30.7%	29.9%	30.8%	30.5%
b	21%	20.6%	19.8%	21.4%	20.6%
c	28%	32.7%	31.6%	29.3%	31.2%
d	20%	16.0%	18.7%	18.5%	17.7%

A single cut along the caudal slope is needed for the tibial implant, at an angle of six degrees when looking at the proximal tibial caudal slope, removing about six

millimeters of bone from the proximal end of the tibia in order to expose cancellous bone for better bone ingrowth of the implant.

3.7.3 Design of femoral implant

Blender was used as the tool for the next step in the design process. The smoothed femur of a canine specimen was imported into the Blender workspace as an STL file. The view was changed from the standard perspective view to orthographic view, as this view allows for better representation of the three-dimensional field by making use of parallel projection for design purposes. Once it was successfully imported, the femur could be aligned in the medial and ventro-dorsal views by making use of the rotational and object move commands, making sure to align with the mechanical axis in the medial view and aligning the distal femur flat on the distal plane in the ventro-dorsal view, shown in Figure 29. The femur was also rotated internally-externally, lining up the condyles in the caudal plane. The initial positioning of the femur was done in this way to enable easier cutting guide generation and to create a constant approach to the femoral implant design regardless of what breed or size canine needs to be designed for. It should be noted that a non-cruciate-ligament-retaining implant design approach was taken.

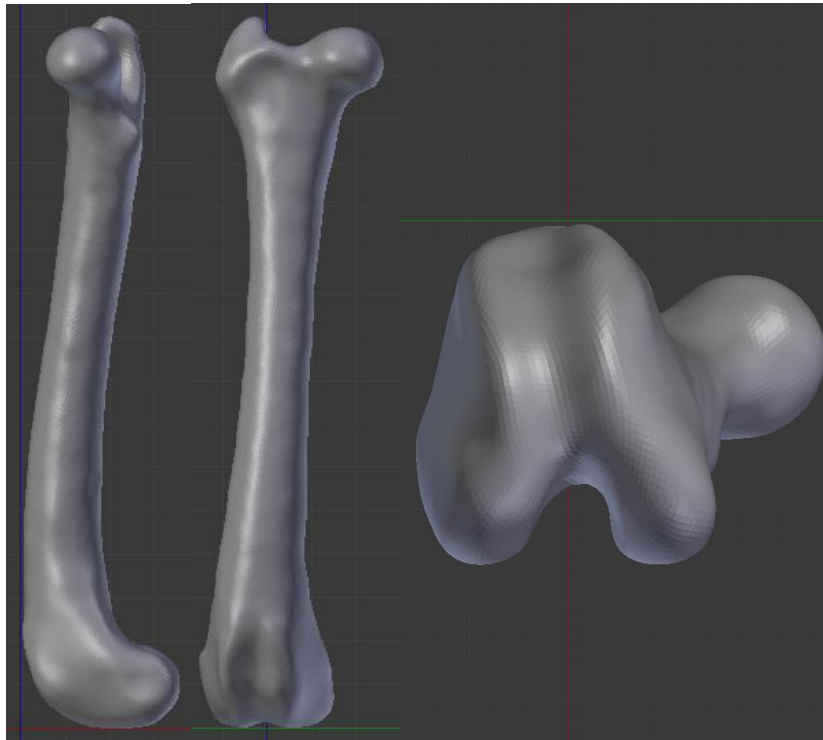


Figure 29: Femoral alignment in the lateral, ventro-dorsal and caudal planes

Once alignment was achieved, the first steps for the femoral implant design could begin. First off, the proposed cutting profile had to be generated. The cutting profile was placed in such a way that it removed about eight millimetres at most from the distal plane of the distal femur. It should be noted that this cutting depth is relevant for the canine sizes studied in this research, and that smaller breeds might require

less bone to be removed from the distal femur for the same effect. The cutting profile could be moved in the cranial and caudal directions until the desired position was achieved for the specific femur. The medial-lateral position does not matter, as the cuts will remain constant regardless of movement in that direction. Once the alignment of the cutting profile is done to satisfaction, the cuts can be implemented onto the femur making use of the Boolean modifier.

Medial slices of the distal femur were created at 2 mm intervals, starting at the midpoint of the patellofemoral groove and moving outwards towards the medial and lateral sides of the femur. The final medial and lateral slices of the femur might not be at an exact 2 mm interval, hence the final slice is created at an interval that is at least 0.5 mm from the edge of the lateral or medial femur and at a distance from the previous slice that is equal to a multiple of 0.4 mm. The reason for this will become evident in the following paragraphs when meshing is implemented. This was once again achieved by making use of the Boolean function.

Once the slices of the distal femur have been generated one can make use of the Blender tool shelf to construct a Bezier circle, which is placed in the same plane as that of the slice generated at the midpoint of the patellofemoral groove. This Bezier circle was transformed until it mimicked the surface geometry of the distal femur slice of interest as close as possible. Transformations can only be done in edit mode and only for one selected object at a time. One should always make sure that the correct mode is selected along with the intended object. Once a satisfactory geometric profile was achieved, the Bezier circle could be copied and moved onto the next plane of interest in both the lateral and medial directions and transformed until a satisfactory result was achieved. The newly generated Bezier circle can be used for the next slice, repeating the process for each slice, until all the planes of interest have Bezier circles representing the surface geometry of the femur for each plane, as displayed in Figure 30.

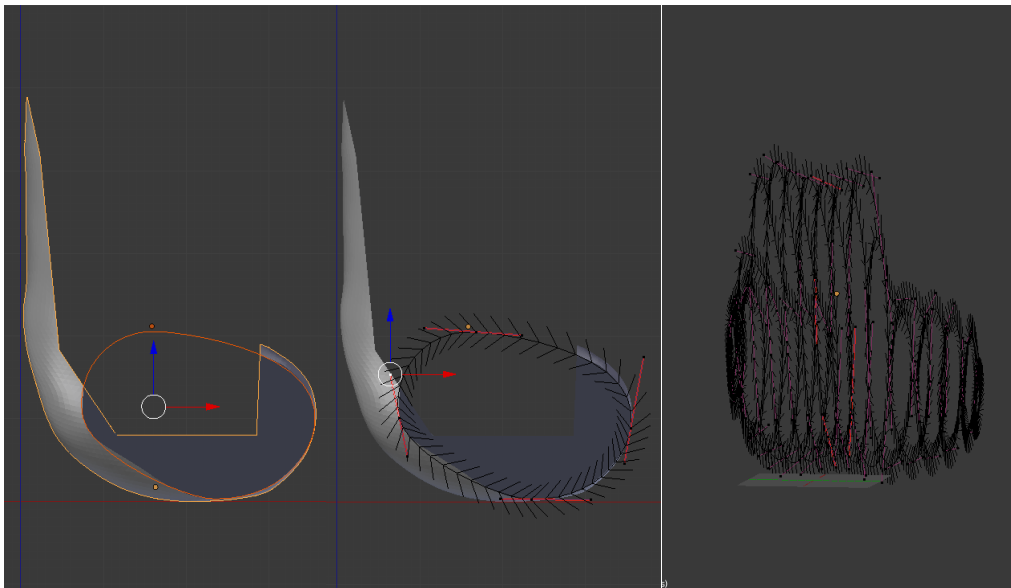


Figure 30: Bezier circle profile generation

This initial design consists of several curves, which are all still separated objects and unrelated to one another. For a connected mesh to be created one must first transform each curve into a mesh in edit mode, as displayed in Figure 31.

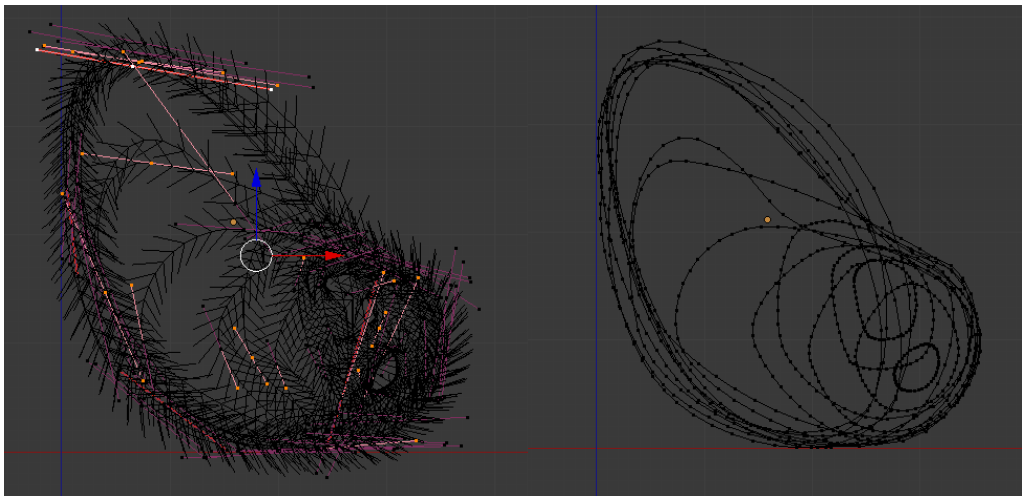


Figure 31: Curve to mesh transformation

Once the all objects are transformed into a mesh and joined, one can make use of the bridge edge loops command to create a semi-watertight mesh. One must make the mesh fully watertight by creating faces on the endcaps found at the medial and lateral sides of the implant. In order to get a higher resolution mesh, more edge loops are added, in preparation for the smoothing process. Four extra edge loops are added between each of the previous mesh loops along the z-axis (axial plane) and y-axis (medial plane), generating a mesh with a resolution of about 0.4x0.4x0.4 mm. This mesh resolution increase step is displayed in Figure 32.

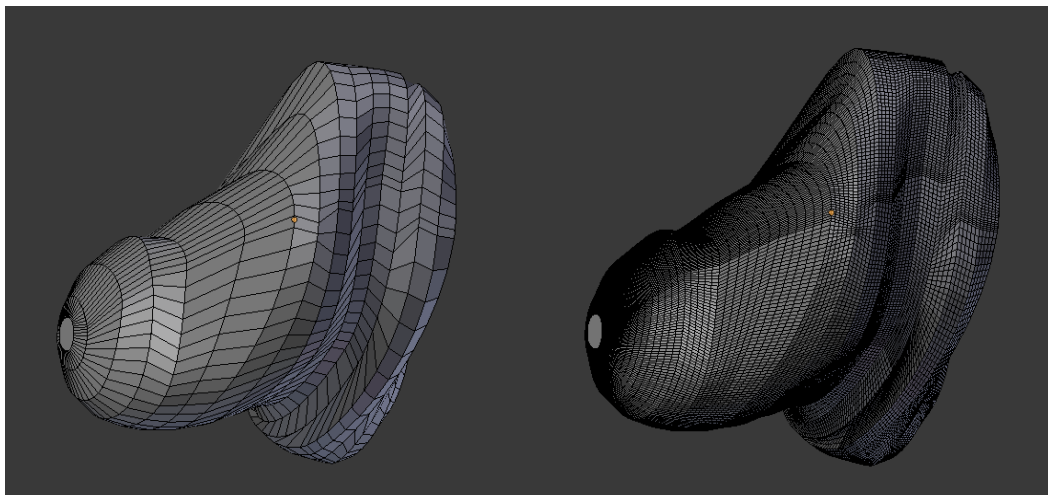


Figure 32: Mesh resolution increase

The triangulation modifier was implemented using the shortest diagonal method for the higher resolution mesh in order to assist the smoothing procedure. Triangular faces remain flat during smoothing, whilst quadrilateral faces have no guarantee of remaining flat post smoothing. This higher mesh resolution was seen as a suitable compromise between quality of the product and computational time needed for smoothing. The resolution is high enough that no faces should be visible to the naked eye after manufacturing, nevertheless it is standard procedure to smooth the frictional surface of an implant after it has been manufactured to make absolutely sure that the joint surface friction is kept to a minimum. The smoothing modifier was implemented at a strength factor of 0.5 for twenty iterations, with the result displayed in Figure 33.

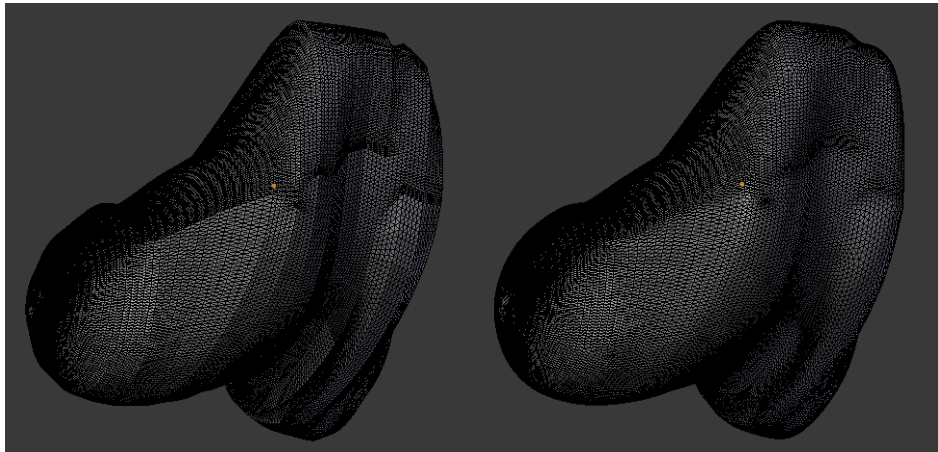


Figure 33: Triangulated mesh before and after smoothing

Having achieved a smoothed profile mimicking the surface geometry of the distal femur, cutting planes can be introduced. This is achieved by making use of the Boolean modifier, as shown in Figure 34. Usually, when making use of the 'Boolean difference' operation, a surface is generated at the interaction surface, however, for all cases throughout the design process for the different implants generated, no interaction surface was generated at this particular step.

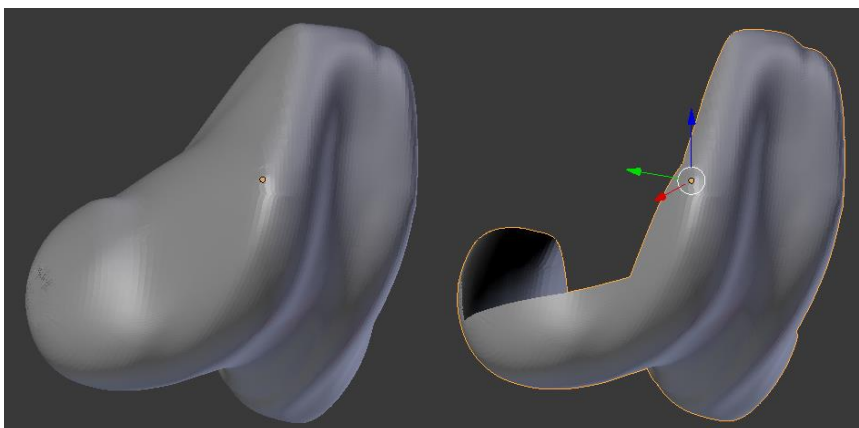


Figure 34: Femoral implant cut-plane interface generation

Cut surfaces were added manually in edit mode by selecting all relevant edges and creating a surface where the cut occurred. Edges had to be added where the cut surfaces met. A fixation pin with a diameter of 5 mm was added where the cranial-distal and distal cuts meet by making use of the Boolean union modifier, as shown in Figure 35. The fixation pin height was determined by imitating the condylar height of the femoral implant. It was decided not to create a longer pin, as a short pin should keep the implant from rotating just as well as a longer pin whilst having a smaller intrusive effect in an already intrusive procedure. Bending of the fixation pin during surgery is also decreased in this way, avoiding possible bone ingrowth problems.

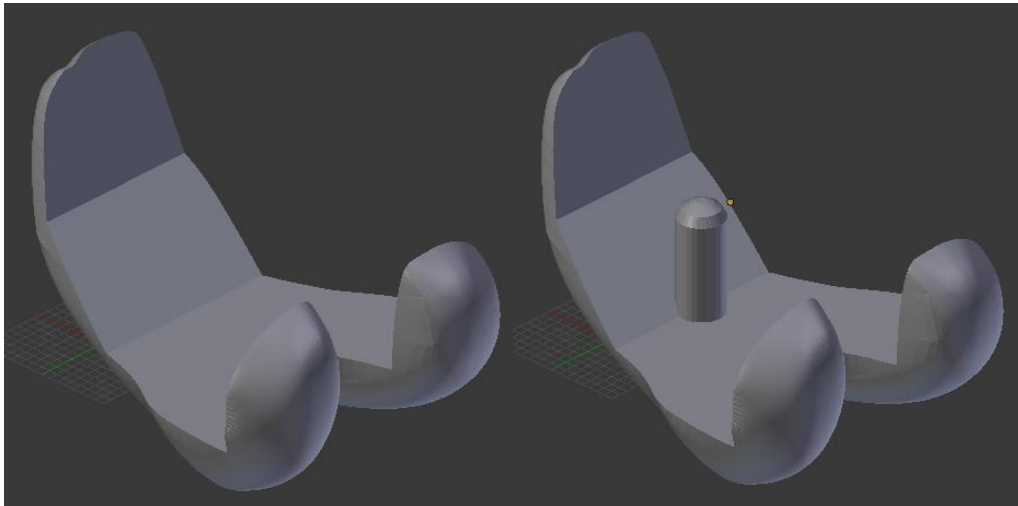


Figure 35: Femoral implant cut surface and fixation pin generation

The 3D-printing add-in was used to identify and repair non-manifold edges. The generated implant geometry is checked against the geometry of the healthy femur, making sure that the cut edges line up with one another. One should also be sure to check the sharpness of the implant edges, as a sharp edge could impede recovery throughout the healing process of the joint post-surgery. The edge sharpness of the implant should be taken into account during the initial Bezier circle geometry generation phase of the implant, as edge sharpness generation can be avoided in this step. A femoral tester, being the femoral implant without a fixation pin, can be generated if a satisfactory result is achieved and one can move onto the design for the tibial implant. A comparison between a healthy femur and the implant component designed for the femur can be seen in Figure 36.

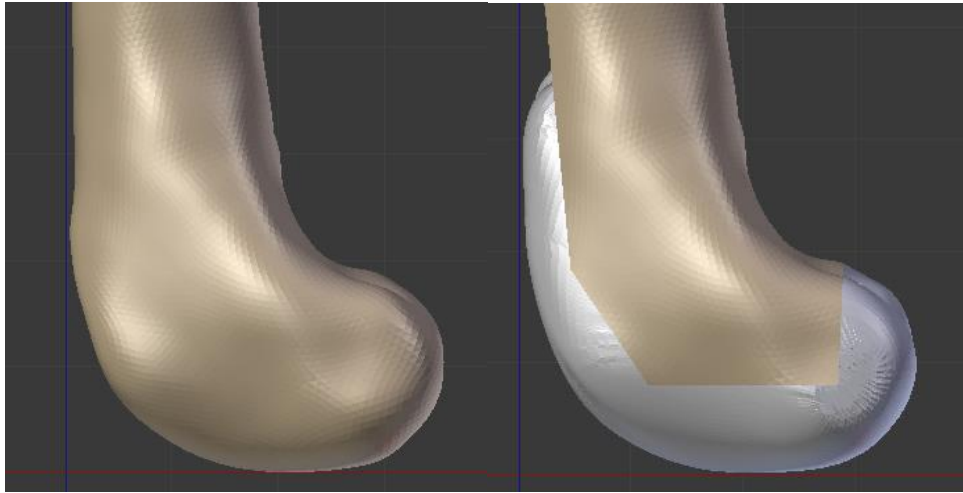


Figure 36: Distal femur pre- and post-implant

3.7.4 Implant thickness calculations

One must make sure that the femoral component is thick enough in order to avoid any mechanical failure post-implantation. Such a mechanical failure would be most likely to occur at the smallest cross-section. Considering the femoral component, this would be in the area where the femoral condyles merge together. At this position, a moment is created by the force that acts on the joint, as the generated contact force does not pass directly through the mechanical axis of the femur. During flexion of the knee joint, the femoral implant would be in a stationary position, with the tibia providing an upward force against the condyles of the distal femur. As the femoral condyles are not in line with the femoral mechanical axis, through which the body weight of the canine is transferred, a failure mode due to a bending moment is generated, hence this can be considered as a simplified equivalent to a loaded beam type problem, as displayed in Figure 37.

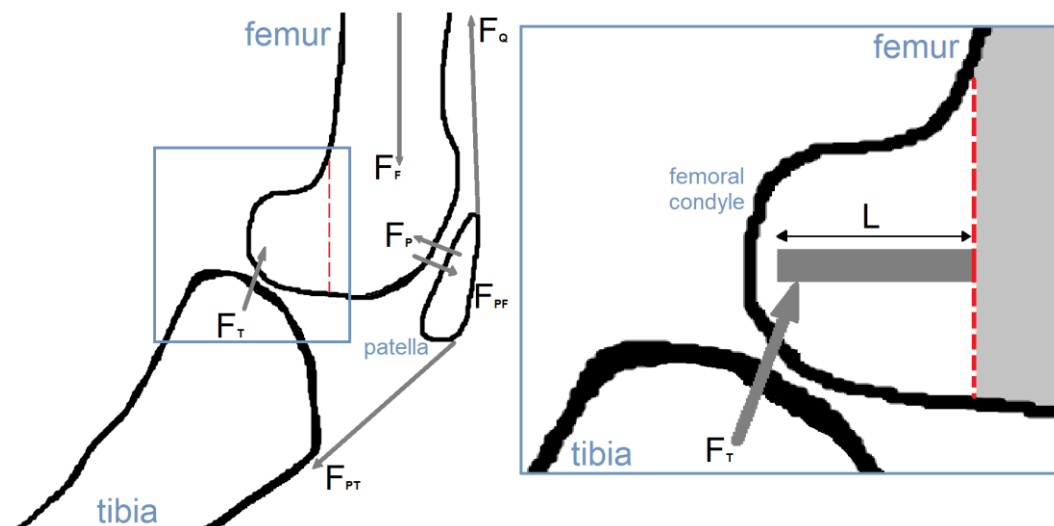


Figure 37: Free body diagram and loaded beam problem setup

The length of the beam can be made equal to the distance between the centre of the furthest point of the condylar surface area, where joint articulation occurs, and the femoral condylar merge plane, where failure is most likely to occur. Considering the 25kg Labrador-cross breed as an example, the bearing weight was considered to be half the body weight distributed across the femoral condyles, resulting in a possible 12.5 kg of weight being distributed across each condyle. The length of the beam was found to be 17 mm at its maximum, with a minimum width of 12.3 mm.

Taking the following equations into account and considering cobalt-chromium and titanium alloys as possible femoral implant materials, one can calculate the minimum thickness required at the point of interest for the implant component to succeed.

$$\text{Yield Strength}_{\text{Cobalt-chromium}} = \sigma_{CoCr} = 1600 \text{ MPa} \quad [35](3.7.4.1)$$

$$\text{Yield Strength}_{\text{Titanium alloy}} = \sigma_{Ti} = 970 \text{ MPa} \quad [35](3.7.4.2)$$

$$\text{Bending Moment} = M = F_T L = \text{Contact Force} \times \text{Length} \quad (3.7.4.3)$$

$$\text{Deflection} = y = t/2 = (\text{thickness of condyle})/2 \quad (3.7.4.4)$$

$$\text{Moment of Inertia}_{\text{rectangular cross-section}} = I = bh^3/12 = by^3/12 = (\text{breadth of condyle})(\text{deflection})^3/12 \quad (3.7.4.5)$$

$$\sigma = My/I \quad (3.7.4.6)$$

Substituting the values and constants from Equations (3.7.4.1)–(3.7.4.5) into Equation (3.7.4.6) one can solve for the minimum thickness of implant needed at the condylar point of interest at which failure is most likely to occur, in order to avoid failure. Taking the labrador specimen as an example one could find that the minimum thickness for the femoral implant should be 0.8 mm or 1.02 mm for a cobalt-chromium and titanium alloy implant respectively. The final designed femoral implants were more than four times thicker than the calculated minimum requirement at the thinnest portion of the area of concern, allowing for a good safety factor to be implemented along with the simplified thickness calculation approach.

The tibial implant thickness, consisting fully of an UHMWPE material, was based on tibial implants being used in industry today. BioMedtrix makes use of tibial implants consisting of three standard tibial implant thicknesses. The thicknesses used are 5 mm, 7 mm and 9 mm [8].

3.7.5 Design of tibial implant

Once a successful femoral implant is generated, one can move onto the tibial implant generation, which relies on the femoral implant design. The smoothed tibia of a canine specimen was imported into the Blender workspace as an STL file, aligning the tibia in the medial and ventro-dorsal views by making use of the

rotational and object move commands, making sure to align with the tibial mechanical axis in both the medial and ventro-dorsal views. The tibial tuberosity was used as a landmark for internal-external rotational positioning, facing the landmark in the cranial direction, as displayed in Figure 38. The initial positioning of the tibia was done in this way to create a constant approach to the tibial implant cutting profile and design regardless of what breed or size canine needs to be designed for.

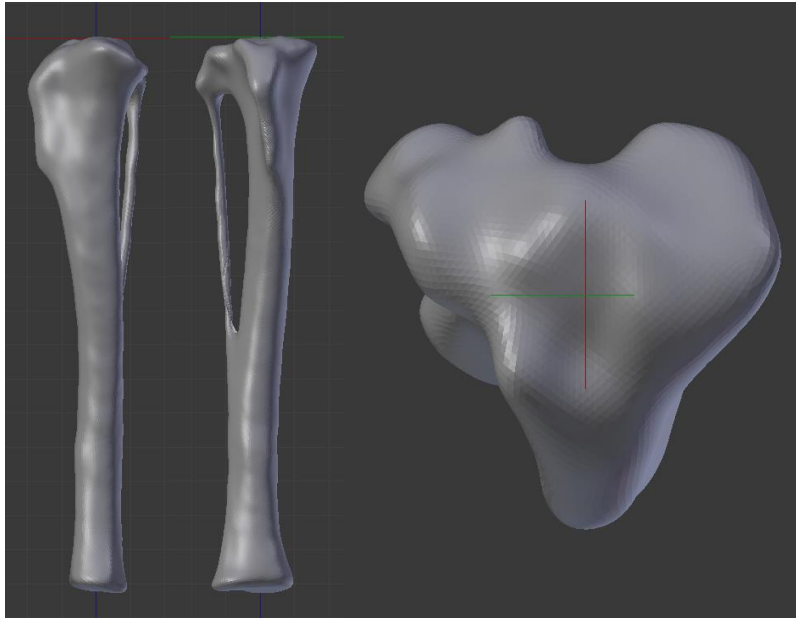


Figure 38: Tibial alignment in the lateral, ventro-dorsal and caudal planes

Once the alignment was done to the satisfaction of the designer, the first steps for the tibial implant design could begin. Using the Boolean difference operation, the ventro-dorsal cut was made at a six degree angle, removing about 6 mm of the proximal tibia, when measured in a distal direction from the epicondylar eminence, as shown in Figure 39.

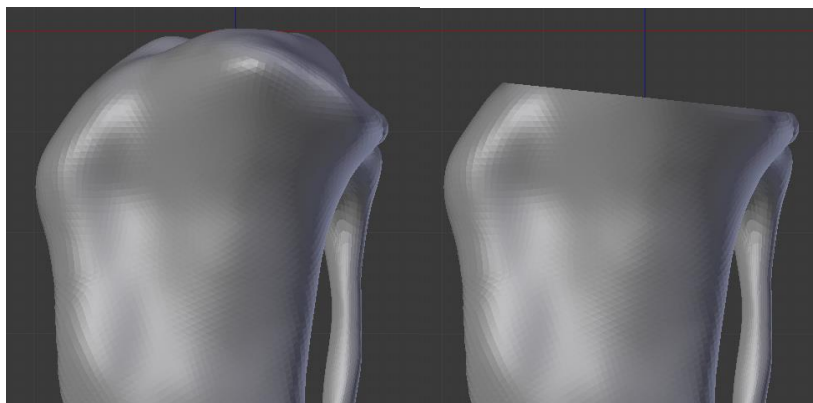


Figure 39: Ventro-dorsal proximal tibial cut

Nurbs circles were generated on the proximal plane of the tibia, mimicking the outer shape of the cut surface area when viewed on the transverse plane in the distal direction, as seen in Figure 40. These curves were transformed into a mesh and edited until a single profile geometry remained.

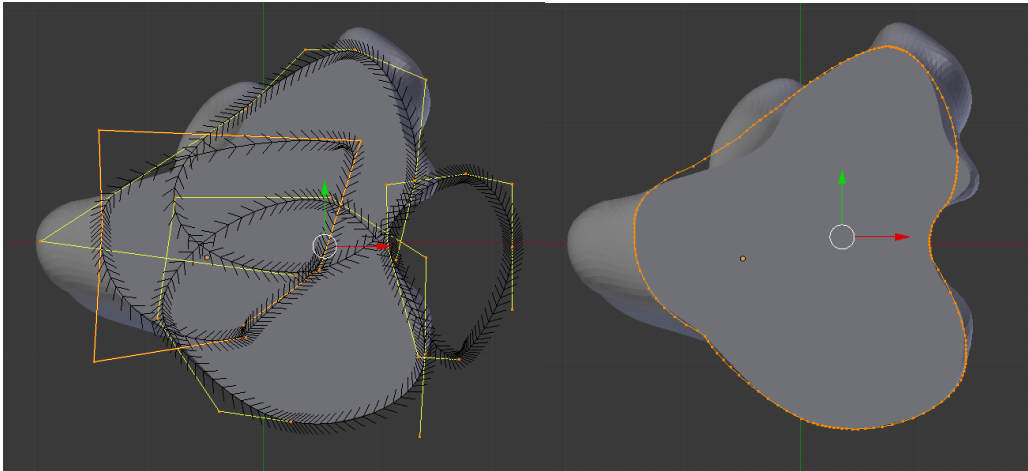


Figure 40: Nurbs circle generation and mesh conversion

A face could be generated from this mesh, which was extruded onto the cut surface of the tibia in the distal direction, where the Boolean difference operation could be used to create a six degree ventro-dorsal cut. This basic extrusion was used as the marble slab from which the tibial component is cut free. The designed femoral implant was used in the following steps. When being viewed from the medial and lateral sides, the profile of the femoral implant with the smallest diameter had to be chosen as the area of interest from which the articular surface of the tibial component would be generated. This requirement was generally found along the caudal edge diameter of the femoral implant. Hence the femoral implant was rotated, so that the femur would be aligned at a ninety degree flexion state at a height of 5 mm above the surface of the tibial cut at the point closest to the cut surface. Only the condyles of the femoral implant were required for the articular surface geometry generation. The Boolean difference operation was used to separate the condyles from the femoral implant, making design tasks easier. New object origins were created for each of the condylar objects in edit and object mode alike, marking the new origin at the point where the condyle is at its closest to the tibial cutting surface. From this point of origin, the condylar objects were scaled in all directions by a factor of four, as shown in Figure 41. This method approach to tibial articular surface design was adapted from a knee implant patent, designed by Steines et al. [36], which scaled a two-dimensional cranio-caudal curve obtained from the femoral geometry to create their tibial insert geometry. The approach in this design made use of the full 3D condylar shape to create the articular surface shape generated for this tibial implant.

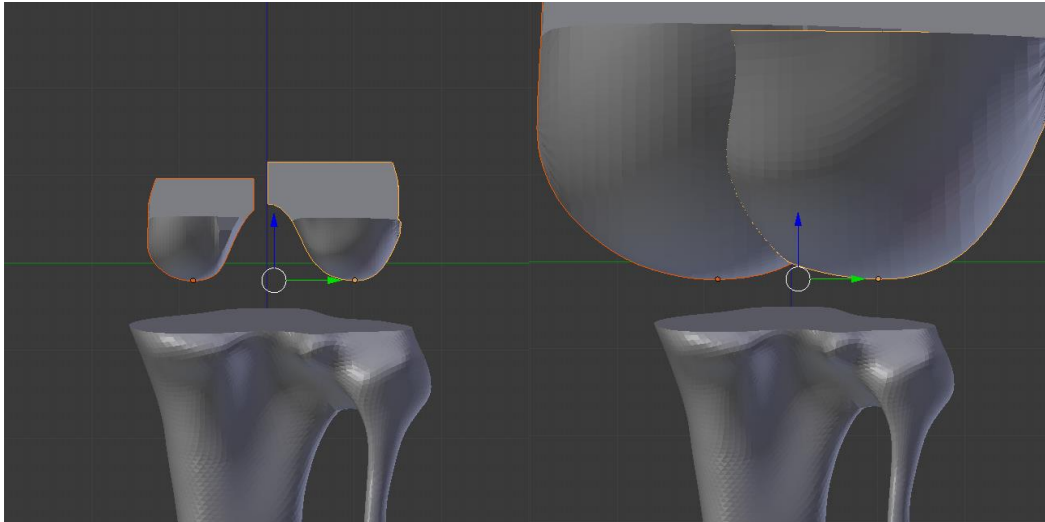


Figure 41: Femoral condyle scaling for tibial implant articulating surface generation

The resolution of the scaled condylar components is important, as this will affect the quality of the eventual produced tibial implant. Surface programming for computer aided manufacturing software makes use of small linear movements of 0.1 mm spacing each. In most design software this is not a problem, as parameterizations can be created. This is not a possibility in Blender, hence a mesh with a resolution of this standard or higher is needed for smooth geometric profile generation that is on par with a profile geometry generated from a curved surface model. The tibial implant is to be manufactured from UHMWPE. A component consisting of this material is created by machining operations, which is a manufacturing method that follows the exact geometry of the designed component. This is coupled with the fact that UHMWPE cannot be smoothed post-manufacturing, making the higher resolution a necessity. Resolution increases may result in delayed rendering or reaction times of the program, sometimes causing it to crash, hence it is very important to save the work for each step until the final tibial implant is generated.

Having scaled the condylar components, the condyles are used one at a time to create the articular surface of the tibial implant by making use of the Boolean union command. Unwanted vertices, edges and faces are removed. The tibial implant articular geometry generation is displayed in Figure 42, using a low-resolution mesh for visualisation purposes.

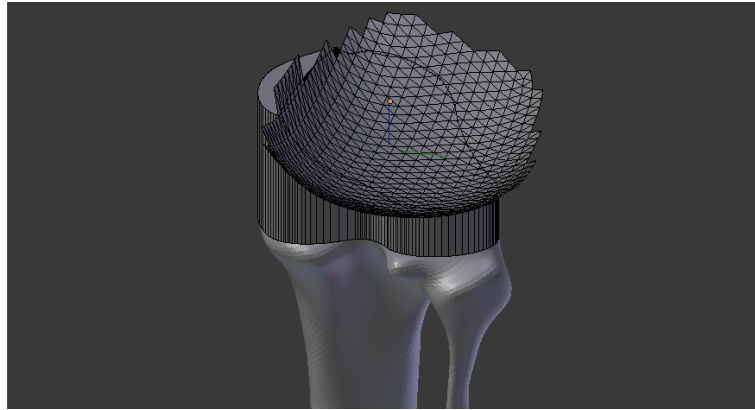


Figure 42: Tibial implant articular geometry generation

Once the articular surface geometry is generated, fixation pins are added to the cut-surface interface of the implant by making use of the Boolean union operation. Three pins are added, with the main fixation pin being inserted along the tibial mechanical axis, with a diameter of 5 mm and a depth of 8 mm. The two remaining pins are placed at the midpoints of the medial and lateral articular surfaces, with a diameter of 1.6 mm and depth of 3 mm each, displayed in Figure 43. With three fixation points, the tibial implant can be fixed effectively to the cut tibia, with no movement likely to occur throughout joint motion.

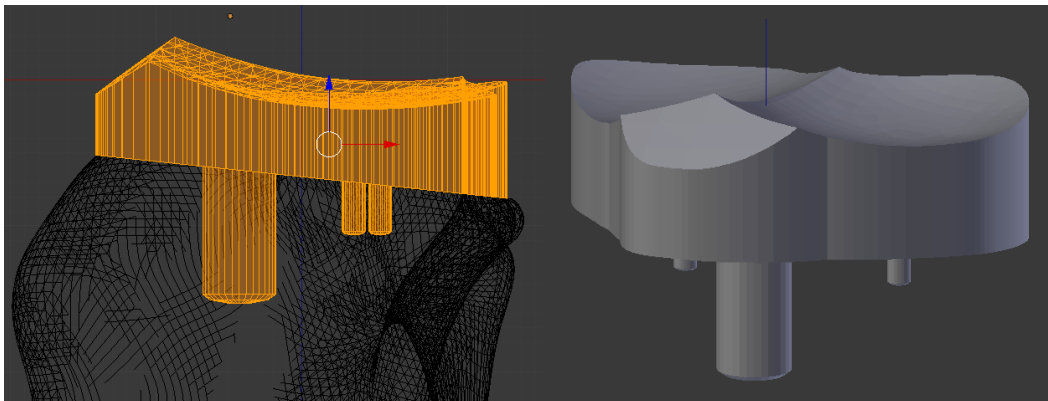


Figure 43: Generated tibial implant

Three tibial implants are generated, which all have the same articular surface geometry, but with three different implant thicknesses. These implants have a thickness of 5 mm, 7 mm and 9 mm. The correct implant thickness can be chosen during the surgery procedure, depending on the depth of proximal tibia being removed and the joint capsule tightness being needed after the removal of ligaments such as the cruciate ligaments and menisci. Tibial testers were created for this purpose, as shown in Figure 44, so that the surgeon can test which implant thickness functions the best, along with the femoral tester, after cuts have been made. Should the process be executed successfully, the tibial and femoral implants will have articular surface geometries that complement one another.

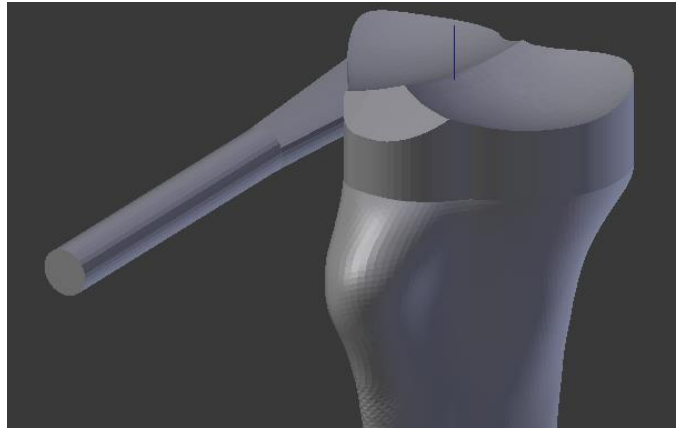


Figure 44: Tibial tester

3.7.6 Design of instrumentation

Total knee replacement implants cannot be effective without a working surgical procedure and robust surgical equipment. Surgery can determine the success of an implant, regardless of the quality of the design. The surgical procedure and necessary equipment was based on the approach used by Liska et al. [4], which also shaped the surgical equipment used in industry today. It should be noted that the standard pins used for fixation during most surgical procedures are 1 mm and 1.6 mm in diameter. For sawing guide design, the S82-104 multi saw blade was considered [37], as it is a common blade used in veterinary practices in South Africa. This blade is 70 mm in length, 25 mm in width and 0.81 mm in thickness, creating a cut thickness of 1.2 mm.

The tibial cutting alignment guide consists of six components, displayed in Figure 45, with each lower-case letter denoting a different cutting guide component. 'Lower cylindrical alignment' (TLCA, a) and 'upper cylindrical alignment' (TUCA, b) components of the tibial cutting guide make up the main body and allow for adjustments to be made in the distal and proximal directions of the tibia. The TUCA component has provisions made for 1.6 mm fixation pins, so that fixation can occur along the tibial tuberosity. Pins of this diameter were chosen as they provide more rigidity to the setup than the smaller 1 mm diameter pins. A sliding fit was designed for the upper and lower cylindrical components, according to ISO specifications, as this type of fit allows parts to be turned easily, slide freely and accurately. Accuracy and easy movement are important for a surgical setup; hence the designed components were created keeping these specifications in mind for all parts. The 'lower pin fixation guide' (TLPG, c) is used to anchor the tibial cutting guide along the distal half of the tibia at two points along the medial and lateral sides, with fixation pin guide provisions being made for 1.6 mm pins. The 'sawing guide' (TSG, d) component, attached at the upper cylindrical alignment component, was designed keeping rotational alignment in mind, allowing the user to get the required proximal tibial caudal slope cut at the right angle. Provisions were made for 1.6 mm fixation pins, allowing for extra stability, should it be needed. The final two components consist of the 'drilling adjuster' (TDA, e) and 'drilling guide' (TDG, f) components. The TDA having the function of its name, to adjust

the caudo-cranial angle and positioning of the drilling guide. The TDG component allows for accurate holes to be drilled into the proximal tibia, so that the tibial implant fixation pins can be attached to the proximal tibia rigidly. The components are designed to be fixed together once a desired configuration is attained by making use of M3 hexagonal socket cap screws. Five of the six tibial alignment guide components can be re-used for different total knee replacement surgeries, with the TDG component being patient specific, requiring different drilling sites for different sized canines.



Figure 45: Tibial cutting alignment guide components

Four components were designed to create the femoral cutting guide, displayed in Figure 46, with each lower-case letter denoting a different cutting guide component. The 'initial pin location' (FIPL, g) component is used to accurately locate the first drill site and guide a 1.5 mm diameter drill into the bone at an angle parallel to that of the mechanical axis of the femur, from which the femoral 'cutting guide block' (FCGB, i) can be accurately positioned. The FCGB component is designed to attach at the distal end of the femur. This component guides the sawing blade for correct cuts to be made. Fixation pins can be inserted at multiple sites along the medial, lateral and cranial sides of the distal femur, with provisions being made for 1.6 mm fixation pins. The FCGB doubles as a drilling guide,

allowing for an accurate hole position to be drilled at the site where the femoral implant fixation pin is to be inserted. A 'fixation pin sleeve' (FFPS, h) component was designed to be placed around a 1.6 mm fixation pin, so that the FCGB could be attached to this sleeve rigidly for initial alignment, doubling as another point of fixation. The 'caudal alignment' (FCA, j) component is used to align the FCGB at the correct angle, with regards to internal-external rotation. Three femoral cutting guide components are patient specific, only the FFPS component can be re-used for different total knee replacement surgeries.

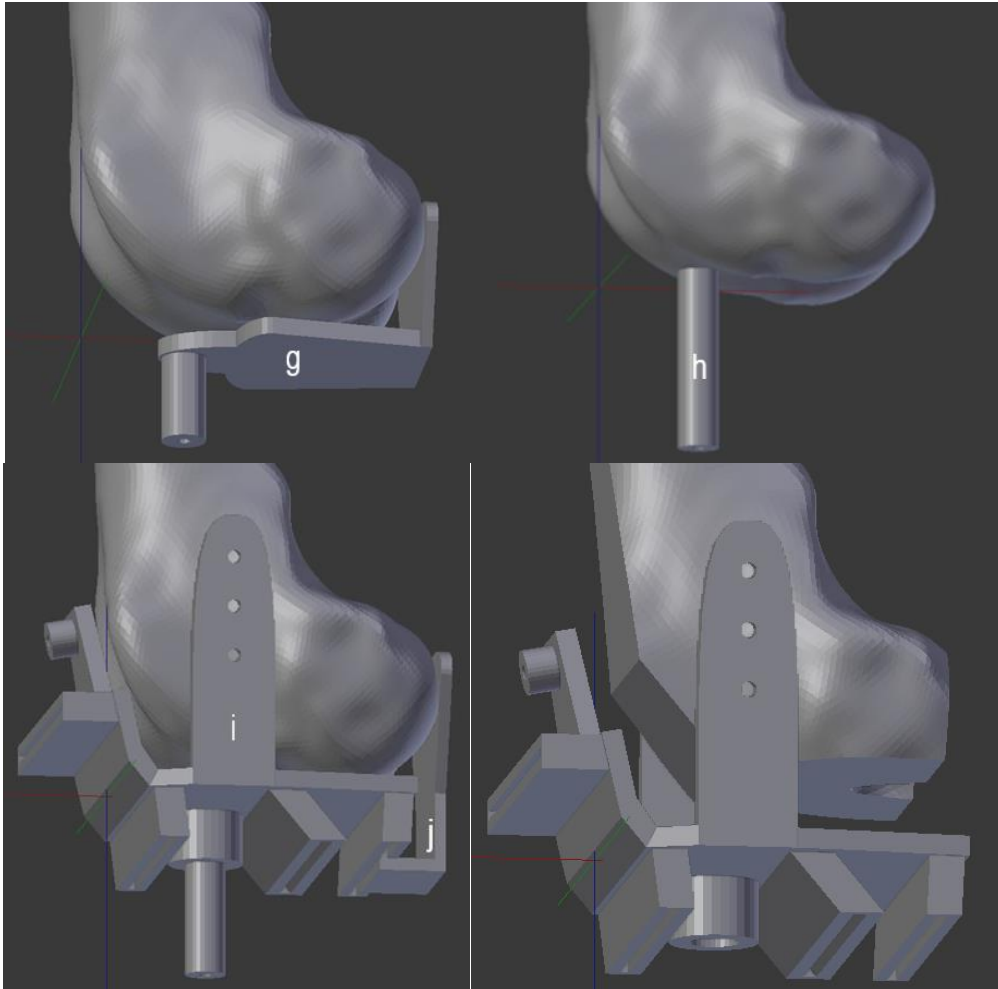


Figure 46: Femoral cutting guide components

4 Testing procedure

4.1 Overview

Implants and surgical equipment were manufactured using rapid prototyping methods. Casted bone models were created for preliminary tests in order to establish the validity of the testing procedure approach, before cadaveric specimen tests could be performed. The testing procedure implemented an Oxford-type knee rig in an open-chain configuration, along with an NDI motion tracking system, to track joint motion and quadriceps forces experienced throughout induced knee extension. Multiple tests were done before and after implant insertion. The surgical procedure and kinematic calculation methods used are also outlined in this section.

4.2 Steps taken to generate test model and implants

CT scans obtained from a bull terrier were used to create bone models on which preliminary testing could take place. Preliminary tests were performed on a model of a canine knee in order to establish the validity of the testing procedure approach, before cadaveric tests could be implemented. Firstly, bone models of the tibia and femur, as well as the designed implants and accompanying surgical instrumentation, were exported as STL files for 3D printing purposes. These STL files could be imported into a 3D-printing software for rapid manufacturing purposes.

Filament deposition modelling is a material extrusion process, where additive manufacturing is achieved by pre-determined melted layers of material being deposited on top of one another, one layer at a time until the desired three-dimensional shape is achieved. One must take factors such as warping, layer adhesion, support structure, infill density and shell thickness into account when preparing a model for printing. Materials such as acrylonitrile butadiene styrene (ABS) and polylactic acid (PLA) are used commonly in this process. ABS material has good strength and temperature resistance but is more susceptible to warping and PLA is easy to print with and has excellent visual quality but has a low impact strength. This manufacturing technology is a cost-effective way of efficiently producing thermo-plastic parts and prototypes.

Both Z-suite and Cura (1.1 beta) open-source software's were used to set up designs for 3D-printing. Polyactic acid (PLA) filament was used for manufacturing of all bone, implant and surgical components for initial tests, for its high strength, high stiffness, low shrinkage and thermoforming dimensional stability properties. The printing setup was done in Cura, where the components were rotated and translated into better positions, so that the best quality product could emerge from printing. After specifying the printer properties, a G-code file was generated and exported onto a memory stick for information transfer onto the Wanhao Duplicator 6 FDM printer. This G-code file informed the printer exactly at what printing temperature, build plate temperature, infill density, wall thickness, layer height, quality and speed it should print, along with other customised settings. Once the print had completed, the components could be cleaned, removing any supporting material. Acrylonitrile butadiene styrene (ABS) filament was used to manufacture the implant components for later tests using cadaveric specimens, as

the surface finish was smoother, with near invisible layer seams. The surface finish could be further improved with the careful post-print exposure to acetone. For ABS FDM printing, the Zortrax M200 printer was used, along with Z-suite software for setup purposes.

Selective laser sintering (SLS) is a process in which powder is heated to a temperature that is just below its melting point by a powerful laser, which causes the powder to sinter together in order to form a predetermined shape. The material powder is heated to a point just short of its melting point, requiring only a small temperature change to achieve its melting point. Since this is a thermal process, lasers are used which have a higher thermal effect, such as long pulse or wave lasers. The fresh powder layer is applied after each sintered layer, until the component is fully formed.

It is a very effective process, as there is very little material waste, with the unused powder being reused for the next laser sintering process. This process has been used extensively in the medical industry to manufacture prosthetics as well as surgical equipment used throughout surgical procedures [38]–[40]. The surgical instrumentation, for later tests using cadaveric specimens, was manufactured by making use of SLS, with the exception of the TLCA and TUCA components. These components were manufactured using machining procedures, such as turning, drilling and threading, to manufacture the components from a soft steel metal. The SLS components were manufactured using a polyamide material suitable for medical application requiring USP Class-VI compliance or biocompatibility [41]. It has good durability for functional testing and excellent surface resolution, necessary for cutting guide components where accuracy is required.

The tibial and femoral PLA bone prints could be used to generate a mould, so that a casted bone could be created that resembled the strength of bone more closely. In order to create a mould, a wooden mould box had to be built that could easily assemble and disassemble, for removal of casted objects and re-use purposes. It had to be large enough to accommodate both the FDM printed tibial and femoral components. A shutter-like approach was used to align the mould box sides for the desired dimensions, as displayed in Figure 47. The advantage of this approach is that the wall dimensions can be changed as required, being limited only by the length of the wood panel used for each side. The generated mould box had inner dimensions of 92 mm x 120 mm x 184 mm with regards to width, length and height. It was fastened with ten M5 x 50 mm wood screws, eight attached along the edges and two along the base, for which pilot holes were drilled before-hand in order to avoid splitting of the wood.



Figure 47: Mould box

The moulding material chosen was Mold Star™ 30 [42], produced by AMT Composites, which is a platinum silicone with a low viscosity that does not require vacuum degassing. It has a one-to-one volume mix ratio, making application easy. Once cured, it is a soft, strong rubber which resists tearing and is observed to have very low shrinkage over an extended period. The cured material is heat resistant up to 232 °C, which is advantageous when an exothermic reaction is utilised in the casting process. The FDM tibia and femur were placed with the articular surfaces facing the bottom, but not touching the bottom. They were held in place by use of cable ties and a rubber-like temporary adhesive. The correct one-to-one volume of the moulding material was mixed together and poured into the moulding box, as seen in Figure 48, to be left to cure for twelve hours.

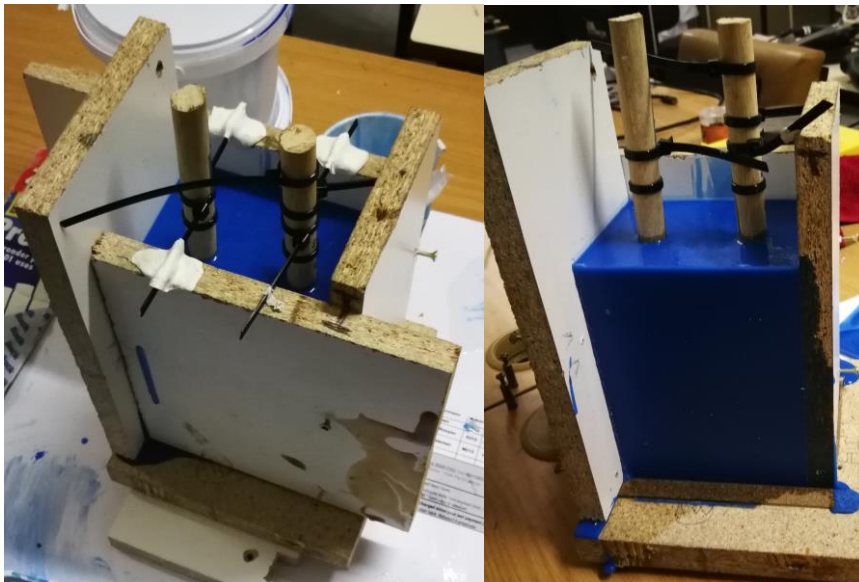


Figure 48: Moulding process

Once cured, the mould box was disassembled so that the mould could be removed. Incisions were made into the moulding material with a utility knife, moving in a vertical direction from the top of the mould towards the bottom, stopping before reaching the base. Care was taken to cut all the way to the object being moulded, so that the mould could be parted without formation of tears. Once enough cuts were made, the moulded tibia and femur could be removed.

F180 Fastcast [42], from AMT Composites, was chosen as the casting material. It is a quick setting fastcast polyurethane resin with very low shrinkage and good impact resistance. The mixing is done by weight, using a one-to-one ratio, which causes an exothermic reaction with a glass transition temperature of 112 °C. It has a tensile strength of 57 MPa, similar to that of the tensile strength seen in bone, which ranges from 50 MPa to 70 MPa, depending on the direction of the force and which bone is measured [43]. The polyurethane sets quickly and can be demoulded after a thirty-minute time period. The mould box was disassembled after the demoulding period was observed, so that the casted femoral and tibial models could be removed, shown in Figure 49. These casted models could be used for initial testing of the functionality of the designed surgical instrumentation, as well as to validate the methodology of the surgical approach and the accuracy of generated femoral and tibial cuts with the help of a veterinary surgeon.



Figure 49: Casted bone models between FDM printed bone models

Further models were generated using the moulding and casting process, to be used as proof of principle for the testing procedure. A casted model of the pre-implant bones was generated, as well as a casted model of the post-implant bones. Both models had insertion points placed on the tibia and femur where organic ligament insertion points would be located. Medial and lateral collateral ligament insertion points, as well as insertion points for the patellar ligament at the tibial tuberosity were added, with ligaments being represented by cotton rope. These ligaments were chosen as they are the stabilising ligaments that remain after a total knee replacement surgery. The pre-implant bone model had a lateral and medial meniscus added to assist joint motion, made from a non-crack elastic clay.

The patella was represented by a smooth hemispheric metal component of a similar diameter to that of the natural measured patellar length. Both the pre-implant and post-implant casted models can be seen in Figure 50.



Figure 50: Free-standing pre-implant casted models (a) and post-implant casted models in joint test rig (b)

4.3 Specimen preparation for kinematic tests

Before any testing could take place, the hind limb was removed from sub-zero temperatures and left to thaw for nine to twelve hours. Once thawed, the paw and skin were removed from the specimen. The proximal half of the femur and the distal half of the tibia were cleaned, so that only bone remained, without any soft tissue present, as seen in Figure 51. All the parts that were removed distally of the knee capsule were weighed, so that a similar weight could be added to the distal tibia during testing, in order to mimic lower limb weights that would normally be similarly experienced. The musculature and soft tissue surrounding the joint itself was not removed to ensure that the joint capsule remained intact for testing. The quadriceps muscles were isolated from the surrounding soft tissue, so that the quadriceps could be attached to an actuator for tensile load generation, in order to facilitate joint movement. Potting was done for both the proximal tibia and distal femur, making sure to align the centre of the mechanical axis for each potted bone with the centre of the pot, whilst quick-set cement was used to generate a pot for each bone.



Figure 51: Specimen leg pre- and post-preparation for potting

4.4 Testing procedure using open-chain configuration

The measurement values of interest in a total knee replacement are what type of kinetic and kinematic differences and similarities occur before and after such a surgical procedure, the most important kinematic motion of interest being flexion-extension of the stifle. This is the primary motion required, as it has the biggest rotational range and biggest functional importance for a canine. When looking at ways of collecting kinematic data of the knee joint, there is a history of a six degrees-of-freedom Oxford knee test rig system or a test rig based on that design being used, with a wide range of data having been obtained in this manner for human knees. The Oxford knee test rig was designed specifically for biomechanical testing of the human knee, making use of cadaveric specimens due to the invasive nature of this type of testing.

The Oxford knee test rig, shown in Figure 52 as described by Zavatsky et al. [44], allows for translational movement of the hip assembly in the vertical direction relative to the ankle assembly, rotation about both the ankle and hip assemblies in the flexion-extension and abduction-adduction directions, and rotation about the knee joint in the flexion-extension, abduction-adduction and internal-external directions. Flexion and extension are achieved by the vertical displacement of the hip assembly, mimicking a squatting motion. The assembly is constrained at the hip and ankle joints, different than what is seen as physiologically normal, however it has been shown that testing in this type of a setup captures knee joint movement as well as any other in-vitro system, allowing for the same six degrees-of-freedom joint motion as of that in a normal knee [45].

In order to gain accurate force measurements of the quadriceps muscles during motion, a rope-type tension force sensor was used (Lorenz K-range Force Sensor, Lorenz messtechnik gmbh [46]). This sensor could be attached to the quadriceps at one end and the actuator at the other end. This allows for tensile force to be measured throughout actuator induced joint motion. The sensor can accurately measure induced force in 0.25 N steps.

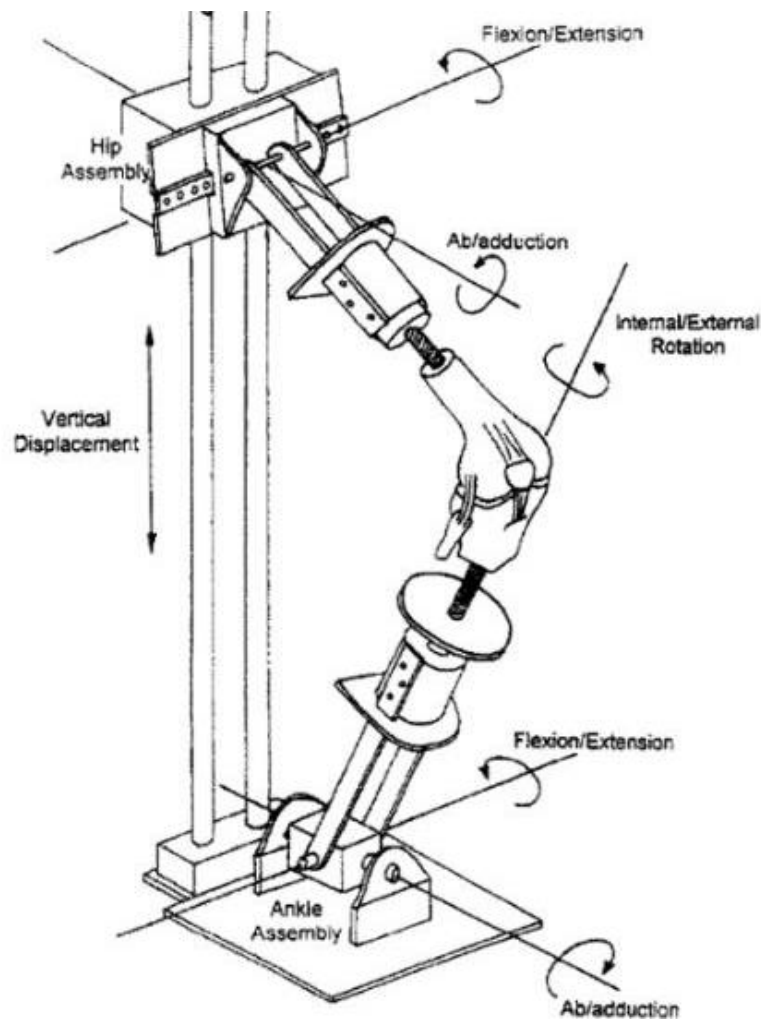


Figure 52: Oxford knee test rig as described by Zavatsky et al. [44]

After securing the potted femur into the Oxford-type knee test rig, which was set up in an open-chain motion testing configuration, a quadriceps clamp was attached to the quadriceps muscle of the prepared specimen, as seen in Figure 53a. A nylon strap (Figure 53b) was used to attach this clamp to the Lorenz force sensor (Figure 53c), which was attached to an actuator (Figure 53d). By inducing a retraction and extension motion in the actuator the quadriceps could be engaged or disengaged, resulting in flexion-extension of the joint. It should be noted that the test setup was such, that the knee would be in a flexed start position, followed by extension, induced by the actuator pulling the quadriceps in a proximal direction relative to femur, before the actuator retracted again, causing flexion, until the cycle was completed. The tibial pot was then secured with the relevant weight added at the distal end of the tibia (figure 53e). Using the Labrador specimen as an example, all the parts that were removed distally of the knee capsule were measured to be 426 g in weight. The weight added to the lower tibia for this scenario was equal to 430 g, with the tibial pot weighing 238 g and the added quick-set cement added weighing 192 g. With no knowledge of the added tibial weight needed for the casted models, an assumed weight of 400 g was added to the distal end of the

tibia for experimental tests. Having set up the test specimen in the test rig, the motion tracking components could be added (Figure 53f). Provisions were made on both pots, so that the tracking markers could be screwed in securely, allowing fixed body tracking for the tibia and femur.

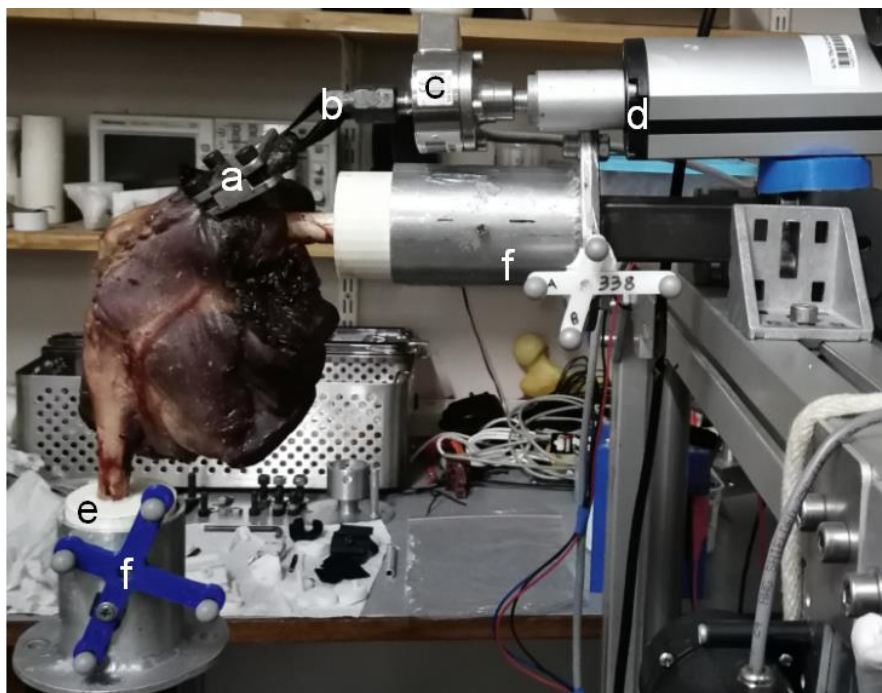


Figure 53: Labelled open-chain test rig setup

Modernised motion tracking techniques make use of multiple cameras to track a marker in space. This can be thought of as the same process that humans and most animals use, where two eyes are used in order to observe an object's three-dimensional positioning in a space. Similarly, in modernised motion tracking, two or more cameras are placed in pre-determined stationary positions and a marker's position is triangulated based on the positioning of the cameras in a three-dimensional environment in order to get the position of the marker relative to a global coordinate system in a calibrated field. NDI tracking tools make use of this technology and have been used to study kinematics in both humans and animals [6], [47]–[50]. This type of system has been accepted as a reliable way of acquiring three-dimensional spatial data. It is not without its faults, losing data points if a tracked marker accelerates suddenly or adding more data points should other reflective surfaces interfere with the actual tracking markers, however the advantages outweigh these minor disadvantages.

The NDI Polaris Spectra sensor (Northern Digital Inc.) was used to track markers on fixed tracking tools and to establish virtual marker positions within a predetermined volume, as displayed in Figure 54. Tracking tools were established by attaching retroreflective spherical markers to a rigid structure at four points. A tool definition file used to describe the tool geometry and the tool's marker geometry was uploaded into the tracking software for each tracking tool used. The

software could therefore track the orientation and position of each tool, as well as the position for each marker defined on the tracking tool. To establish virtual marker positions, a pointer/probe tool was described and uploaded into the system. In order to determine the tool tip offset, the spherical tool tip was positioned in a hemispherical divot of the same size and pivoted around the vertical, making sure that the sensor was in line of site of the spherical markers throughout the pivoting process. If a satisfactory RMS error value was achieved (~ 0.2) the offset could be applied.

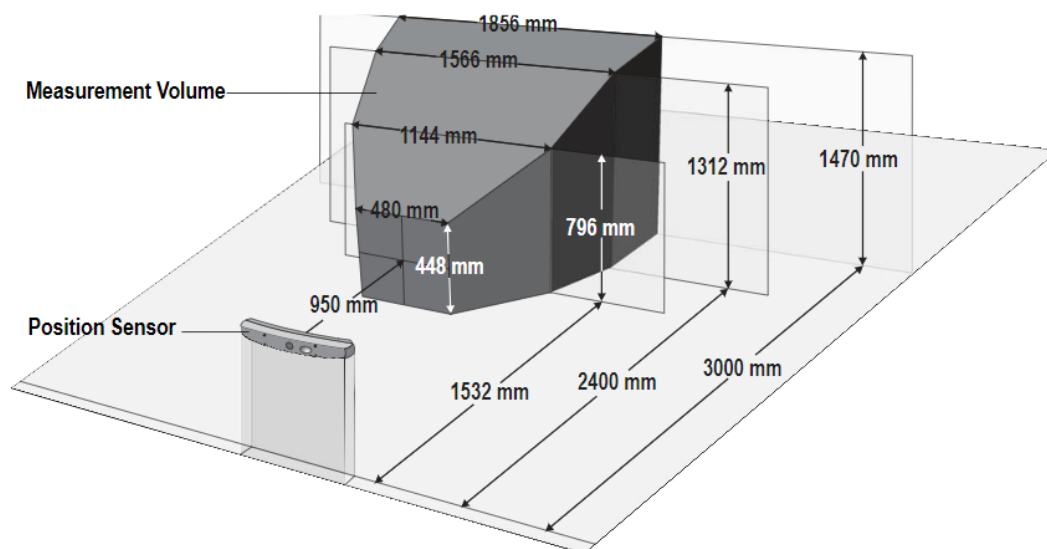


Figure 54: Polaris Spectra Measurement Volume (Northern Digital Inc.) [51]

With the femoral fixed and tibial fixed tracking tools attached at their respective positions, the femoral tracking tool was set to be the global reference tool. The probe tool was used to define four virtual marker points on both the femur and tibia relative to the global reference respectively, which could later be used to establish an anatomical coordinate system for both the femur and tibia. The virtual proximal femoral point is located along the mechanical axis of the femur, but as the femur is already potted, this mechanical axis line is followed and the virtual point is marked on the proximal side of the femoral pot, where a mark was made for repeatability purposes. The virtual distal femoral point is located inbetween the lateral and medial condyles on the posterior surface at the most distal point. For the medial and lateral virtual femoral points, the medial epicondyle and tibial epicondyle are chosen. The virtual distal tibial point is located along the mechanical axis of the tibia, but as the tibia is already potted, this mechanical line is followed and the virtual point is marked on the distal side of the tibial pot, where a mark was made for repeatability purposes. For the virtual proximal tibial point, it is located at the most proximal midpoint of the intercondylar eminence. The medial virtual tibial point is located at the most medial bone prominence of the medial tibial condyle. The lateral virtual tibial point is located at the most lateral bone prominence of the lateral tibial condyle. These virtual marker points can be seen in Figure 55. Each virtual marker point was recorded relative to the global reference (fixed femoral tool), with the fixed tibial tool orientation and positioning known at the time of recording for each virtual point.

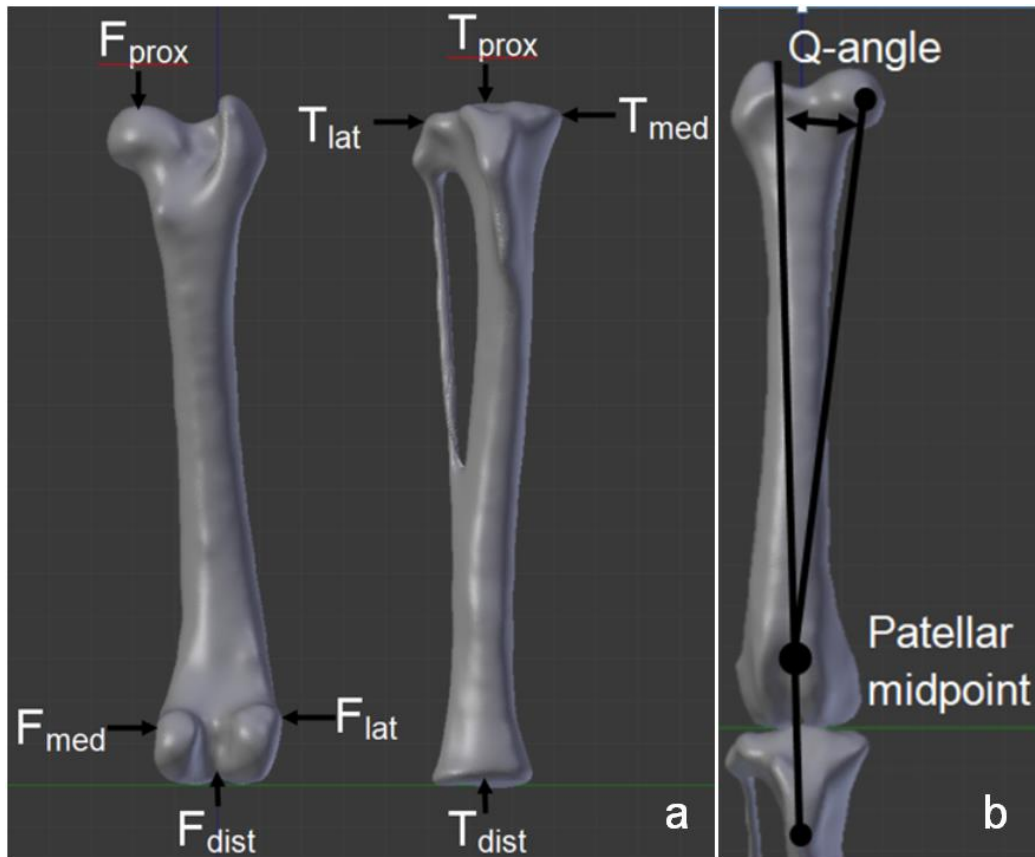


Figure 55: Virtual marker point locations shown for a posterior femur and anterior tibia in a. Quadriceps-angle description from an anterior view in b.

The actuator was aligned to have a quadriceps-angle that was observed to be natural to the specimen being tested, as described in Figure 55. Quadriceps-angles of canines can range anywhere from 2.7° to 29.7° , as described by Pinna et al [52]. It is important to make sure that quadriceps-angle is correct so that the patellar alignment is correct to ensure stability, as instability in the patella can result in patellar luxation during joint motion. The actuator was manually retracted and extended to check the natural open-chain flexion-extension joint range for which the quadriceps muscle would be activated, as seen in Figure 56. The points where maximum and minimum joint extension occurred were marked on the shaft of the actuator. The range was checked multiple times to ensure that the marked maximum and minimum points were indeed correct. The maximum joint extension point was determined as the natural stop-point of the joint. The actuator was manually extended or retracted until the joint was in its least extended position where quadricep activation for flexion would no longer have an impact on the joint. At this position, the Lorenz force measurement is set to zero. The start position was hence chosen at the position where force was no longer applied to the Lorenz force measurement tool, but where a force would immediately be present again for retraction induced joint extension.

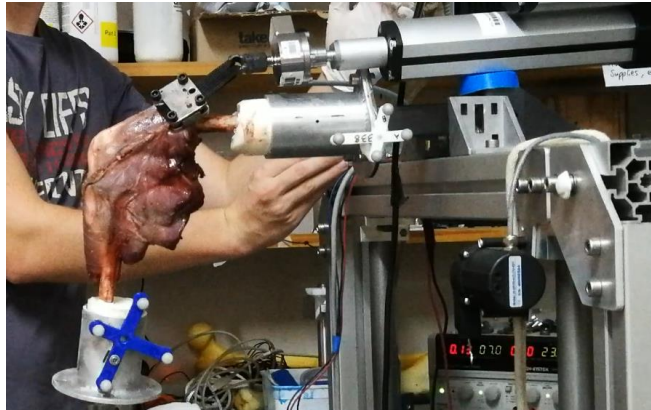


Figure 56: Open-chain experimental setup for knee joint in flexion

With the joint in the correct starting position, both the motion tracking system and force measurement system were started at the same time, recording data at 20 Hz each. The actuator was manually turned on for retraction until the mark for maximum joint extension was reached. The actuator was turned off for five seconds at this joint position, before it is turned on again for extension to induce joint flexion. The actuator was turned off again once the start position is reached. The motion tracking system and force measurement system data recorders are stopped at the same time and recorded data can be saved. After at least five seconds of waiting, the next extension-flexion cycle could begin. The pause between the flexion and extension phase of the joint is done to avoid any inaccuracies during data collection resulting from a sudden change of direction, which could have the effect of introducing an impact force to the recorded data. The same testing procedure is performed, until at least five successful recordings are established, so that a wide recorded data range is acquired. The described testing procedure steps are followed for the joint after TKR is performed once again, so that pre- and post-implant joint motion ranges can be compared to one another for validation purposes.

4.5 Surgical procedure and implantation

After many iterations of the cutting guide components were designed, and initial testing on casted models was done, a surgical procedure could be generated with the help a qualified veterinary surgeon. A medial approach is used to open the knee capsule, using the patella as an identifying feature to create a stab incision, from which the knee capsule can be opened. The patella is displaced in the lateral direction, exposing the knee joint from the straight patellar ligament to the proximal end of the trochlear groove. Full flexion is created in the joint to expose the entire tibial plateau, allowing for an easier approach for the tibial cut, which is done before the femoral cuts. The tibial menisci, cruciate ligaments and infrapatellar fat pad are removed, exposing the bone articular surfaces of the joint.

For the tibial cut it is important to get the depth and angle of the cut correct, so that healthy cancellous bone is exposed. It was noted that the depth of the cut could become a problem, removing too much of the proximal tibia which could cause a loose joint capsule post-surgery, hence special care needs to be taken to ensure

that this problem does not occur. Additionally, a precision cut needs to be made so that no injuries are incurred on the collateral ligaments throughout the procedure. With the TUCA, TLPFG and TLCA components already assembled, the TLPFG is attached to the distal half of the tibia from a cranial approach, using two fixation pins to attach the component to the tibia percutaneously. Adjustments can be made cranially, caudally, laterally and medially by moving the TLPFG and TLCA components along the assembly, using the trochlear groove and intercondylar eminence as an additional centre line guide. The TUCA rests against the tibial tuberosity in an ideal alignment scenario. Once the components are aligned with the mechanical axes of the tibia from medial and cranial perspectives, the desired configuration is fastened at the TLCA and TLPFG interface by making use of a M3 screw. Proximal and distal positioning is done by sliding the TUCA up or down the shaft of the TLCA. A provision has been made at the proximal end of the TUCA, which allows for a 1.6 mm pin to be inserted through the component from the cranial side. When this pin rests on the intercondylar eminence it is used as an indication that correct proximal-distal positioning is attained. With correct alignment reached, the configuration can be fastened using a M3 fixation screw and a third point of fixation can be added through the TUCA, inserting at the tibial tuberosity, to secure the alignment guide components into place, as seen in Figure 57.

The TSG is inserted at the proximal end of the TUCA using a medial approach, where it can be rotated and aligned to create a six degree caudal slope along the proximal end of the tibia, by making use of degree line indications present on the medial side of the proximal TUCA. Once correct alignment is achieved, the configuration is secured with a M3 screw, and additional fixation pins can be added through the medial side of the TSG to further secure the sawing guide. The tibial cutting guide is secured with at least three fixation pins before any cut can be made, usually with five, with two more being added through the TSG. With the joint in full flexion, the cut can be made using the allocated saw guide slot of the TSG, sweeping in a lateral and medial motion from the cranial side in a caudal direction, taking care not to injure any of the collateral ligaments. Once the proximal tibial cut is made, the bone segments can be removed so that a perfectly flat tibial surface with exposed cancellous bone remains, as seen in Figure 58.

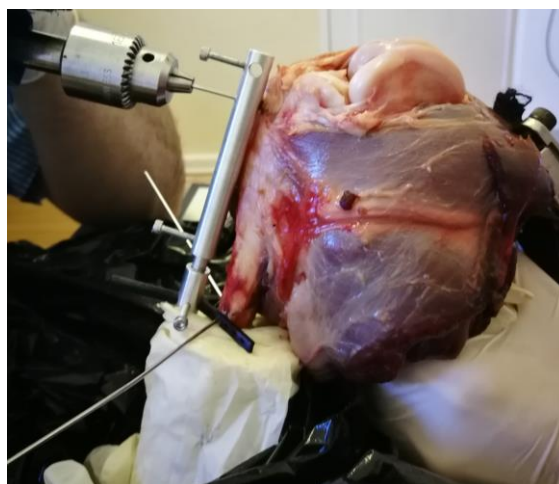


Figure 57: Fixation of the tibial alignment guide

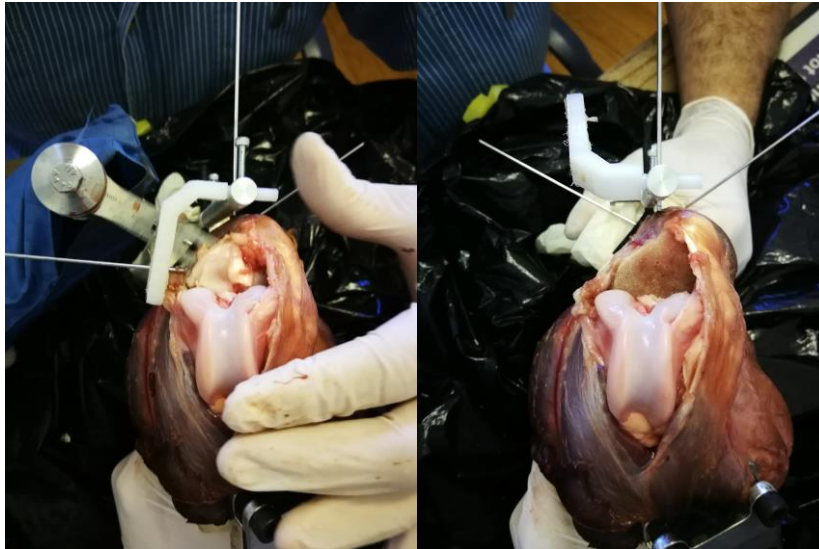


Figure 58: Tibial cut being made and resultant flat tibial surface

The fixation pins holding the TSG in place are removed, followed by the TSG, where the TDA is positioned in its stead, which is rotated in the same plane as flexion-extension of the knee joint. The TDG is inserted into the TDA and rotated until it is positioned perpendicular with the TUCA. Medial-lateral and caudo-cranial positioning can be achieved by moving the TDA and TDG components along their sliding joints respectively. Once the desired configuration is achieved, it is secured using a M3 screw. A proximal approach is used for drilling, creating holes in which the tibial implant pins will be inserted for secure fixation. The drill bit diameters being 5 mm and 1.5 mm, where 1.6 mm diameter fixation pins are used to increase the hole diameters at the medial and lateral tibial implant insertion points. The TDG and TDA components are removed. If the fixation pin hole is too tight for the tibial implant to be inserted, the drill can be used to increase the hole size without the use of the drilling guide. Smaller drill holes can be made along the tibial surface to promote fixation once implant cement is introduced in final stages of surgery. A tibial tester can be used to see which thickness of the implant component will be most suitable. The remaining components can be removed or kept in place, functioning as a visual alignment guide or extra handle to move the tibia around, depending on the needs of the surgeon.

For the femoral cuts, the joint is positioned in a flexed position. The FIPL is placed to make contact against the distal and caudal end of the femur, positioned perpendicular to the mechanical axis of the femur, with both condyles being positioned flush against the component. The mediolateral positioning is determined by aligning the drill insertion point slightly medially of the centre of the patella-femoral groove, or along the mechanical axis of the femur instead of the anatomical axis of the femur. The origin of the common digital extensor can be used as an indication of correct alignment, with the fixation pin location being slightly above the origin of the extensor when viewed from the distal end. A fixation pin is inserted at least 10 mm into the distal femur using the FIPL as a guide. Once inserted, the FIPL can be removed and the FFPS component is placed about the fixation pin. The FCGB component is positioned onto the FFPS using a distal approach until

pressed up against the femur. Mediolateral and caudocranial alignment being achieved, the FCA is inserted into the caudal saw guide slot of the FCGB in order to get correct internal-external rotational alignment. Once the correct alignment configuration is achieved, the FCGB is secured into position with a 1.6 mm fixation pin on the medial and lateral distal femoral sides, where provisions have been made for fixation pins to be inserted, as seen in Figure 59.

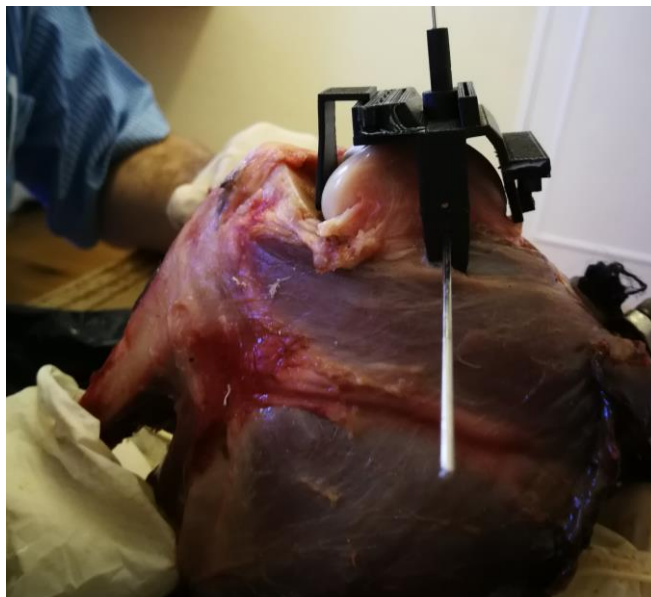


Figure 59: Fixation of FCGB with FCA still attached

With three points of fixation present, the FCA is removed. Four cuts are made, starting with the saw blade against the bone surface and avoiding hitting the guide slot sides, which could loosen the cutting guide. These cuts follow the same sequence of cranial, caudal, distal and cranial-distal each time. Fixation points are changed between the second and third cuts, removing the first fixation pin that was inserted into the distal femur, along with the FFPS. Another fixation point is utilized at the proximal cranial side of the FCGB, achieving three points of fixation once again, allowing the next distal cut to be made, as seen in Figure 60. Fixation points are changed, as this allows each cut to be made without any interference from the entry point to the exit point of the blade. The hole of the femoral fixation pin can be drilled. A 5 mm diameter drill bit is used for this procedure, following the drilling guide of the FCGB to a depth suitable for the designed femoral component implant. The final cranial-distal cut is made after the hole has been drilled.

Once all four cuts and hole have been made, the FCGB and remaining fixation pins can be removed. Creation of a notch is most likely to occur for the cranial cut, and should be avoided if possible, as this can create a higher femoral stress, which has a possibility of leading to femoral bone fracture. Should a notch be present, the surgeon should attempt to remove the notch by free-hand sawing to reduce stresses. If ideal alignment is achieved, a notch should not occur. Bone fragments and any soft tissue attachments remaining are removed, so that exposed cancellous bone remains, as seen in Figure 60.



Figure 60: Proximal fixation pin added proximally and exposed cancellous bone after femoral cuts have been made

A femoral tester is used to check the completeness of all cuts, allowing the surgeon to complete any unsatisfactory cuts free hand, being careful to create a cut in the exact plane as intended. The femoral and tibial testers are placed at their respective sites, checking for correct joint tightness. Once the correct tibial thickness is selected and cuts have been identified to be satisfactory, the exposed surfaces of the distal femur and proximal tibia are cleaned in preparation for final implantation. The femoral implant should be cemented into place, making sure to use compressive force for good fixation, followed by the tibial implant being cemented into place, with any excess cement identified outside of the implant perimeters to be removed before it can harden. The implants were not cemented into place for this study, as they only had to remain fixed for a few hours throughout the testing procedure and the design of the implants allowed for a tight enough fit that cementing was deemed as unnecessary for short term purposes. The joint was cleaned before the patella could be placed back into position, in the patellofemoral groove. Suturing of the joint is the final step in the knee replacement process, making sure to close the incision in order to restore joint capsule tautness as close to natural as possible, as seen in Figure 61.



Figure 61: Knee with implants inserted before and after suturing

4.6 Angle and translation calculation method

The following section describes the computational procedure that was followed in order to convert data obtained from the motion tracking system into translations and angles that have medical relevance. A description of the code used in this section can be found in Appendix D. An overview of the computational steps followed are as follows:

1. Define translation vectors.
2. Generate rotational matrices from femur and tibia (joint coordinate systems) to their anatomic coordinate systems (cartesian coordinate systems) and define anatomic coordinate system's origins.
3. Generate rotational matrix from tibial tool joint coordinate system to world (femoral) coordinate system and tibial tool positioning in terms of world coordinate system for dynamic data.
4. Generate anatomic coordinate systems (cartesian coordinate systems) of femur and tibia for dynamic data.
5. Generate joint coordinate system for dynamic data.
6. Calculate angles and translations for joint shape relationship based on generated rotation matrices.

The above steps provided the baseline which was used to guide the calculation steps. As mentioned before, the virtual markers were placed on predetermined bone landmarks, so that repeatability could be increased. The calculations that follow are based on the right hind limb of a canine.

After making sure that the fixed femoral tracking tool was set to act as the global reference during data recording, the virtual marker tool positioning for tibial bone landmarks could be defined relative to the world (femoral) coordinate system at the time of recording, denoted as $\mathbf{t}_{probe\ to\ world}$. The tibial tool positioning could also be defined relative to the world coordinate system at the time of recording, as seen in Figure 62a, denoted as $\mathbf{t}_{tool\ to\ world}$.

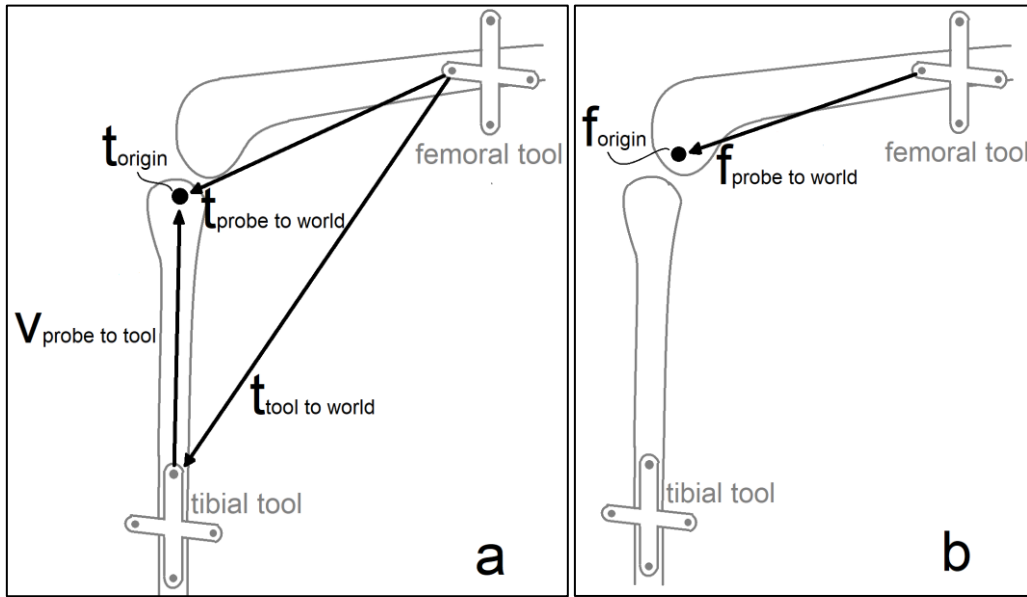


Figure 62: Joint coordinate and cartesian coordinate systems relationship

Quaternion rotation was recorded from the world coordinate system to the fixed tibial tool coordinate system, denoted as q . All tibial virtual marker points should be denoted in terms of the fixed tibial tool coordinate system ($v_{probe\ to\ tool}$); hence a rotation matrix is needed in order to create a constant vector from the tibial fixed tool to each of the tibial virtual marker points. This is done for all tibial bone landmarks chosen, namely the medial, lateral, distal and proximal tibial points. The equations to achieve this are as follows:

$$q = w + ix + jy + kz \quad (4.5.1)$$

$$Q_{rot\ matrix} = \begin{bmatrix} 1 - 2y^2 - 2z^2 & 2xy - 2zw & 2xz + 2yw \\ 2xy + 2zw & 1 - 2x^2 - 2z^2 & 2yz - 2xw \\ 2xz - 2yw & 2yz + 2xw & 1 - 2x^2 - 2y^2 \end{bmatrix} \quad (4.5.2)$$

$$v_{probe\ to\ tool} = Q_{rot\ matrix}' * (t_{probe\ to\ world}' - t_{tool\ to\ world}') \quad (4.5.3)$$

The origin for the tibial anatomic coordinate system is located at the proximal tibial probe point relative to the fixed tibial tool, denoted as t_{origin} . The tibial anatomic coordinate system can be generated by creating a system of axes located at the chosen bone landmarks relative to the fixed tibial tool, as visualised by Grood et al. [12] in Figure 4. This is done as follows:

$$z = t_{proximal\ probe\ to\ tool} - t_{distal\ probe\ to\ tool} \quad (4.5.4)$$

$$y = z \times (t_{lateral\ probe\ to\ tool} - t_{medial\ probe\ to\ tool}) \quad (4.5.5)$$

$$x = z \times y \quad (4.5.6)$$

Unit vectors for each axis of the tibial anatomic coordinate system, is generated as follows:

$$\hat{\mathbf{x}} = \mathbf{x}/|\mathbf{x}| \quad (4.5.7)$$

$$\hat{\mathbf{y}} = \mathbf{y}/|\mathbf{y}| \quad (4.5.8)$$

$$\hat{\mathbf{z}} = \mathbf{z}/|\mathbf{z}| \quad (4.5.9)$$

Due to rigid body properties, the rotation matrix of the fixed tibial tool coordinate system to anatomic coordinate system always remains the same and can be displayed as follows:

$$\mathbf{R}_{\text{tibial tool to anatomic}} = [\hat{\mathbf{x}} \hat{\mathbf{y}} \hat{\mathbf{z}}] \quad (4.5.10)$$

The virtual marker tool positioning for femoral bone landmarks could be defined relative to the world (femoral) coordinate system at the time of recording, as seen in Figure 62b, denoted as $\mathbf{f}_{\text{probe to world}}$. As the femoral tool is already set as world coordinate system, the tool position relative to the world did not need to be recorded, as it was already established. The origin for the femoral anatomic coordinate system is located at the distal femur probe point relative to the fixed femoral tool, denoted as $\mathbf{f}_{\text{origin}}$. The femoral anatomic coordinate system can be generated by creating a system of axes located at the chosen bone landmarks relative to the fixed femoral tool, as visualised by Grood et al. [12] in Figure 4. This is done as follows:

$$\mathbf{Z} = \mathbf{t}_{\text{proximal probe to tool}} - \mathbf{t}_{\text{distal probe to tool}} \quad (4.5.11)$$

$$\mathbf{Y} = \mathbf{Z} \times (\mathbf{t}_{\text{lateral probe to tool}} - \mathbf{t}_{\text{medial probe to tool}}) \quad (4.5.12)$$

$$\mathbf{X} = \mathbf{Z} \times \mathbf{Y} \quad (4.5.13)$$

Unit vectors for each axis of the femoral anatomic coordinate system is generated as follows:

$$\hat{\mathbf{X}} = \mathbf{X}/|\mathbf{X}| \quad (4.5.14)$$

$$\hat{\mathbf{Y}} = \mathbf{Y}/|\mathbf{Y}| \quad (4.5.15)$$

$$\hat{\mathbf{Z}} = \mathbf{Z}/|\mathbf{Z}| \quad (4.5.16)$$

Due to rigid body properties, the rotation matrix of the fixed femoral tool coordinate system to anatomic coordinate system always remains the same and can be displayed as follows:

$$\mathbf{R}_{\text{femur tool to anatomic}} = [\hat{\mathbf{X}} \hat{\mathbf{Y}} \hat{\mathbf{Z}}] \quad (4.5.17)$$

Motion data is used to get the orientation of the tibial tool relative to the world coordinate system, displayed in quaternions. For each point of tracked motion, a rotation matrix is created, denoted as $R_{\text{tool to world}}$. The same motion data is used to track the position of the tibial tool for each point of tracked motion, denoted as $p_{\text{tool to world}}$, as visualised in Figure 63.

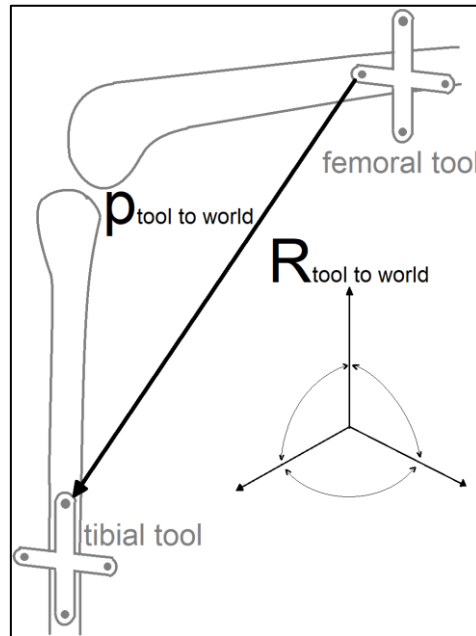


Figure 63: Tibial tool positioning and orientation relationship

Similarly, the following calculations are done for each point of tracked motion. For rotational information, the joint coordinate system must be obtained. Firstly, the cartesian coordinate system is described for the tibia, with the base vectors for each respective axis of the tibia being denoted by \mathbf{i} , \mathbf{j} and \mathbf{k} . For a $m \times n$ matrix:

$$\mathbf{i} = R_{\text{tool to world}}(1, n) * R_{\text{tibia tool to anatomic}}(1, n) \quad (4.5.18)$$

$$\mathbf{j} = R_{\text{tool to world}}(2, n) * R_{\text{tibia tool to anatomic}}(2, n) \quad (4.5.19)$$

$$\mathbf{k} = R_{\text{tool to world}}(3, n) * R_{\text{tibia tool to anatomic}}(3, n) \quad (4.5.20)$$

Secondly, the cartesian coordinate system is described for the femur, with the base vectors for each respective axis of the femur being denoted by \mathbf{I} , \mathbf{J} and \mathbf{K} . For a $m \times n$ matrix:

$$\mathbf{I} = R_{\text{femur tool to anatomic}}(1, n) \quad (4.5.21)$$

$$\mathbf{J} = R_{\text{femur tool to anatomic}}(2, n) \quad (4.5.22)$$

$$\mathbf{K} = R_{\text{femur tool to anatomic}}(3, n) \quad (4.5.23)$$

The nonorthogonal unit base vectors for the body fixed axes are described as \mathbf{e}_1 and \mathbf{e}_3 respectively, with \mathbf{e}_2 being described for the floating axis. Together they form the rotation matrix from the world coordinate system to the joint coordinate system. These can now be calculated as follows:

$$\mathbf{e}_3 = \mathbf{R}_{tool\ to\ world} * \hat{\mathbf{z}} \quad (4.5.24)$$

$$\mathbf{e}_1 = \hat{\mathbf{X}} \quad (4.5.25)$$

$$\mathbf{e}_2 = \mathbf{e}_3 \times \mathbf{e}_1 \quad (4.5.26)$$

$$\mathbf{R}_{World\ CS\ to\ Joint\ CS} = [\mathbf{e}_1\ \mathbf{e}_2\ \mathbf{e}_3] \quad (4.5.27)$$

Therefore flexion-extension, internal-external rotation and adduction-abduction can be calculated by making use of the calculation method described by Grood et al. [12].

$$\text{flexion} = \alpha = 180^\circ - \cos^{-1}(\mathbf{J} \cdot \mathbf{e}_2) \quad (4.5.28)$$

$$\text{tibial rotation} = \gamma = \sin^{-1}(\mathbf{e}_2 \cdot \mathbf{I}) \quad (4.5.29)$$

$$\text{joint adduction} = \beta = \cos^{-1}(\mathbf{I} \cdot \mathbf{k}) - 90^\circ \quad (4.5.30)$$

In order to calculate translations, the tibial origin relative to the world coordinate system must be calculated, denoted by $\mathbf{t}_{oACStoW}$, for each data sample of tracked motion. This is done so that the vector from the femoral anatomic coordinate system origin to the tibial anatomic coordinate system origin can be calculated, denoted by \mathbf{s} .

$$\mathbf{t}_{oACStoW} = \mathbf{p}_{tool\ to\ world} + \mathbf{R}_{tool\ to\ world} * \mathbf{t}_{origin} \quad (4.5.31)$$

$$\mathbf{s} = \mathbf{R}_{World\ CS\ to\ Joint\ CS} * (\mathbf{t}_{oACStoW} - \mathbf{f}_{origin}) \quad (4.5.32)$$

Therefore, mediolateral tibial shift, denoted by q_1 , can be described along the \mathbf{e}_1 -axis. Anterior-posterior drawer, denoted by q_2 , can be described along the \mathbf{e}_2 -axis. Distraction or compression of the joint, denoted by q_3 , can be described along the \mathbf{e}_3 -axis. These can be calculated by making use of the calculation method described by Grood et al. [12] as follows:

$$q_1 = s_1 + s_3 \cos(\beta + 90^\circ) \quad (4.5.33)$$

$$q_2 = s_2 \quad (4.5.34)$$

$$q_3 = -s_3 - s_1 \cos(\beta + 90^\circ) \quad (4.5.35)$$

5 Results

5.1 Obtained data

Results were obtained for open chain tests of pre- and post-implant knee joints. Kinematics were compared for the joint extension cycle of the test. Kinematics such as internal-external rotation, adduction-abduction angular rotation, mediolateral tibial shift, displacement of the tibial origin along the floating axis (drawer) and the height of the femoral origin above the tibial transverse plane (distraction) were measured against the extension angle of the joint, as the test setup determined the flexion-extension range achieved. The angle measurement convention used for extension is displayed in Figure 64. The quadriceps force experienced throughout the extension phase of the joint was recorded and plotted against the extension angle of the joint.

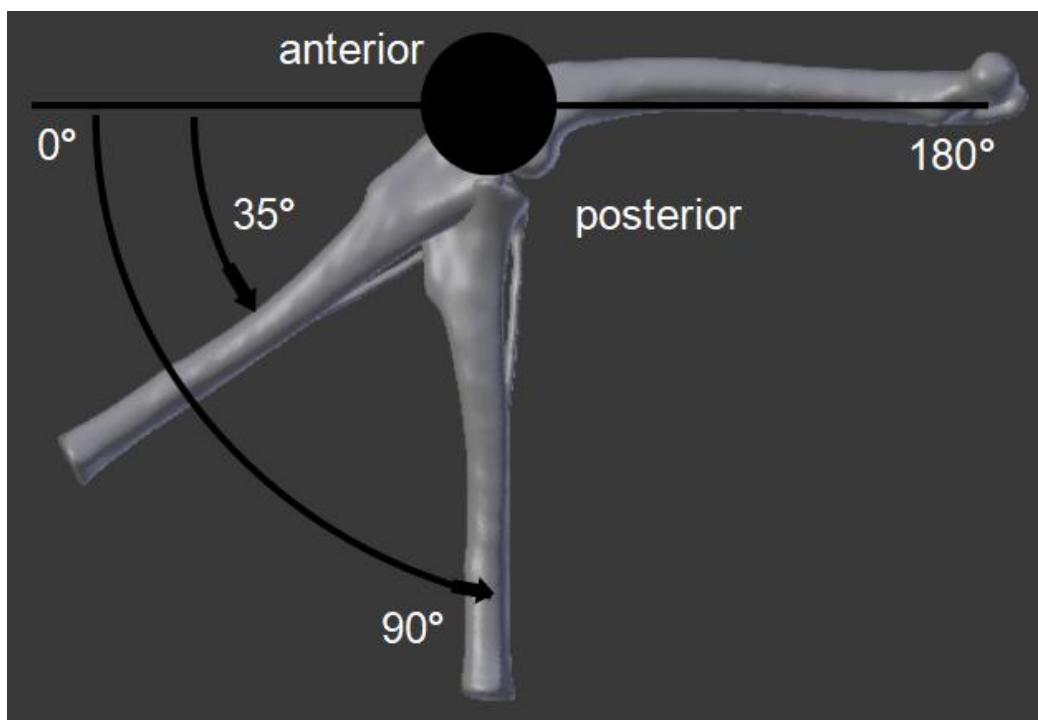


Figure 64: Flexion-extension angle measurement convention

5.2 Casted bone model results

The casted bone model design, based on a bullterrier, was used as proof of concept for the test setup and measurement method. After numerous iterations, the test approach in section 4.2 was developed and the following results were obtained for the pre-implant casted bone model and post-implant casted bone model. Eleven tests were performed for both the pre-implant and post-implant models to obtain the visualised data seen in Figure 65, showing a mean curve with a 95% confidence interval. Figure 66 displays the difference comparison between pre- and post-implant test results achieved.

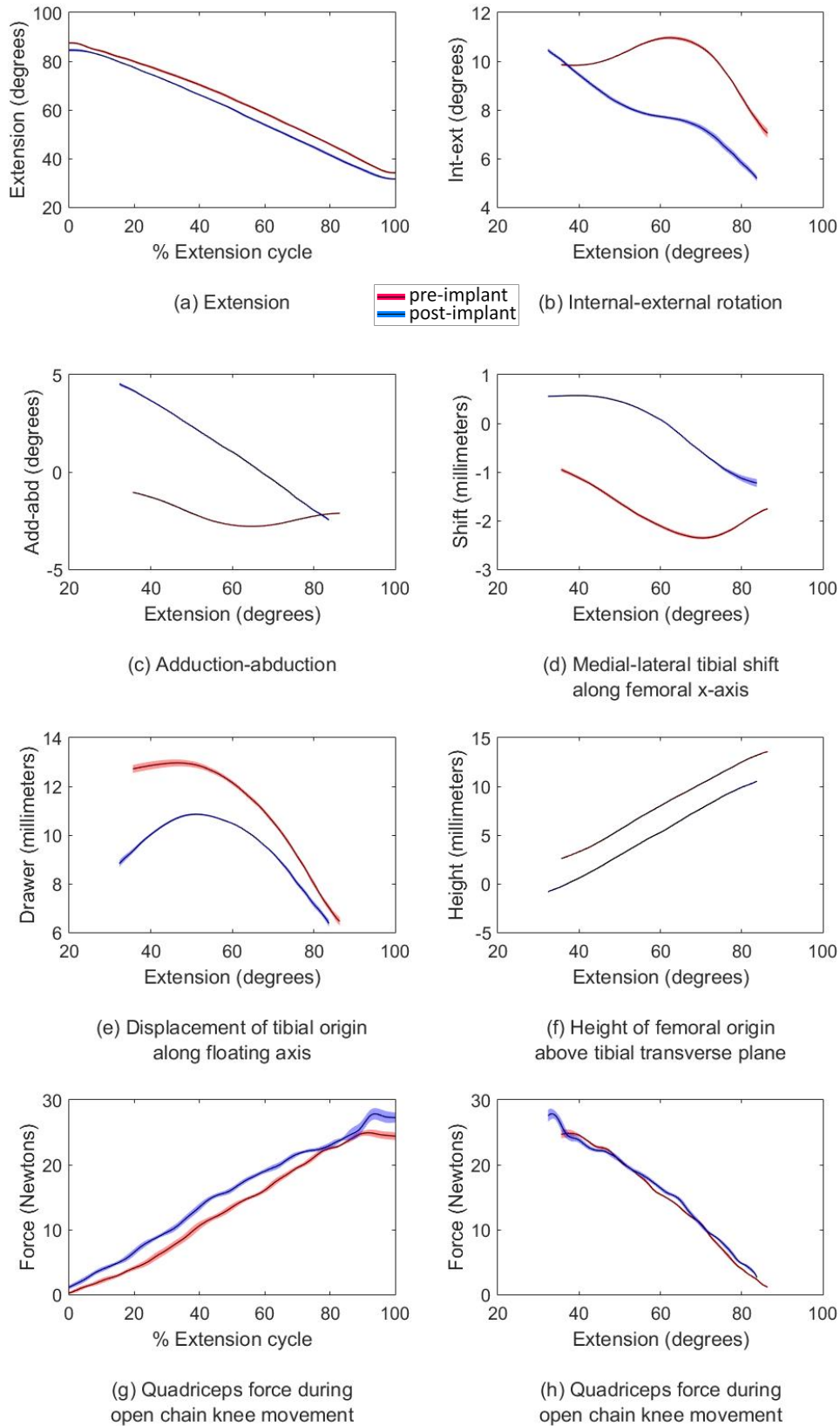


Figure 65: Pre- and post-implant kinematic results for casted bone model tests

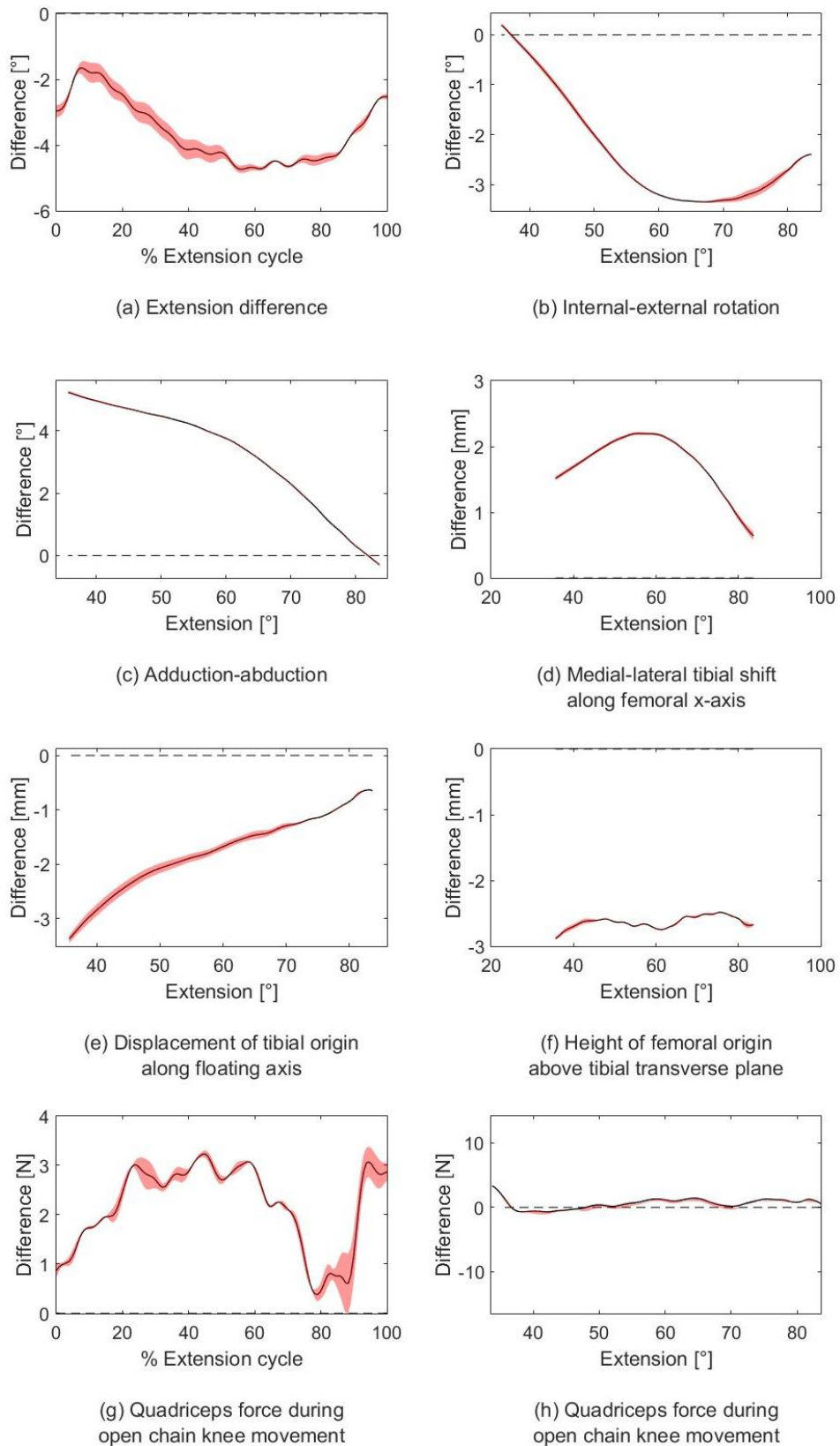


Figure 66: Difference comparison between pre- and post-implant results for casted bone model tests

Similar curve trajectories were observed for both the pre-implant kinematic curves and post-implant kinematic curves, with a noticeable increase in range of motion being observed for internal-external rotation (1.36°) and adduction-abduction (5.24°) post-implant. A noticeable decrease in range of motion for anterior-posterior drawer was also observed post-implant (2.03 mm). An increase in extension could be associated with an increase of external rotation, with a slight decrease of external rotation in the later parts of the extension phase pre-implant. An increase in abduction and lateral tibial shift along the femoral x-axis could generally be associated with an increase in the later part of extension, with a decrease being experienced in the initial stages of extension pre-implant. Translation curves for anterior-posterior drawer and joint distraction-compression were similar in shape pre- and post-implant. A summary of the kinematic test results can be seen in Table 4, with a 95% confidence interval deviation shown in brackets.

Table 4: Kinematic comparison between tests for pre-implant and post-implant casted bone models

Angles and translations	Pre-Implant			Post-Implant		
	Minimum (95% CI)	Maximum (95% CI)	Range of motion	Minimum (95% CI)	Maximum (95% CI)	Range of motion
(a) Flexion-extension [°]	37.06 (1.18)	87.01 (0.88)	49.95	32.46 (0.32)	84.48 (0.52)	52.02
(b) Internal-external [°]	7.04 (0.19)	10.96 (0.06)	3.92	5.18 (0.13)	10.46 (0.08)	5.28
(c) Adduction-abduction [°]	-2.79 (0.03)	-1.05 (0.02)	1.74	-2.47 (0.04)	4.53 (0.08)	7
(d) Shift [mm]	-2.36 (0.03)	-0.95 (0.04)	1.41	-1.23 (0.08)	0.57 (0.01)	1.8
(e) Drawer [mm]	6.45 (0.17)	12.96 (0.14)	6.51	6.37 (0.16)	10.85 (0.03)	4.48
(f) Distract [mm]	2.58 (0.04)	13.57 (0.07)	10.99	-0.84 (0.04)	10.53 (0.06)	11.37

Quadriceps forces increased as extension increased, with a maximum median force of 24.75 N pre-implant and a maximum median force of 27.75 N post-implant shown in Figure 65(g). Pre- and post-implant correlation data is displayed in Table 5, which shows the maximum and minimum differences between the two data ranges, as well as the root mean square error and coefficient of determination. A high statistical correlation was present for all parameters besides (b), (c) and (d), which have a coefficient of determination of 28.4%, 41% and 50.5% respectively.

Table 5: Pre- and post-implant correlation data for casted bone models

Figure 66	(a) [°]	(b) [°]	(c) [°]	(d) [mm]	(e) [mm]	(f) [mm]	(g) [N]	(h) [N]
Min diff	-1.65	0	0	0.64	-0.63	-2.48	0.38	0
Max diff	-4.73	-3.35	5.24	2.2	-3.37	-2.88	3.24	3.37
RMS Error	0.803	0.748	0.392	0.30	0.5	0.073	0.856	0.5
R² [%]	99.8	28.4	41	50.5	93.2	99.9	98.9	99.5

5.3 Labrador specimen results

The following results were obtained for the pre-implant and post-implant joint tests for the Labrador specimen. Seven test run results were included for the pre-implant visualised data and five test run results were included for post-implant visualised data, seen in Figure 67, showing a mean curve with a 95% confidence interval. Figure 68 displays the difference comparison between pre- and post-implant test results achieved.

Similar curve trajectories were observed for both the pre-implant kinematic curves and post-implant kinematic curves, with a noticeable increase in range of motion being observed for adduction-abduction (5.24°), mediolateral shift (4.13 mm) and joint distraction-compression (3.95 mm) post-implant. A noticeable decrease in range of motion for internal-external rotation was observed post-implant (9.89°). An increase of internal rotation could be associated with an increase in extension, with a slight decrease of internal rotation in the later parts of the post-implant extension phase. An increase in abduction and lateral tibial shift along the femoral x-axis could generally be associated with an increase in extension, with a decrease in abduction being experienced in the initial stages of pre-implant extension. Anterior drawer translation increased during the initial stages of extension, with an increase in posterior drawer being experienced in the later stages of extension. Joint compression increased as joint extension increased. A summary of the kinematic test results can be seen in Table 6, with a 95% confidence interval deviation shown in brackets.

Quadriceps forces increased as extension increased, with a maximum pre-implant median force of 33.75 N and a maximum post-implant median force of 137.75 N being observed, as seen in Figure 67(g). Pre- and post-implant correlation data is displayed in Table 7, which shows the maximum and minimum differences between the two data ranges, as well as the root mean square error and coefficient of determination. A high statistical correlation was present for all parameters besides (c) and (e), which have a coefficient of determination of 69.8% and 12.9% respectively.

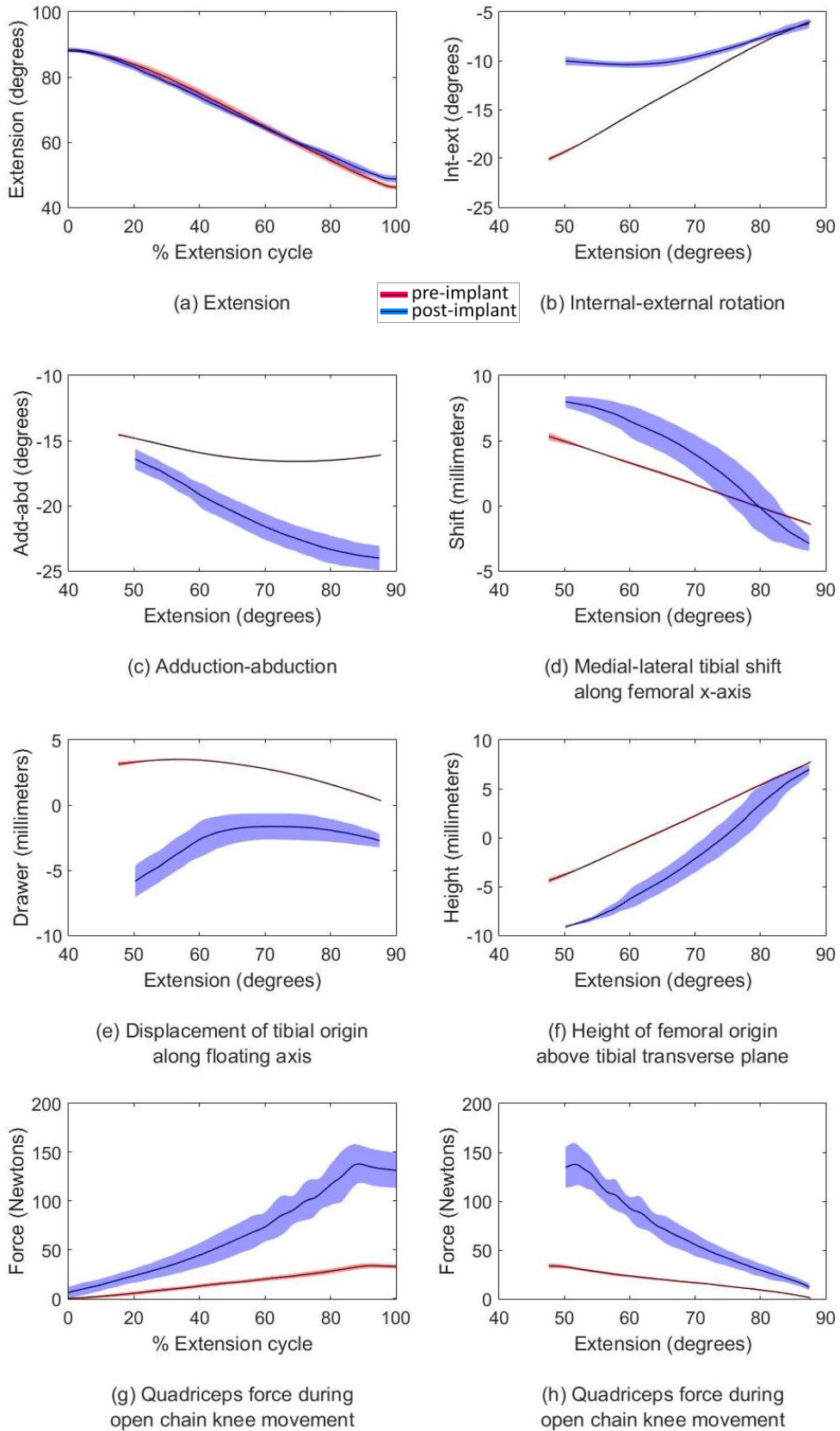


Figure 67: Pre- and post-implant kinematic results for Labrador specimen

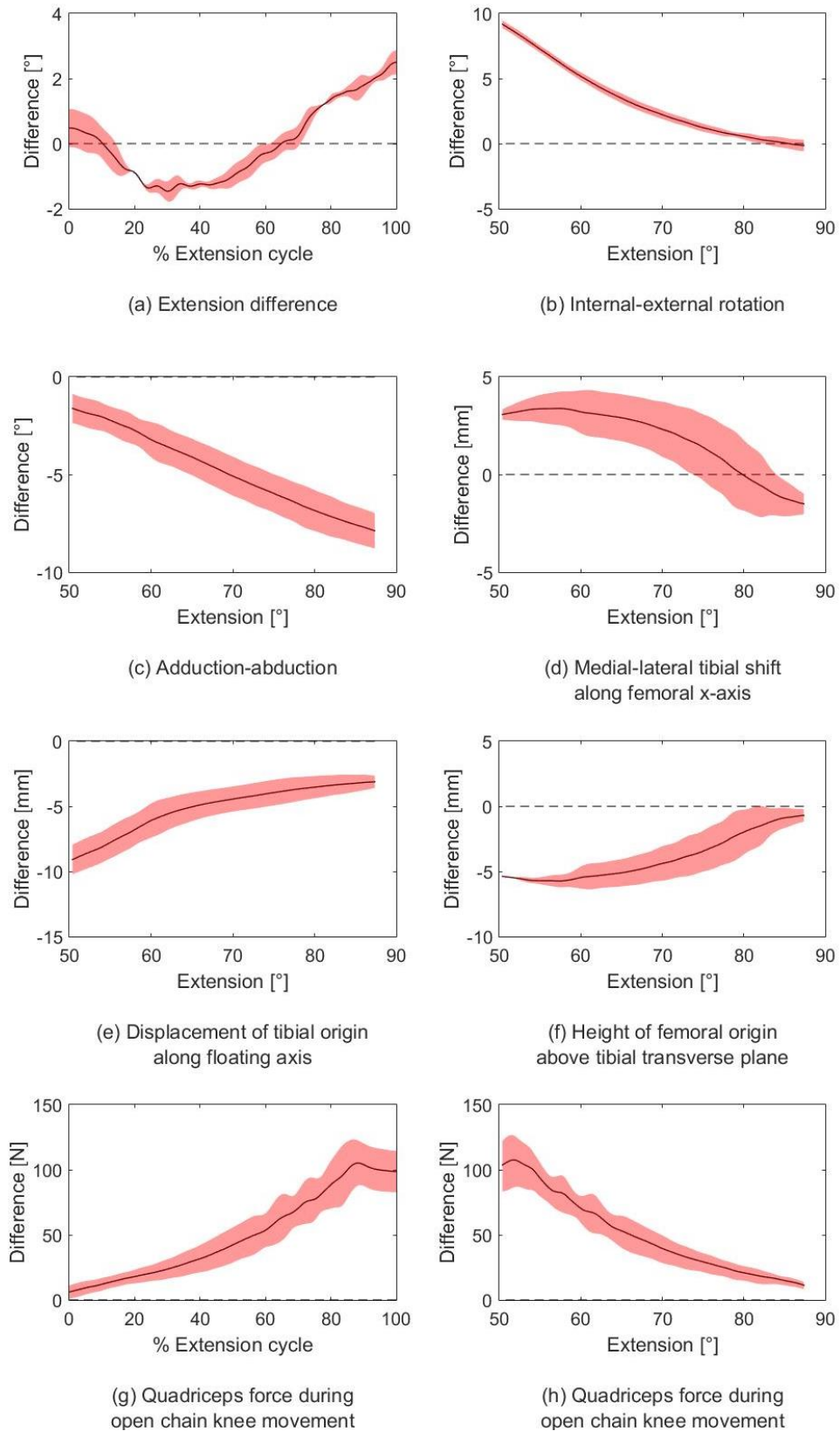


Figure 68: Difference comparison between pre- and post-implant results for Labrador specimen

Table 6: Kinematic comparison between tests for pre-implant and post-implant Labrador specimen

	Pre-Implant			Post-Implant		
Angles and translations	Minimum (95% CI)	Maximum (95% CI)	Range of motion	Minimum (95% CI)	Maximum (95% CI)	Range of motion
(a) Flexion-extension [°]	46.39 (1)	87.82 (0.14)	41.43	48.89 (1.33)	88.05 (1.01)	39.16
(b) Internal-external [°]	-20.07 (0.22)	-5.96 (0.04)	14.11	-10.4 (0.31)	-6.18 (0.5)	4.22
(c) Adduction-abduction [°]	-16.6 (0.01)	-14.55 (0.08)	2.05	-24.03 (0.93)	-16.41 (0.79)	7.62
(d) Shift [mm]	-1.44 (0.06)	5.32 (0.21)	6.76	-2.9 (0.56)	7.99 (0.42)	10.89
(e) Drawer [mm]	0.33 (0.06)	3.51 (0.02)	3.18	-5.87 (1.19)	-1.65 (1)	4.22
(f) Distract [mm]	-4.41 (0.27)	7.76 (0.05)	12.17	-9.14 (0.17)	6.98 (0.51)	16.12

Table 7: Pre- and post-implant correlation data for Labrador specimen

Figure 68	(a) [°]	(b) [°]	(c) [°]	(d) [mm]	(e) [mm]	(f) [mm]	(g) [N]	(h) [N]
Min diff	0	0	-1.61	0	-3.12	-0.7	6.1	11.2
Max diff	2.5	9.17	-7.88	3.39	-9.09	-5.74	105.2	107.5
RMS Error	0.854	1.66	0.266	0.298	0.989	0.349	1.21	1.61
R² [%]	99.6	84.1	70	97.7	12.9	99	98.7	96.6

An additional passive range of motion test was performed before and after the surgery by a qualified veterinarian surgeon. Passive range of motion tests were performed for flexion-extension, adduction-abduction and internal-external rotation. All tests were repeated at least five times by the surgeon and relied on the surgeon's practical experience to ascertain when the joints maximum or minimum range had been reached. The motion of the knee joint was tracked throughout each test and additional angular kinematic information could be obtained. Flexion-extension passive ranges of motion were observed to be 122.4° and 117.1° for pre-implant and post-implant tests respectively, resulting in a post-implant range very close to that of the pre-implant joint specimen. Internal-external passive ranges of motion were observed to be 10.78° and 16.3° for pre-implant and post-implant tests respectively. Adduction-abduction passive ranges of motion were observed to be 4.85° and 6.79° for pre-implant and post-implant tests respectively.

5.4 German Shepherd specimen results

The following results were obtained for the pre-implant and post-implant joint tests for the German Shepherd specimen. Seven test run results were included for both the pre-implant and post-implant visualised data, seen in Figure 69, showing a mean curve with a 95% confidence interval. Figure 70 displays the difference comparison between pre- and post-implant test results achieved.

Similar curve trajectories were observed for both the pre-implant kinematic curves and post-implant kinematic curves, with medial-lateral tibial shift pre- and post-implant curve trajectories being the exception. An increase in post-implant range of motion was observed for adduction-abduction (3.35°). A noticeable decrease in range of motion for internal-external rotation (2.83°) and joint distraction-compression (3.08 mm) was observed post-implant. An increase of internal rotation could be associated with an increase in extension, with a slight decrease of internal rotation in the early parts of the post-implant extension phase. An increase in abduction could be associated with an increase in extension. Medial-lateral shift trajectories during extension differed pre- and post-implant, with an increase of lateral shift with an increase of extension being observed pre-implant, but an increase of medial shift with an increase of extension being observed post-implant. Anterior drawer translation increased during the initial stages of extension, with an increase in posterior drawer being experienced in the later stages of extension. However, pre-implant anterior drawer increased for a longer time as extension increased, compared to post-implant drawer, which saw an earlier change to posterior drawer increase. Joint compression increased as joint extension increased pre- and post-implant. A summary of the kinematic test results can be seen in Table 8, with a 95% confidence interval deviation shown in brackets.

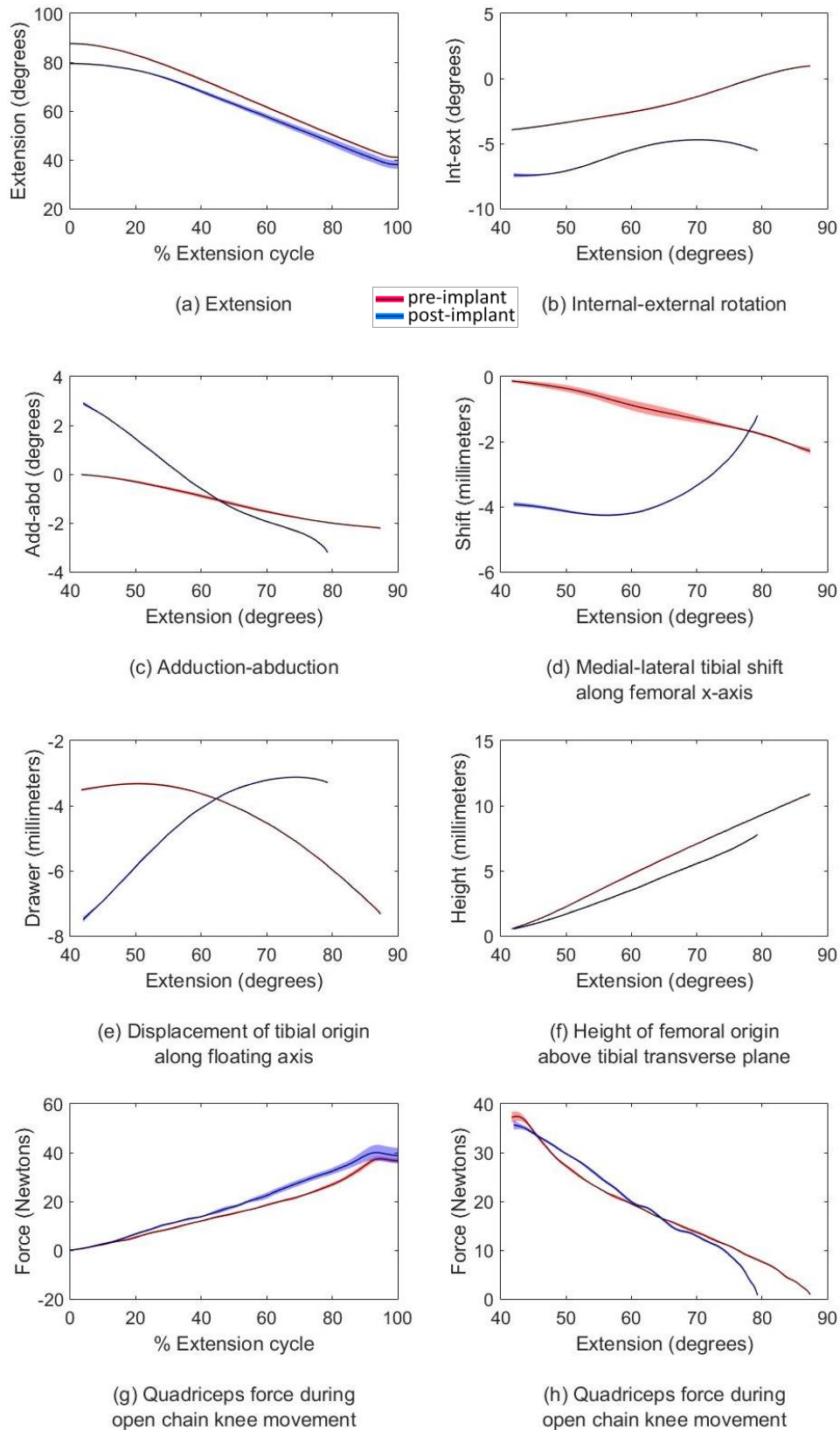


Figure 69: Pre- and post-implant kinematic results for German Shepherd specimen

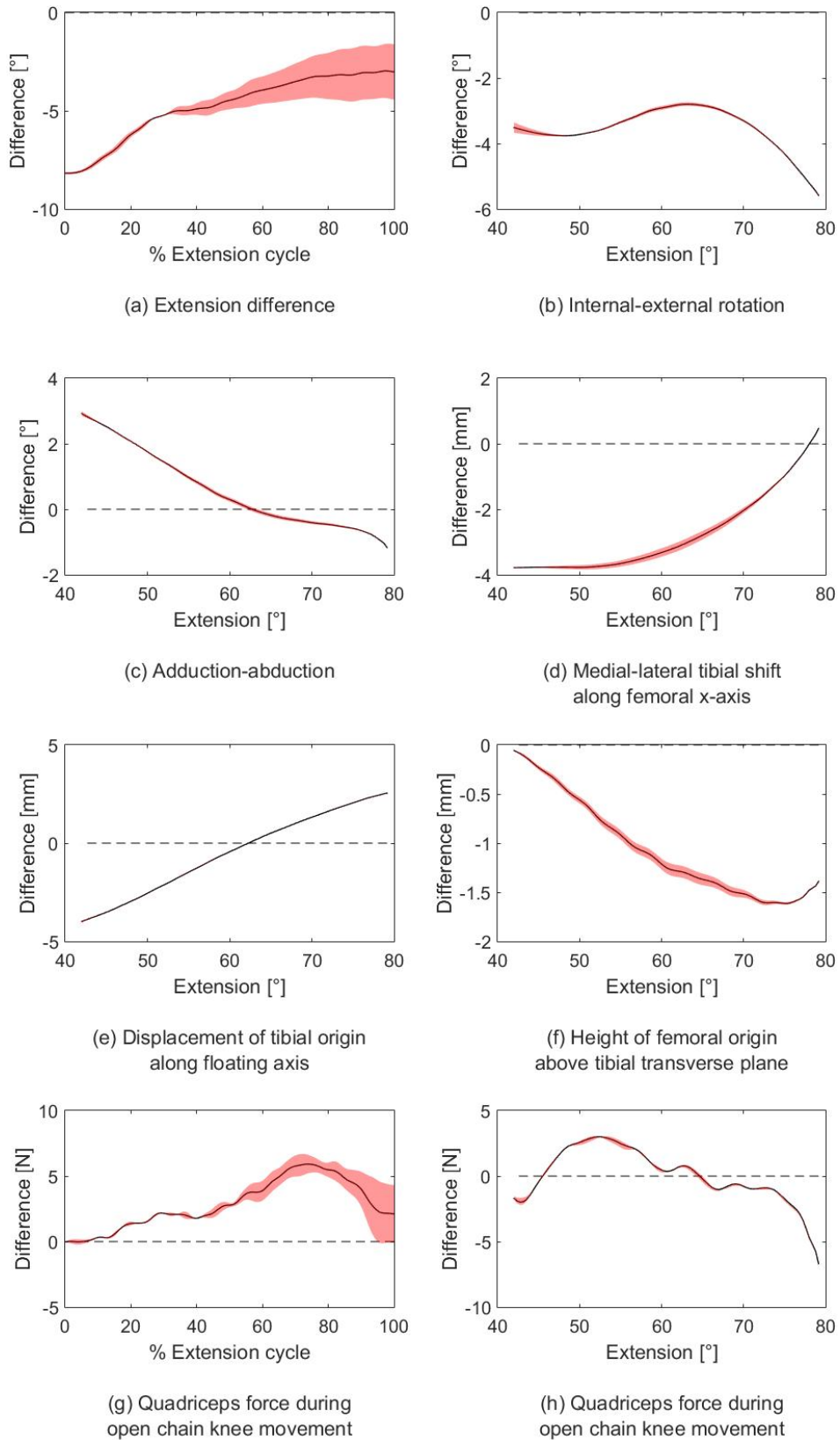


Figure 70: Difference comparison between pre- and post-implant results for German Shepherd specimen

Table 8: Kinematic comparison between tests for pre-implant and post-implant German Shepherd specimen

Angles and translations	Pre-Implant			Post-Implant		
	Minimum (95% CI)	Maximum (95% CI)	Range of motion	Minimum (95% CI)	Maximum (95% CI)	Range of motion
(a) Flexion-extension [°]	41.2 (0.45)	87.48 (0.11)	46.28	38.03 (1.72)	79.43 (0.04)	41.4
(b) Internal-external [°]	-3.94 (0.01)	0.96 (0.06)	4.9	-2.07 (0.07)	0 (0.02)	2.07
(c) Adduction-abduction [°]	-2.21 (0.04)	-0.02 (0.01)	2.19	-1.39 (0.02)	4.15 (0.07)	5.54
(d) Shift [mm]	-2.29 (0.1)	-0.14 (0.05)	2.15	-4.18 (0.03)	-0.81 (0.04)	3.37
(e) Drawer [mm]	-7.33 (0.05)	-3.32 (0.03)	4.01	-7.41 (0.08)	-3.1 (0.01)	4.31
(f) Distract [mm]	0.53 (0.04)	10.91 (0.03)	10.38	0.44 (0.06)	7.74 (0.01)	7.3

Quadriceps forces increased as extension increased, with a maximum pre-implant median force of 37.5 N and a maximum post-implant median force of 35 N being observed, resulting in similar joint forces being experienced pre- and post-implant, as seen in Figure 69(g). Pre- and post-implant correlation data is displayed in Table 9, which shows the maximum and minimum differences between the two data ranges, as well as the root mean square error and coefficient of determination. A high statistical correlation was present for all parameters besides (b), (d) and (e), which have a coefficient of determination of 69.7%, 62% and 55.1% respectively.

An additional passive range of motion test was performed before and after the surgery by a qualified veterinarian surgeon. Passive range of motion tests were performed for flexion-extension, adduction-abduction and internal-external rotation. All tests were repeated at least five times by the surgeon and relied on the surgeon's practical experience to ascertain when the joints maximum or minimum range had been reached. Flexion-extension passive ranges of motion were observed to be 125.8° and 109° for pre-implant and post-implant tests respectively. Internal-external passive ranges of motion were observed to be 17.1° and 22.7° for pre-implant and post-implant tests respectively. Adduction-abduction passive ranges of motion were observed to be 7.01° and 8.8° for pre-implant and post-implant tests respectively.

Table 9: Pre- and post-implant correlation data for German Shepherd specimen

Figure 70	(a) [°]	(b) [°]	(c) [°]	(d) [mm]	(e) [mm]	(f) [mm]	(g) [N]	(h) [N]
Min diff	-2.97	-2.8	0	0	0	-0.06	0	0
Max diff	-8.18	-5.58	2.92	-3.78	-3.99	-1.61	5.92	-6.69
RMS Error	0.644	0.652	0.107	0.309	0.514	0.177	1.18	1.65
R² [%]	99.8	70	97.2	62	55.1	99.5	98.9	96.2

6 Discussion and conclusion

6.1 Discussion and recommendations

The open-source design approach was implemented multiple times with encouraging results being achieved for the total knee replacement implants compared to the kinematic performance of healthy knees. A novel contribution to the field is obtained with the femoral and tibial implant design approach, based on healthy articulating knee joint geometry, in combination with the exclusive use of open-source software throughout the design process.

The main functional objective of the implant was to mimic kinematic mobility as close as possible to that of the healthy canine knee, especially in the flexion-extension phase of the knee. From the passive range of motion tests performed pre- and post-implant, discussed in chapter 5, a flexion-extension range of 95.6% and 87.2% was restored for the Labrador and German Shepherd specimens respectively. The obtained passive flexion-extension ranges were 122.4° and 125.8° pre-implant, and 117.1° and 109° post implant for the Labrador and German Shepherd specimens respectively, with very strong pre- and post-implant kinematic motion correlations being found. Liska et al. provided flexion-extension data in two cases where the outcome after implementation of canine total knee replacement surgery was obtained. One study resulted in a 120° flexion-extension range of motion being restored to the operated knee compared to the flexion-extension range of 124° of the healthy knee [53]. Another resulted in a 115° flexion-extension range being achieved post-implant, compared to the flexion-extension range of 100.7° pre-implant [4]. Allen et al. [5] showed knee flexion-extension ranges after TKR and a one-year recovery time, with a flexion-extension range of $112 \pm 5^\circ$ unoperated, compared to a flexion-extension range of $87 \pm 16^\circ$ post-implant. The post-implant flexion-extension results achieved in this research are similar, or in some cases better, to results seen in past studies.

Kinematic correlation for internal-external rotation and adduction-abduction was encouraging, with a minimum coefficient of determination of 70% for both cadaveric specimens. This is an encouraging sign for the recreation of healthy knee joint kinematics with regards to angular motion during extension. Strong post-implant correlation was achieved for compression-distraction translational motion as well.

Due to the nature of total knee replacement surgery, the cruciate ligaments and menisci are removed, which form part of a knee joint's main source of stability. In an attempt to counter the possible stability losses incurred from such a procedure, the tibial implant was designed to have a concave articular joint shape that compliments the femoral component, with raised edges on all sides of both the lateral and medial tibial condyles of the articular joint surface, meant to restore stability and inhibit larger ranges of motion being experienced than what the natural knee would experience pre-implant. Such a design was also implemented to lower the chance of luxation taking place, with the absence of the removed ligaments.

A decrease of internal-external rotational range of motion was incurred post-implant for both the Labrador and German Shepherd specimens, with good kinematic motion correlation present. A decrease in range of motion for this parameter is a better outcome than an increase, as an increase would result in injury due to unnatural joint movement, solving the joint degradation related problem with an implant, but causing a motion related problem. A decrease in range of motion lowers the risk of any motion-related injury without impacting the overall kinematic performance of the knee joint, hence this result is still favourable.

Post-implant anterior-posterior drawer ranges were similar to that of the healthy knee for both the Labrador and German Shepherd specimens, however a very low motion correlation was achieved. This change of motion during extension is attributed to the absence of the cruciate ligaments and menisci, which assist in the natural anterior-posterior drawer of the femur and tibia throughout joint motion. Considering the motion profile differences in combination with the range of motion similarities, a reasonable anterior-posterior result is achieved that will still be functional.

Significant increases in both adduction-abduction and mediolateral shift motion ranges were observed for the post-implant knee of both the Labrador and German Shepherd specimens. A possible contribution to the increase in adduction-abduction and mediolateral shift motion ranges could be due to the use of defrosted cadaveric specimens during testing. In a healthy knee, fibrosis would take place during the healing process along the sutured incision before any movement is applied to the joint, forming excess fibrous connective tissue and adding stability in the mediolateral directions of the joint, whereas an increase over time for muscle fibre laxity was observed in the cadaveric specimen during tests. This should be considered for future research work.

Testing on the Labrador knee specimen in chapter 5.3 revealed post-implant forces more than four times larger in magnitude during the extension phase when compared to pre-implant joint forces during extension. This was attributed to faulty tibial implant thickness selection, resulting in joint motion inhibiting tautness. With higher forces being exerted throughout extension, a probability increase of hyper-extension and luxation was induced. With an unplanned higher force needed to get the knee into a fully extended position, the robustness of the implant component could be observed, showing favourable resistance to hyper-extension related joint subluxations under high joint forces. The post-implant quadriceps forces experienced during extension for the German Shepherd specimen were very similar, with a near exact force curve correlation being present when compared to that of the healthy knee. This also highlights the importance of correct joint implant thickness selection, as the surgical procedure and implementation can have a major impact on the success of a TKR.

A previous study, conducted by Liska et al. [4], used a lateral approach during the surgical procedure, however the surgical approach used in this research and described in Chapter 4.4 made use of a medial approach, after it was observed that a lateral approach was more likely to cause damage to ligaments and musculature that needed to be preserved during the cutting procedure compared to the same likelihood of damage from the medial side. Both approaches could be

implemented with success, but the preference of the surgeon was deemed to be a medial approach. The alignment and cutting profiles generated for the implants during surgery were successfully made and the implants had a good fit, fixing in place at the implant-bone surface interfaces without any visible movement. Cancellous bone was present for all femoral and tibial cuts made during surgical procedures, important for the promotion of bone ingrowth and improved recovery time when considering implementation on a live patient.

The main areas of concern with regards to repeatability are for the segmentation process, the articular surface profile generation using Blender and the identification of landmarks used to define anatomic coordinate systems. The segmentation process was reliant on the skill of the user, done manually, following the same procedure described in Chapter 3.5 and 3.6. An automated process could possibly standardise this step and allow a more consistent result being attained across multiple segmentation processes, however the manual approach allows for variabilities of the bone structure between different breeds to be observed and kept for patient-specific design considerations. The articular surface generation of the joint relied on the skill of the user, as a manual approach was used. An automated or semi-automated approach might fast-track this part of the design process and produce a more consistent design across different sizes and breeds, warranting further research in this area. The identification of landmarks for anatomic coordinate system generation was entirely user-dependant. This process can only be done manually, with position variability being incurred during location determination of a specific landmark, due to the presence of soft tissue in the knee joint. This made it difficult to determine the exact location of virtual marker landmark points as described in chapter 4.3. With the assistance of a veterinary professional, the points were located as best as possible, allowing for kinematic comparisons of the same specimen, but making comparisons of kinematic data across different specimens difficult.

For a constant test procedure and force analysis of the quadriceps during motion, the Oxford-type knee rig was used for testing in this research, which was designed to be used on humans. Future work could include developing a standardised potting procedure for usage in a closed-chain setup for an Oxford-type knee test rig, to ensure that the closed-chain testing can be used in addition to open-chain testing for validation purposes of implants or kinematic and kinetic analysis of a healthy canine knee. A potting protocol could be beneficial as the hip and ankle have to be lined up directly above one another in order for the rig to work for a closed-chain scenario and does not allow test subjects to line up naturally. This could cause several problems during closed chain testing, resulting in joint dislocations, as the probability of making manual errors during the potting procedure is very high and the correct initial alignment for proper flexion-extension is difficult to achieve on a reliably repeatable basis. Due to this fact, the open chain testing approach was preferred, as this ensured that the ankle could line up naturally with the hip, without testing setup error being a concern throughout the testing process.

FDM manufacturing methods used for implant generation were effective and generated articular surface shape geometries as designed. However, sometimes suboptimal articular joint smoothness profiles were achieved, as the FDM

approach would cause layer seams. This was smoothed out before implementation of the implant in this research, but the concern remains that it could result in some unwanted results should a sharp edge be missed. Hence, it would be beneficial in future studies to manufacture a femoral component from a titanium alloy or cobalt-chromium alloy and a tibial component from UHMWPE, as they will most likely give a more consistent smoother surface finish and in turn a better estimation of expected joint kinematic motion when used in joint motion testing. This is the next natural step, as actual implants cannot be manufactured using FDM and one would have to manufacture implants using these biomaterials for real-world implementation.

The design approach of this study was based on a healthy articular knee joint surface geometry. The implementation of this patient-specific design approach would also be possible in a specimen with unhealthy articular knee joint surface geometry; however, the design process would then rely heavily on the expertise and experience of the user in knowing what a healthy femoral articular joint surface would look like. Further research into standardised component development might help in this regard or further research into a process that is semi-automated, where data from healthy femoral articular geometry shapes could be used to generate a component that will fit an unhealthy joint. Nevertheless, the novel design approach used has shown encouraging results and could be used to generate functional patient-specific implants with accompanying surgical instrumentation.

6.2 Conclusion

A canine knee implant modelled after healthy knee geometry was achieved for three different specimens. The femoral component was modelled after healthy canine articular surface geometry, whilst the tibial component was modelled after the complementing articular surface geometry of the generated femoral implant. Throughout the design process, open-source software was used, and a repeatable work-flow process was generated, as described in chapter 3. Healthy knee kinematics were successfully compared with knee kinematics after the implementation of a patient-specific implant, with encouraging results being achieved. Patient-specific implants have the potential to restore kinematic motion to a patient similar to that of a healthy knee. The design process for a patient-specific solution relies on the skill of the user; however, this research provides the user with the ability to follow a workflow that makes the skill-level required more attainable.

Overall, the joint kinematics of the open-source design approach compared well to the motion profiles of a healthy knee, generating implant components for three different cases, with promising kinematic results. A design model was generated that has evident commercial potential for canine TKR implementation. The femoral and tibial implant design approach, based on healthy articulating knee joint geometry, in combination with the exclusive use of open-source software throughout the design process, amounts to a novel contribution to the field.

References

- [1] BioMedtrix, "06d012e56c62ddf331ad257b5ef6ea0a971dc401 @ biomedtrix.com." [Online]. Available: <https://biomedtrix.com/total-knee-replacement/>.
- [2] M. Sharkey, "The challenges of assessing osteoarthritis and postoperative pain in dogs," *AAPS J.*, vol. 15, no. 2, pp. 598–607, 2013.
- [3] [www.fitzpatrickreferrals.co.uk](https://www.fitzpatrickreferrals.co.uk/orthopaedic/canine-total-knee-replacement/), "Canine total knee replacements." [Online]. Available: <https://www.fitzpatrickreferrals.co.uk/orthopaedic/canine-total-knee-replacement/>.
- [4] W. D. Liska and N. D. Doyle, "Canine total knee replacement: Surgical technique and one-year outcome," *Vet. Surg.*, vol. 38, no. 5, pp. 568–582, 2009.
- [5] M. J. Allen, K. A. Leone, K. Lamonte, K. L. Townsend, and K. A. Mann, "Cemented total knee replacement in 24 dogs: Surgical technique, clinical results, and complications," *Vet. Surg.*, vol. 38, no. 5, pp. 555–567, 2009.
- [6] D. L. Millis and I. A. Ciuperca, "Evidence for Canine Rehabilitation and Physical Therapy," *Vet. Clin. North Am. - Small Anim. Pract.*, vol. 45, no. 1, pp. 1–27, 2015.
- [7] L. C. Hieu *et al.*, "Integrated approaches for personalised cranio-maxillofacial implant design and manufacturing," *IFMBE Proc.*, vol. 27, no. November 2015, pp. 119–122, 2010.
- [8] A. Matthew, "Biomechanical Considerations for Total Knee Arthroplasty," pp. 484–487.
- [9] D. H. Carpenter and R. C. Cooper, "Mini review of canine stifle joint anatomy," *Anat. Histol. Embryol.*, vol. 29, no. 6, pp. 321–329, 2000.
- [10] "9050_Canine_Knee_2008 @ www.anatomynow.com." [Online]. Available: http://www.anatomynow.com/filebin/supplier_images/gpi/325px/9050_Canine_Knee_2008.jpg.
- [11] [www.homeofbob.com](http://www.homeofbob.com/glossaries/VeterinarianAnatomicalPositions.html), "Veterinarian Anatomical Positions." [Online]. Available: <http://www.homeofbob.com/glossaries/VeterinarianAnatomicalPositions.html>.
- [12] E. S. Grood and W. J. Suntay, "A joint coordinate system for the clinical description of three-dimensional motions: Application to the knee," *J. Biomech. Eng.*, vol. 105, no. 2, pp. 136–144, 1983.
- [13] Health City Cayman Islands, "Top Reasons for Knee Replacement

- Surgery.” [Online]. Available: <https://www.healthcitycaymanislands.com/top-reasons-for-knee-replacement-surgery/>.
- [14] “9051_K9_4-Stage_Osteo_Knee-2 @ www.anatomynow.com.” [Online]. Available: https://www.anatomynow.com/filebin/supplier_images/gpi/325px/9051_K9_4-Stage_Osteo_Knee-2.jpg.
- [15] S. Comitini *et al.*, “Evolution in Knee Replacement Implant,” *Single-Cell Biol.*, vol. 4, no. 2, 2014.
- [16] “500-ajrr-releases-2017-annual-report-on-hip-and-knee-arthroplasty-data @ www.ajrr.net,” *American Academy of Orthopaedic Surgeons*, 2018. [Online]. Available: <http://www.ajrr.net/media-news/press-releases/500-ajrr-releases-2017-annual-report-on-hip-and-knee-arthroplasty-data>. [Accessed: 07-Nov-2018].
- [17] M. Saini, “Implant biomaterials: A comprehensive review,” *World J. Clin. Cases*, vol. 3, no. 1, p. 52, 2015.
- [18] Innoplast, “GenuSys Knee.” [Online]. Available: <https://www.innoplast-vet.de/knee.html>.
- [19] S. Amiri, D. Cooke, I. Y. Kim, and U. Wyss, “Mechanics of the passive knee joint. Part 2: Interaction between the ligaments and the articular surfaces in guiding the joint motion,” *Proc. Inst. Mech. Eng. Part H J. Eng. Med.*, vol. 221, no. 8, pp. 821–832, 2007.
- [20] H. Pandit *et al.*, “Influence of surface geometry and the cam-post mechanism on the kinematics of total knee replacement,” *J. Bone Jt. Surg. - Ser. B*, vol. 87, no. 7, pp. 940–945, 2005.
- [21] C. K. Fitzpatrick, M. A. Baldwin, P. J. Laz, D. P. FitzPatrick, A. L. Lerner, and P. J. Rullkoetter, “Development of a statistical shape model of the patellofemoral joint for investigating relationships between shape and function,” *J. Biomech.*, vol. 44, no. 13, pp. 2446–2452, 2011.
- [22] J. M. Cottrell, E. Townsend, J. Lipman, T. P. Sculco, and T. M. Wright, “Bearing surface design changes affect contact patterns in total knee arthroplasty,” *Clin. Orthop. Relat. Res.*, no. 464, pp. 127–131, 2007.
- [23] W. Mesfar and A. Shirazi-Adl, “Biomechanics of the knee joint in flexion under various quadriceps forces,” *Knee*, vol. 12, no. 6, pp. 424–434, 2005.
- [24] Q. Rong, J. Bai, Y. Huang, and J. Lin, “Presurgery design and biomechanical evaluation of patient-specific knee implant,” *J. Mech. Med. Biol.*, vol. 15, no. 6, pp. 1–11, 2015.

- [25] A. Marković, T. Mišić, J. L. Calvo-Guirado, R. A. Delgado-Ruíz, B. Janjić, and M. Abboud, "Two-Center Prospective, Randomized, Clinical, and Radiographic Study Comparing Osteotome Sinus Floor Elevation with or without Bone Graft and Simultaneous Implant Placement," *Clin. Implant Dent. Relat. Res.*, vol. 18, no. 5, pp. 873–882, 2016.
- [26] D. Ji, P. Wang, X. Zhang, and X. Chen, "Feasibility study on accurate rapid prototyping for human hand bones and affiliated artery," *Rapid Prototyp. J.*, vol. 23, no. 1, pp. 96–100, 2017.
- [27] A. Soni, Y. Kumar Modi, and S. Agrawal, "Computed tomography based 3D modeling and analysis of human knee joint," *Mater. Today Proc.*, vol. 5, no. 11, pp. 24194–24201, 2018.
- [28] E. C. S. Júnior, A. T. Nogueira, B. A. Rocha, W. M. N. E. Filho, and A. D. Meneses, "Reconstrução virtual tridimensional como ferramenta de planejamento pré-operatório de fístulas anais complexas," *J. Coloproctology*, vol. 38, no. 1, pp. 77–81, 2018.
- [29] T. Simmons-Ehrhardt, C. Falsetti, A. B. Falsetti, and C. J. Ehrhardt, "Open-source tools for dense facial tissue depth mapping of computed tomography models," *Hum. Biol.*, vol. 90, no. 1, pp. 63–76, 2018.
- [30] T. Dovramadjiev, "Modern accessible application of the system Blender in 3D design practice," *Nhk 技研*, vol. 151, no. 4, pp. 10–17, 2015.
- [31] KetanKumar Ramniklal Jalal, "Custom Design and Manufacturing of Canine Knee Implant," p. 125, 2003.
- [32] Simtk.org, "GeometryGeneration," 2019. [Online]. Available: <https://simtk.org/plugins/moinmoin/openknee/Specifications/GeometryGeneration>.
- [33] Y. Ohtake, A. Belyaev, and I. Bogaevski, "Mesh regularization and adaptive smoothing," *CAD Comput. Aided Des.*, vol. 33, no. 11, pp. 789–800, 2001.
- [34] D. P. Huttenlocher, W. J. Rucklidge, and G. A. Klanderman, "Comparing images using the Hausdorff distance under translation," *Proc. IEEE Comput. Soc. Conf. Comput. Vis. Pattern Recognit.*, vol. 1992-June, no. 9, pp. 654–656, 1992.
- [35] Matweb, "SpecificMaterial." [Online]. Available: <http://asm.matweb.com/search/SpecificMaterial.asp?bassnum=MTP641>.
- [36] D. Steines and A. Zhuravlev, "United States Patent, Patent No.: US8,234,097 B2," 2012.
- [37] A. H. S. Company, *Veterinary Instrumentation*, 6th ed. 2017.

- [38] S. D. Gittard and R. J. Narayan, "Laser direct writing of micro- and nano-scale medical devices," *Expert Rev. Med. Devices*, vol. 7, no. 3, pp. 343–356, 2010.
- [39] F. G. Mangano, B. Cirotti, R. L. Sammons, and C. Mangano, "Custom-made, root-analogue direct laser metal forming implant: A case report," *Lasers Med. Sci.*, vol. 27, no. 6, pp. 1241–1245, 2012.
- [40] F. Mangano *et al.*, "Custom-made, selective laser sintering (SLS) blade implants as a non-conventional solution for the prosthetic rehabilitation of extremely atrophied posterior mandible," *Lasers Med. Sci.*, vol. 28, no. 5, pp. 1241–1247, 2013.
- [41] 3D Systems, "DuraForm ® PA Plastic Properties," 2017.
- [42] A. Composites, "AMT Composites Products." [Online]. Available: <https://www.amtcomposites.co.za/>.
- [43] University of Cambridge, "Mechanical properties of bone." [Online]. Available: http://www.doitpoms.ac.uk/tlplib/bones/bone_mechanical.php.
- [44] A. B. Zavatsky, "A kinematic-freedom analysis of a flexed-knee-stance testing Rig," *J. Biomech.*, vol. 30, no. 3, pp. 277–280, 1997.
- [45] K. M. Varadarajan, R. E. Harry, T. Johnson, and G. Li, "Can in vitro systems capture the characteristic differences between the flexion-extension kinematics of the healthy and TKA knee?," *Med. Eng. Phys.*, vol. 31, no. 8, pp. 899–906, 2009.
- [46] A. Pcr and L. Kit, "Tension and Compression Force Sensor K-1427 Data Sheet," pp. 0–1, 2012.
- [47] J. K. Hofer, R. Gejo, M. H. McGarry, and T. Q. Lee, "Effects on tibiofemoral biomechanics from kneeling," *Clin. Biomech.*, vol. 26, no. 6, pp. 605–611, 2011.
- [48] C. Anglin *et al.*, "Biomechanical Consequences of Patellar Component Medialization in Total Knee Arthroplasty," *J. Arthroplasty*, vol. 25, no. 5, pp. 793–802, 2010.
- [49] K. M. Ghosh, A. M. Merican, F. Iranpour, D. J. Deehan, and A. A. Amis, "Length-change patterns of the collateral ligaments after total knee arthroplasty," *Knee Surgery, Sport. Traumatol. Arthrosc.*, vol. 20, no. 7, pp. 1349–1356, 2012.
- [50] K. M. Ghosh, A. M. Merican, F. Iranpour-Boroujeni, D. J. Deehan, and A. A. Amis, "Length change patterns of the extensor retinaculum and the effect of total knee replacement," *J. Orthop. Res.*, vol. 27, no. 7, pp. 865–870, 2009.

- [51] I. NDI, "Passive Polaris Spectra User Guide," vol. Revision 7, no. September, 2012.
- [52] S. Pinna and N. Romagnoli, "Radiographic measurement of the quadriceps angle in dogs," *PLoS One*, vol. 12, no. 10, pp. 1–10, 2017.
- [53] W. D. Liska, D. J. Marcellin-Little, E. V. Eskelinen, C. G. Sidebotham, O. L. A. Harrysson, and A. K. Hiem-Björkman, "Custom total knee replacement in a dog with femoral condylar bone loss," *Vet. Surg.*, vol. 36, no. 4, pp. 293–301, 2007.
- [54] G. D. D'Angelo, "Blender Infographics Map," 2014. [Online]. Available: <https://www.giudansky.com/illustration/infographics/blender-map>.

Appendices

A 3DSlicer segmentation protocol

The following steps were followed to start the process of unprocessed 3D model reconstruction using 3DSlicer:

- Load DICOM Data
- Volume Rendering
 - Enable Crop & Display ROI
- Crop Volume, making sure to include the tibial, fibular, patellar and femoral bone segments
 - Apply when ready and repeat as needed
- Select the Editor
 - Anatomy Layers
 - Paint Effect
 - Threshold paint – select a lower threshold paint limit of about 230 ~ 300 as shrinkage is likely to occur during the smoothing process
 - Apply the threshold paint effect to each slice of the CT scan, making sure to include the relevant anatomies, i.e. the tibial, fibular, patellar and femoral bone segments.
 - Make model effect
- Go to Model Maker
 - Select label map volume
 - Define the model name and labels
 - Set smoothing and decimation levels to zero
- Select the Editor
 - Make Model Effect
 - Deselect smoothing, name the model
 - Apply settings when ready
- Generated models can be viewed in the Models tab
- Save and export the STL-file

B Meshlab smoothing protocol

A smoothing protocol developed for the human knee was used as a guideline [32]. Unfortunately, Meshlab is prone to regular crashes, making it important to save the generated component after each step taken. Saving work is also important, as one cannot 'undo' an action in Meshlab, hence it would be easier to recall a previous save file than to restart the entire process from the start should one make a mistake. In order to change orientation or to move about a selected mesh, either the left mouse button or the number pad can be used to change to different orientations. Toggling between orthogonal and non-orthogonal views can be done by pressing five on the number pad. Zooming and translation of the selected mesh can be achieved by either holding in or scrolling the middle mouse button.

Once the raw STL file has been loaded, initial cleaning of the mesh can take place. When importing the mesh, a prompt will appear to unify duplicate vertices. This should be applied as the first cleaning step. From the "Filters" drop-down menu one can select several cleaning and repairing options, as required for the imported mesh. One can also make use of the "Edit" drop-down menu to select faces in a rectangular field or to select connected components in a region. This can be used to remove floating vertices or unwanted objects from the workspace. Should unwanted holes be present in the mesh, one can remove these by selecting "Remeshing, Simplification and Reconstruction" in the "Filters" drop-down menu, which will give the user the opportunity to select "Close Holes" and make the mesh watertight again.

For Laplacian smoothing, the following steps are followed:

- Use the layer dialog panel to select the desired mesh.
- Select Filters
 - Smoothing, fairing and deformation
 - Laplacian smooth (surface preserve)
- Set the number of smoothing steps to the specified amount for the selected mesh.
- Apply the smoothing procedure.

Make sure to save the newly created mesh. This type of smoothing moves each vertex in the average position of neighbour vertices, with the newly generated vertex lying almost on the original surface.

For surface reconstruction, the following steps are followed:

- Use the layer dialog panel to select the desired mesh.
- Select Filters
 - Smoothing, fairing and deformation
 - Surface reconstruction: VCG
- Set the voxel side world unit value to a suitable amount for the selected mesh relative to the original image resolution.
- Enable post merge simplification and apply.

Make sure to save the newly created mesh. This filter is applied to all visible layers present in the layer dialog box. Should fragments appear at the edges of the model, cleaning of the model should be done to remove the unwanted fragments.

For Taubin smoothing, the following steps are followed:

- Use the layer dialog panel to select the desired mesh.
- Select Filters
 - Smoothing, fairing and deformation
 - Taubin smoothing
- Set the lambda and mu values as required.
- The preview function can be used to interactively display the smoothing parameters being applied to the mesh.
- Apply the smoothing procedure.

Make sure to save the newly created mesh. This filter is especially useful in smoothing over any sharp edges on the mesh.

For Iso parametrization, there are two stages to follow. The first stage is done as follows:

- Use the layer dialog panel to select the desired mesh.
- Select Filters
 - Smoothing, fairing and deformation
 - Iso parametrization: Main
- Apply the procedure.

This filter creates a rough surface triangulation that can be projected onto the new mesh without much distortion from the original mesh. This step in the process can be problematic and cause the program to crash. The filter could fail due to excessive topological noise, bad triangulation or because the mesh resolution is too low. Should the “multi component mesh” error message appear, one should remove any meshes besides the one that is required, or it could mean that more cleaning and repairing is needed as there are floating vertices present. Deselecting the double-step option can also fix the problem. The input mesh seems to be non-deterministic with regards to the functionality of the filter.

If the process still does not work, one might have to remove some internal vertices by making use of the following procedure:

- Use the layer dialog panel to select the desired mesh.
- Select Filters
 - Colour creation & processing
 - Apply the ambient occlusion filter
- Select Filters
 - Selection
 - Select by vertex quality
 - Experiment with the sliders to create a low-quality selection, in other words to select all interior vertices that are not visible.
- Select Filters
 - Selection
 - Delete selected vertices

Now stage one of Iso parametrization can be repeated and should be functional.

Stage two of Iso parametrization can be done as follows:

- Use the layer dialog panel to select the desired mesh.

- Select Filters
 - Remeshing, simplification and reconstruction
 - Select Iso parametrization remeshing
- Specify the sampling rate as required.
- Apply the procedure.

Make sure to save the newly created mesh.

Taubin smoothing must be applied one more time as previously described to finish the smoothing process. This final smoothing step will also correct any twisted triangles, should any have been created in the previous step.

The Hausdorff paired mesh distance mapping can be applied as follows:

- Select Filters
 - Sampling
 - Select Hausdorff
 - The sampled mesh is the smoothed mesh created and the reference surface.
 - The target mesh is the original raw mesh.
- Use the layer dialog panel to select the desired mesh.
- Select Render
 - Show Vertex Quality Histogram
- Select Filters
 - Colour creation & processing
 - Colorize by vertex quality
 - Set the minimum to zero and the maximum as apparent by the vertex quality histogram.
 - The preview function can be used to interactively display the distance map being generated on the surface.
 - The previous two steps can be repeated until the desired colorized distance map is generated.
- Apply the procedure

C Blender infographic map

Blender involves a steep learning curve at first, however once the fundamentals are learned, the design process speeds up exponentially. Many of the commands and add-ins used throughout the design process can be seen in the Blender infographic map in Figure 71, adapted from Giudansky [54]. This can be used as a useful tool to streamline the design process, enabling one to input commands in a single step instead of several steps.

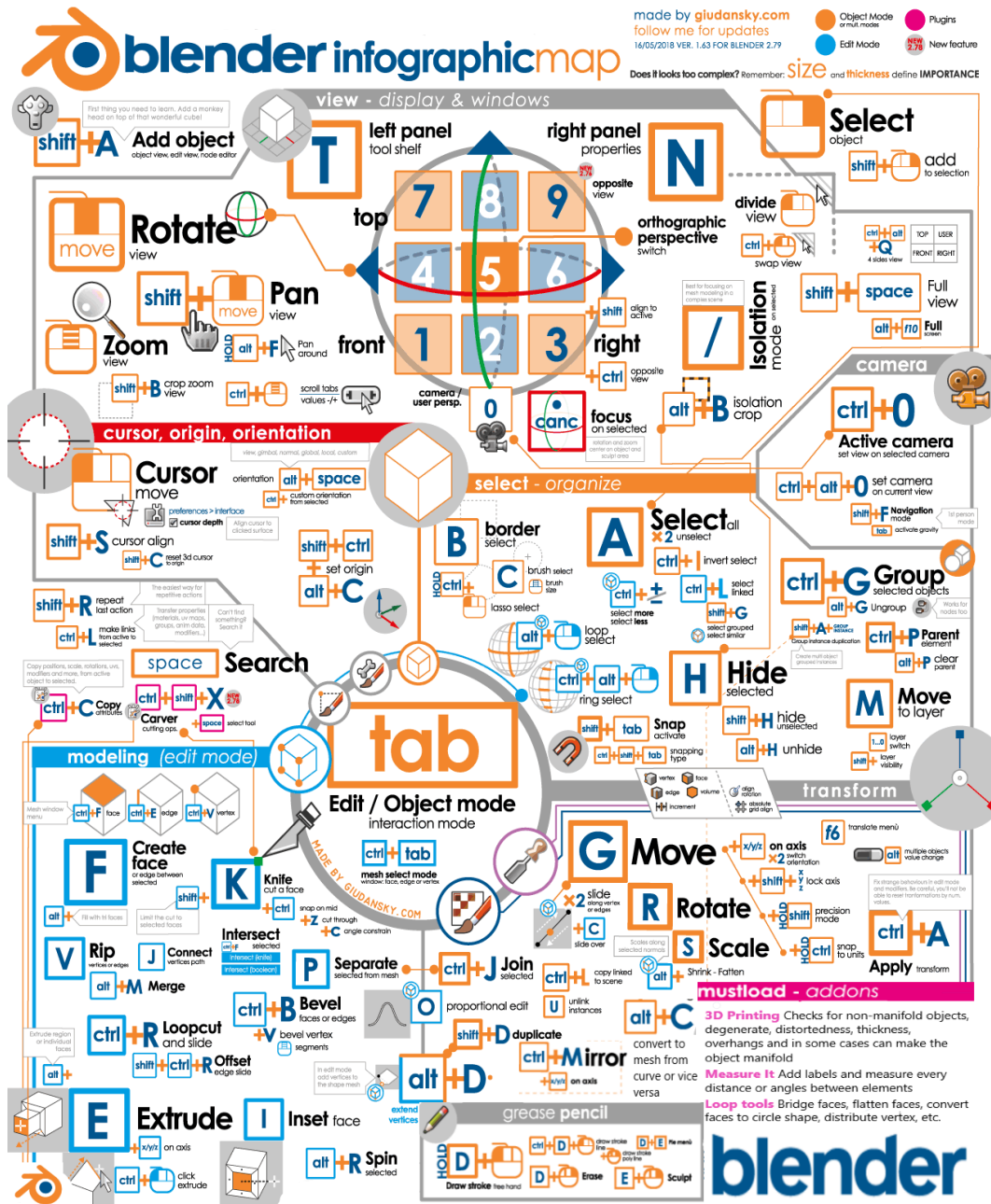


Figure 71: Blender infographic map adapted from Giudansky [54]

Whenever a Boolean modifier is applied, one should make use of the '3D Printing' add-in, found in the tool shelf toolbox. Newly generated components can be checked to see whether they are manifold or not. This is a very useful tool in repairing non-manifold objects, as one can use this to identify and select non-manifold edges, intersect faces, non-flat faces, zero faces and edges. In some cases, when the object geometry is of a lower complexity, the 'make manifold' command can be used to fix an object automatically. This command should be used sparingly and with caution, as it can add additional unwanted geometries to the object in an attempt to fix it.

It should be noted that one can choose three sub-options in the Boolean modifier, namely intersect, union or difference. The Boolean difference modification was used predominantly throughout the design process. The program runs into problems at times and creates a union when an intersection is requested for example, or any combination of the three Boolean options. Fortunately, a preview is generated before one applies a modification and hence one can check whether the requested modification is achieved or not. This problem can arise when a face, edge or vertex from the Boolean mesh is placed directly on top of the target mesh, however this does not always seem to be a determinant factor. Another reason for this could be due to duplicate faces or a non-manifold mesh being used with a manifold mesh during a modifier's application.

Considering the tibial articulating surface design for an implant. When a high-resolution mesh is present, the Boolean difference operation does not always work as intended, hence a different Boolean option such as the Boolean union operation is used. This can be very time consuming when working with a higher resolution mesh, as unwanted vertices, edges and faces must be manually removed. One can make use of the '3D Printing' add-in, found in the tool shelf toolbox, to speed up this process somewhat once all faces and edges have been removed that lie outside of the original intended articular shape profile. If this step is done correctly, one can make use of the 'make manifold' command in the 3D Printing toolbox, which should generate an intended articular surface geometry that is manifold, as intended. Should this process generate unwanted results, one must perform the entire process manually.

D Kinematic calculations code

```

% Set femoral tracking tool as global reference (world coordinate system)
% i.e. fixed femoral tracking tool = world
% =====
% Important abbreviations:
% t2w - tool to world
% t2a - tool to ACS (anatomic coordinate system)
% T - Tibia
% F - Femur
% L - Length of array
% =====
% Read virtual markers located at landmarks. Read tool points.
All_data = xlsread('Virtual and tool point data','Range');
% Read data of tibial tool during motion.
Motion_data = xlsread('Motion Data');
% Read quadriceps force data during motion.
Quadriceps_data = xlsread('Force Data');
ForceQuads = Quadriceps_data(:,2); % relevant force data during motion
% =====
% Establishing anatomic coordinate system at proximal tibia relative to
% tibial tool, located at the bone landmarks, identified with the use of
% the virtual marker points
% Hence a rotation matrix from tibial tool to tibial ACS is established
% p2t - virtual probe marker points relative to tool
% t2w - fixed tool relative to world
% p2w - virtual probe marker points relative to world
% TOrigin_p2t - Tibial ACS origin located at proximal tibial ACS point,
% relative to fixed tibial tool
% =====
xT_lat_p2w = All_data(12,11:13)'; % Generating a column vector.
xT_lat_t2w = All_data(12,6:8)'; % Defining tibial tool positioning rel
% to world when virtual lateral point
% was recorded.
QT_lat_w2t = All_data(12,1:4); % Quaternion rotation from world to
% fixed tibial tool when virtual
% lateral point was recorded.
RT_lat_w2t = quat2rotm(QT_lat_w2t); % Rotation matrix of quaternion.
% =====
xT_med_p2w = All_data(14,11:13)'; % Same process as for lateral
xT_med_t2w = All_data(14,6:8)';
QT_med_w2t = All_data(14,1:4);
RT_med_w2t = quat2rotm(QT_med_w2t);
% =====
zT_distal_p2w = All_data(10,11:13)'; % Same process as for lateral
zT_distal_t2w = All_data(10,6:8)';
QT_dist_w2t = All_data(10,1:4);
RT_dist_w2t = quat2rotm(QT_dist_w2t);
% =====
zT_prox_p2w = All_data(15,11:13)'; % Same process as for lateral
zT_prox_t2w = All_data(15,6:8)';

```

```

QT_prox_w2t = All_data(15,1:4);
RT_prox_w2t = quat2rotm(QT_prox_w2t);
% =====
% All virtual markers should be denoted i.t.o fixed tool coordinate system
% By applying rotation, hence constant vectors created from tibial fixed
% tool 2 virtual marker point i.t.o. axes that define the tibial fixed tool
xT_lat_p2t = RT_lat_w2t' *(xT_lat_p2w - xT_lat_t2w);
xT_med_p2t = RT_med_w2t' *(xT_med_p2w - xT_med_t2w);
zT_dist_p2t = RT_dist_w2t' *(zT_distal_p2w - zT_distal_t2w);
zT_prox_p2t = RT_prox_w2t' *(zT_prox_p2w - zT_prox_t2w);
% Tibial ACS origin located at proximal tibial ACS point, relative to fixed
% tibial tool
TOrigin_p2t = zT_prox_p2t;
% =====
% Anatomic Coordinate System generation for tibia
% - Creating system of axes located at the bone landmarks, identified with
% the use of the virtual marker points
Ztt = zT_prox_p2t - zT_dist_p2t;
xT_temp = xT_lat_p2t - xT_med_p2t;
Ytt = cross(Ztt,xT_temp);
Xtt = cross(Ztt,Ytt);
% =====
% Normalised unit vectors:
XT_p2t = Xtt/ norm(Xtt); % Unit vector of x-axis on tibia ACS, med to lat
YT_p2t = Ytt/ norm(Ytt); % Unit vector of y-axis on tibia ACS, post to ant
ZT_p2t = Ztt/ norm(Ztt); % Unit vector of z-axis on tibia ACS, dist to prox
% =====
% Rotation matrix of fixed tibial tool to ACS, due to rigid body, the value
% remains constant
RT_t2a = [XT_p2t, YT_p2t, ZT_p2t]';
% = [XT_p2t(1) YT_p2t(1) ZT_p2t(1);
%     XT_p2t(2) YT_p2t(2) ZT_p2t(2);
%     XT_p2t(3) YT_p2t(3) ZT_p2t(3)]
% =====
% Establishing anatomic coordinate system at distal femur relative to
% femoral (world) tool, located at the bone landmarks, identified with the
% use of the virtual marker points
% Hence a rotation matrix from femoral (world) tool to femoral ACS is
% established
% p2t          - virtual probe marker points relative to tool
% t2w          - fixed tool relative to world
% p2w          - virtual probe marker points relative to world
% FOrigin_p2t - Femoral ACS origin located at proximal femoral ACS point,
%              relative to fixed femoral tool
% =====
xF_lat_p2w = All_data(2, 11:13)'; % Generating a column vector
% =====
xF_med_p2w = All_data(3, 11:13)';
% =====
zF_dist_p2w = All_data(1, 11:13)'; % Femoral ACS origin position
% =====
zF_prox_p2w = All_data(4, 11:13)';
% =====

```

```

% Anatomic Coordinate System generation for femur
% - Creating system of axes located at the bone landmarks, identified with
%   the use of the virtual marker points
zff    = (zF_prox_p2w - zF_dist_p2w);
xF_temp = (xF_lat_p2w - xF_med_p2w);
Yff    = cross(Zff,xF_temp);
Xff    = cross(Zff,Yff);
% =====
% Normalised unit vectors in world CS:
XF_p2t =Xff/ norm(Xff); % Unit vector of X-axis on femur ACS - med to lat
YF_p2t =Yff/ norm(Yff); % Unit vector of Y-axis on femur ACS - post to ant
ZF_p2t =Zff/ norm(Zff); % Unit vector of Z-axis on femur ACS - dist to prox
% =====
% Femoral ACS origin located at distal femur ACS point, relative to fixed
% femoral/world tool
FOrigin_p2t = zF_dist_p2w;
% =====
% Rotation matrix of fixed femur tool to ACS, due to rigid body, the value
% remains constant
RF_t2a = [XF_p2t, YF_p2t, ZF_p2t]';
% =====

% Motion data
% Fixed Tibia Tool:

% Orientation
Q_wSample = Motion_data(:,1);
Q_xSample = Motion_data(:,2);           % Orientation of tibial tool, in
Q_ySample = Motion_data(:,3);           % quaternions, relative to world
Q_zSample = Motion_data(:,4);           % coordinate system
QT_tool2w = [Q_wSample, Q_xSample, Q_ySample, Q_zSample];
% Fixed tibial tool relative to world coordinate system - Rotation Matrix
RotT_t2w = quat2rotm(QT_tool2w);
% Data samples for motion - length captured
Length = length(QT_tool2w);

% Position
T_xt = Motion_data(:,6);
T_yt = Motion_data(:,7);
T_zt = Motion_data(:,8);
% Fixed tibial tool relative to the world coordinate system - Position
TibT_t2w = [T_xt, T_yt, T_zt];
% =====

for a = 1:(Length)

% Tibia to Femur
% ===== Rotations =====
% Obtaining Joint CS
% Cartesian coordinate system for tibia denoted by i,j and k
i    = RotT_t2w(:, :,a)*(RT_t2a(1, :))';
j    = RotT_t2w(:, :,a)*(RT_t2a(2, :))';
k    = RotT_t2w(:, :,a)*(RT_t2a(3, :))';
% Cartesian coordinate system for femur denoted by I,J and K

```

```

I = RF_t2a(1,:);
J = RF_t2a(2,:);
K = RF_t2a(3,:);

e3 = RotT_t2w(:, :, a)*ZT_p2t;
e1 = XF_p2t;
e2 = cross(e3,e1);
% Rotation matrix from world CS to Joint CS
R_JointCS_t2a = [e1, e2, e3]';

flex(a) = 180 - acosd(dot(J,e2));
rot(a) = - asind(dot(e2,i));
abd(a) = acosd(dot(I, k)) - 90;

% ===== Translations =====
% Tibial origin relative to world CS - during motion
TOrig_ACS2w = TibT_t2w(a, :, :)' + (RotT_t2w(:, :, a)*TOrigin_p2t);
% Vector from femoral ACS origin to Tibial ACS origin
V_FemACS2TibACS = R_JointCS_t2a*(TOrig_ACS2w-FOrigin_p2t);

T_shift(a) = V_FemACS2TibACS(1) + V_FemACS2TibACS(3)*cosd(abd(a)+90);
T_drawer(a) = V_FemACS2TibACS(2);
T_distract(a)= -V_FemACS2TibACS(3) -V_FemACS2TibACS(1)*cosd(abd(a)+90);

end

```

Published with MATLAB® R2015a